

POLITECNICO DI TORINO

Master's Degree Course in Mechanical Engineering

Master's Degree Thesis

**Optimization of the Heating
System in a Bus Cabin:
a Numerical Approach through
OpenFOAM**



Supervisor:
prof. Eliodoro Chiavazzo

Candidate:
Rajiv Haresh Vaswani R.
Student Id: 260469

Academic Year 2019-2020

Abstract

Throughout human history, thermal comfort has been by far the most important factor when evaluating well-being. Although, there are numerous studies regarding thermal engineering in HVAC systems, their scope has primarily been focused on analyzing buildings or automobiles, but have barely fixated on buses. Moreover, in the field of computational fluid dynamics, there is virtually no research aimed towards this kind of vehicles. This thesis tries to fill this void by analyzing the heating system of a public transport bus in Turin, using the ASHRAE-55 standard, which is a guideline for thermal design in enclosed spaces. This work serves as a base reference for all the processes involving CFD simulations and thermal comfort analysis of a bus cabin. The first part covers everything from the retrieval of the bus geometry up to the post-processing of the output data. The second part consists of studying the minimum requirements for input thermal variables to ensure comfort during winter time in Turin. It concludes with the evaluation of the required amount of heat power needed to accomplish such task and the overall performance of the installed heating system. The outcome of this research is the improvement in heating efficiency of the bus without jeopardizing thermal perception on passengers.

*To my family,
my mother, my father,
and the three siblings
life gave me.*

Acknowledgements

First, I would like to thank Alloviz Engineering Services, company who supported this work. Particularly, I would like to thank engineer Valerio Novaresio, who was my tutor during all this process and gave me all the resources available to learn effectively CFD. In addition, I would like to thank the engineers of Gruppo Torinese Trasporto; Marco Zanini and Pietro Urso, who had all the willingness to answer all questions I had and the readiness to make appointments whenever I needed.

My deepest gratitude to my family, who had always the right word in the difficult moments and never stopped encouraging me to accomplish my goals with passion. To my mother María Isabel, my father Ganesham, and my three siblings Dinesh, Fernanda and Varsha. Without you, this would not be possible.

To my friends in Chile, with whom I shared my university process. Even if the distance makes the contact between us a bit seldom, I always have present the good moments with all of you. To those friends that I met here, which I still have contact with, I thank you for being there in every moment.

To those teachers in Chile who always encouraged and challenged us to be better, I give you a big kudos. All of them, from the ones that taught me in school to my professors in the university. Finally, I would like to thank Pontificia Universidad Catolica de Chile and all the workers of the double degree program who made this possible. To all of you, I thank you.

Contents

1	Introduction	1
2	State of the art	3
2.1	HVAC	3
2.1.1	A Brief Historical Review	3
2.1.2	Objective	4
2.1.3	HVAC scope and limitations	5
2.1.4	Modern HVAC	7
2.2	Ergonomics basics	8
2.2.1	Environmental ergonomics	9
2.3	Thermal comfort	11
2.3.1	Research in thermal comfort	12
2.3.2	Thermal comfort in vehicles	13
2.4	Computational Fluid Dynamics	16
2.4.1	CFD basics	19
2.4.2	The absence of thermal simulations in buses	21
3	Geographical context	25
3.1	Turin, Italy	25
3.2	Climate and temperatures	26
4	Bus case setup	28
4.1	Bus CAD geometry	29
4.2	Bus simplification	33
4.2.1	Computational resources and geometrical implications	33
4.2.2	Simplifications	35
4.3	Heating system definition: test bus and scope of simulation	38
4.3.1	Bus test case overview	40
4.3.2	Meshing of the test bus	43
4.3.3	Test bus simulation setup	51
5	Real bus simulation	72
5.1	Geometry	72
5.2	Mesh	75
5.3	Simulation and post-processing	78
6	Thermal comfort assessment and results	82
6.1	Concepts in thermal comfort	82
6.2	Inputs and thermal calculations	83
6.3	Results	84
6.3.1	First simulation: 296.6 K	86
6.3.2	Second simulation: 303.3 K	89
6.3.3	Optimization of inlet temperature	91
6.3.4	Energy requirements	93
7	Conclusions and recommendations	95
8	Bibliography	99

9 Annexes	102
A1 Technical datasheet of GTT bus.	102
A2 Technical description of heating and air conditioning system.	104
A3 Visual Basic code for PMV calculation	111

List of Figures

1 Personal Environmental Model	6
2 Chair ergonomics	10
3 Air conditioning system examples	10
4 Gagge thermal model	14
5 OpenFOAM simulation of motorbike	16
6 Direct Numerical Simulation of jet flow	18
7 Processing units	19
8 Thermal simulation in a car	24
9 Map of Italy	25
10 Po river course	26
11 Types of urban city buses.	28
12 K9 electric bus in Turin.	29
13 Bus CAD designs	31
14 Selected bus geometry	32
15 Interior view of selected bus	33
16 Original seat geometry.	34
17 Isometric views of the original wheel.	35
18 Isometric views of the simplified wheel.	35
19 Simplified chair model.	36
20 Dashboard flattening.	36
21 Chamfer and hole deletion.	37
22 Totem deletion.	37
23 Simplified bus interior	38
24 HVAC layout of a public transport bus.	41
25 Test bus geometry designed with Autodesk® Inventor	41
26 Test bus mesh	45
27 Extractor and inlets mesh blocks	46
28 Interior mesh of test bus.	47
29 Test mesh cutting plane	48
30 Non orthogonal cells in test mesh	48
31 Test mesh maximum included angle cut	49
32 Glass surface boundary conditions in test mesh	50
33 Inflow-outflow boundaries in test mesh	51
34 Bodywork surfaces of test case	57
35 Bus seat chosen for sampling.	62
36 Velocity probes convergence for test passenger.	63
37 Temperature probes convergence for test passenger.	64
38 Heat loss through bus.	66
39 Heat loss through bodywork.	67
40 Heat loss through glass surfaces.	68
41 Residuals plot for each analyzed variable.	70

42	Final bus base geometry	72
43	Grill inlets of BYD K9® bus.	73
44	Blue inlets are evenly distributed throughout the bus length.	73
45	Oval shaped and rectangular shaped grills.	74
46	Air ducts connected to the rooftop AC unit.	74
47	Upper view of final bus geometry	75
48	General view of final mesh.	76
49	Breakpoints in roof’s left side for refinement in near-inlet walls.	77
50	Mesh cut plane for non orthogonality	78
51	Volume ratio cut plane in near inlet zone.	78
52	Sampling locations for thermal evaluation.	81
53	Curve smoothing example	86
54	<i>Cold</i> simulation heat losses.	87
55	<i>Hot</i> simulation smoothing example	90
56	Heat power consumption vs Recirculated air percentage	94

List of Tables

1	Metabolism levels	12
2	Temperature and influence in driving performance	15
3	CFD research in vehicular cabin summary	23
4	Climate conditions during winter in Turin	27
5	Test bus dimensions	42
6	Cell count of test bus	47
7	Sutherland’s coefficients	53
8	Turbulence boundary conditions implemented in test case	54
9	Thermal layers of bodywork.	57
10	Common velocity-pressure systems in OpenFOAM.	58
11	Pressure and velocity assignment.	58
12	Simulation control.	59
13	Average temperature measuring according to ASHRAE-55	62
14	Velocity and temperature probes summary.	64
15	Test passenger values used for PMV estimation.	65
16	Heat loss through surfaces	69
17	Overall energy balance.	71
18	Metrics of the final mesh.	77
19	PMV sensation scale.	83
20	General table used for thermal assessment.	83
21	Output file structure example	85
22	Overall energy balance.	86
23	Thermal comfort results for <i>cold</i> simulation	88
24	Thermal results of <i>hot</i> simulation.	90
25	Optimized inlet temperature for thermal comfort summary.	92
26	Recirculating air properties summary.	93

1 Introduction

The sensation of comfort is completely subjective. By subjective it must be understood that every single person has a different perception of what is comfortable and what is not, even if their responses to certain stimuli could be the same. Of course, it depends on external conditions: sound level, lighting, temperature, humidity and so on. But it also depends on the personal variables defining that particular individual: its emotional state, previous experiences, health, age or gender.

Engineers have practically no influence under personal variables when designing systems for comfort. On the contrary, over environmental variables they have greater control. Mathematical models have been developed throughout the last six decades to model the ideal conditions that make a human feel satisfied with the surrounding environment. Particular interest has been given to the thermal sensations that a human classifies as hot, warm, cool or cold. Dealing with these subjective variables is a difficult task: it is nearly impossible to ensure pleasant conditions for every user. In the thermal comfort field, statistical models for the representation of comfort have been developed and validated, so that standardized parameters for a satisfactory thermal environment are ensured within certain limits.

In the literature, thermal comfort has been left aside in the buses field. Even if this topic should be a cornerstone in the design of such a vehicle, researchers tended to focus in other types of vehicles. Particularly, Computational Fluid Dynamics has rarely been used as a tool for assessing occupants perception of the thermal environment in buses. This study tries to fill the void that has been in literature by simulating the heating of a bus during winter conditions in Turin, using a steady state solver.

A detailed explanation of how to construct a CFD simulation will be provided here. The four steps of retrieving the geometry, meshing the obtained tridimensional design, set up the CFD solver and post-processing the results are demonstrated for didactic purposes. Indeed these steps are iterative ones, since the all the models and geometries are prone to fail. But errors in the design are not the only reason, iteration in the design are needed to test different situations. Geometrical features, quality of the mesh, boundary conditions or diverging solutions are some of the issues that could lead to repeat part of the design process.

The open source software `OpenFOAM` will be the CFD solver code. Three kind of simulations will be achieved during this work. The first one has as the objective of testing the CFD code in the bus cabin to find suitable parameters that work in the following two simulations, which require longer periods of running. The second, will simulate a low temperature cabin, which is hopefully near the Best Operation Point (BOP). Finally, the third simulation will emulate a higher temperature than the second but also it is

expected to be near the BOP. With the latter two simulations accomplished, the values will be extrapolated so to find the point that minimizes energy while ensuring thermal comfort in steady-state conditions.

2 State of the art

2.1 HVAC

According to the Merriam–Webster dictionary the abbreviation HVAC stands for "Heating, Ventilation and air-conditioning"[1]. The previous definition gives a simple insight about the acronym meaning, not explaining what is its purpose, origins nor its utility in a modern society with customers who want to satisfy their needs regarding the *treatment of air*.

2.1.1 A Brief Historical Review

During the 19th century, almost all people used paper for whatever purpose: writing, drawing, sketching, journal printing, among other uses. The main problem was air humidity, since paper turns to be completely useless in humid conditions. With this problem in mind, in 1902 engineer Willis Carrier developed a basic solution for the humid air, consisting in blowing the humid air into cold coils to control temperature and humidity of the air. The newly created device was called the *Apparatus for Treating Air*, and got its patent on 1906 [3].

This milestone marked the beginning of the standards for the air conditioning systems purpose:

- Control temperature
- Control humidity
- Control air circulation and ventilation
- Cleanse air

Within the following years, new improvements and uses for the air conditioning systems were made. For instance, the air conditioning system developed by William Carrier was brought to the theaters, where people could enjoy movies and relief from the heating of the outside. This exhibited that HVAC was not only meant for technical purposes, such as dehumidifying paper, but can also be used for comforting purposes. Moreover, in 1939, the first air conditioned car is released and, in the 1950's, almost every house in the United States had at least one air conditioner.

Nowadays, HVAC systems are found everywhere in the industry, where thermal comfort is the cornerstone which drives the continuous improvement of climate devices. The main uses of HVAC can be summarized as:

- **Residential:** People normally inhabit and use the interior spaces of the living place to do their own personal activities, which does not involve exhausting or demanding physical labors in general. Thus, requiring the monitoring of the key comfort metrics, in order to sustain healthy life at the interior of residential places. Houses, buildings, hotels and even senior suites are among this category. The latter being critical, considering that elder people who live in an uncomfortable environment could have serious consequences.
- **Non-Residential:** Generally speaking, people do not spend the majority of the time in these installations, but a considerable part of it. Moreover, these installations, even if not used all day long, need a careful analysis of adequate comfort, because the inner environment is not only affected by comfort variables, but could also be affected by health variables, such as an inhospitable environment. Heat, ventilation and humidity can have a major impact in those. Hospitals, offices, industries and educational facilities are in this category. The HVAC system of an hospital or an industry workplace not only must be comfortable, but has to maintain suitable conditions to avoid contamination of rooms, such as bacteria or chemical products suspended in air.
- **Vehicular:** The vehicular use of HVAC is fundamental in a world where almost all the population moves in all kinds of transport, covering longer distances as new transport technologies are developed. Even if the time spent in a vehicle is less than that spent on residential or non-residential buildings, it is of a comparable size. Moreover, according to *ABC's* journal, people spend 9 hours and 35 minutes weekly in their cars in average [4]. On the other hand, comfort at the interior of a vehicle can be a difficult task to achieve due to the potentially extreme conditions that can be found in the external environment, such as extreme temperatures and velocities in the exterior of an aircraft, or the high temperatures due to the heat of the engine or the radiated surface of a black vehicle. Cars, buses, trains, aircrafts and ships are types of vehicles where HVAC is fundamental to ensure comfort of people using it.

2.1.2 Objective

Even with the definition of HVAC stated and several references to *comfort*, the purpose of this branch of engineering might still not be clear. At the beginning, the only purpose of William Carrier was to develop a simple solution to not ruin paper by humidity and created an air conditioning system. Throughout the years this concept has changed dramatically as technology evolved and more standards of comfort have been added.

Air conditioning systems are used in the internal cabin of an aircraft to maintain the

adequate temperature conditions, since the exterior temperature in-flight can be as low as $-50\text{ }^{\circ}\text{C}$, fatal for humans. They can either be installed in buses, to create thermally acceptable conditions for passengers.

A heater could be used to keep a warm temperature at the interior of a house, specially where climate conditions could be extreme. For instance, Finland in winter can have a temperature down to $-30\text{ }^{\circ}\text{C}$ [5], lethal for any human exposed to this temperature levels in a couple of hours.

A ventilation system of a building exchanges the internal humid room air, concentrated with CO_2 and pollutants, for less contaminated and tempered fresh air of the exterior. This process is carried out continuously during the day, since the CO_2 concentration comes from the exhaling air of people.

With the previous examples, the common denominator results evident to understand HVAC: *people's well-being and comfort in relation to the surrounding environment*. And this sentence is highly related to the ergonomics concept, which will be analyzed later on.

Even if the HVAC concept is related to ergonomics, this is not the only usage of the acronym. Moreover, according to the *Fundamentals of HVAC* book, "Often, the objective is to provide a comfortable environment for the human occupants, but there are many other possible objectives: creating a suitable environment for farm animals, regulating a hospital operating room, maintaining cold temperatures for frozen food storage or even maintaining temperature and humidity to preserve wood and fiber works of art." [7]. The previous quote contemplates not only human welfare, but also productive reasons to design reliable HVAC systems.

2.1.3 HVAC scope and limitations

Creating comfortable conditions may sound as an easy task to be achieved. In reality is a difficult multi-variable task, as shown in Figure 1.

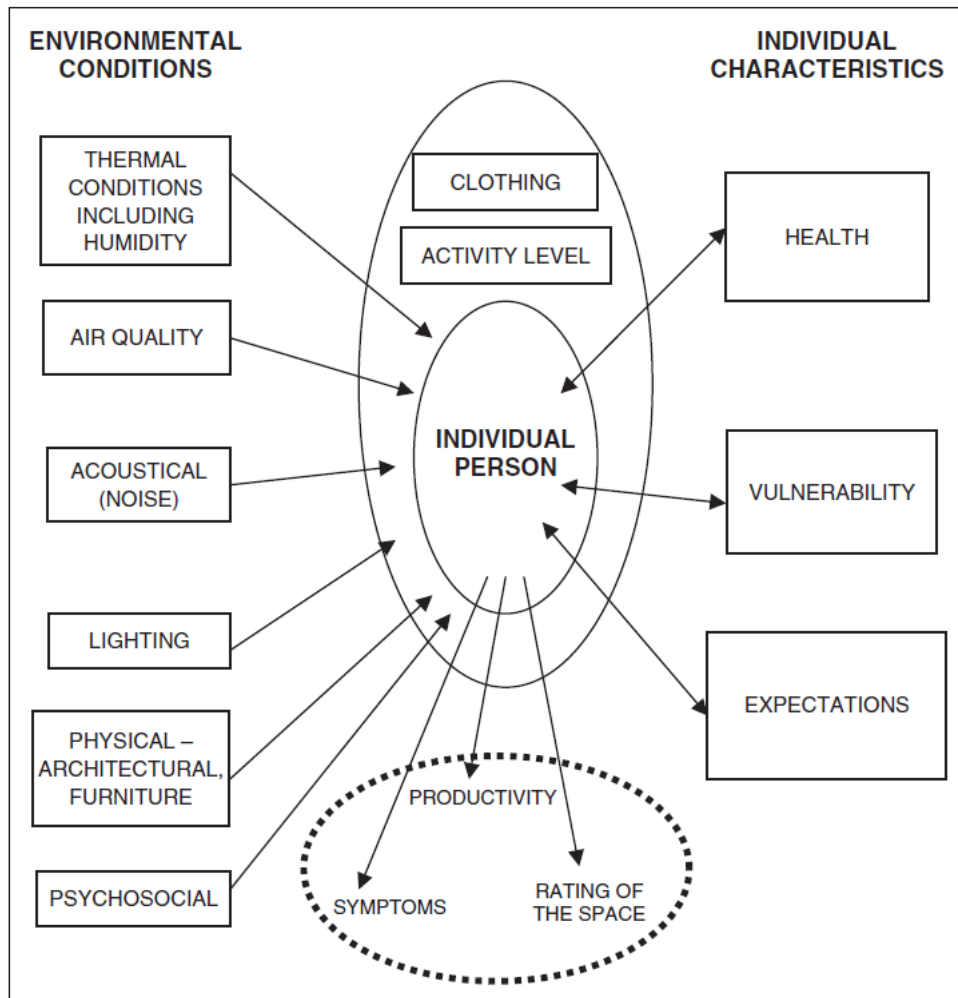


Figure 1: Personal Environmental Model, retrieved from *HVAC Fundamentals* [7]

The Personal Environmental Model shows the variables that affect comfort of the occupants in a closed space. These can be divided in three major groups:

- **Spatial attributes.** Most HVAC systems interact and modify the parameters related to these variables, but can act directly or indirectly.
 - *Thermal conditions:* this is a direct consequence of the HVAC system because, as mentioned in Section 2.1.1, the standards of HVAC were driven in the beginning by controlling thermal and humidity variables. Thermal conditions include more than just air temperature, for instance it also includes air velocity.
 - *Air quality:* another direct consequence of the HVAC system. Air quality is modified through respiration of the occupants and the particle material of the location. The concentration of these levels is controlled by exchanging the interior polluted air by outer fresh air.
 - *Lighting:* lighting in conjunction with HVAC systems affect directly the comfort perception of the environment. Light has a spectrum of radiation, and as

such produces heat in surfaces, leading to a rise of superficial temperature. In a non-thermal perspective, it affects the perception of luminosity of a room. Architects tend to fixate on this issue due to the internal sensation of comfort that light produces.

– *Acoustical environment, physical space and psychosocial situation:* these variables are not directly affected by the design of an HVAC system, but are here mentioned as factors that affect perception of comfort.

• **Characteristics of the individuals.** HVAC systems cannot affect these variables by itself, since these are particular for each person and are part of their nature, but it can take into account them in order to improve comfort. These variables can be summarized as:

– *Health:* People with health issues tend to get uncomfortable with different environmental conditions. For instance, an ambulance must adapt the conditions to maintain stability of the patient being carried to the hospital.

– *Vulnerability.* People do not respond equal under the same conditions, they depend on the physical exposure they are. A post-surgery patient can experience extreme pain if exposed to cool air, whereas a healthy person does not.

– *Expectations:* Even if related to psychological factors, expectations make people have an estimated idea of what to expect in a particular space; there should be an important difference between the expected "quality of air" in a kitchen and the one expected in a fancy hotel lobby room.

• **Clothing and activity of the individual.** The choosing of clothing is a matter of concern and debate, particularly during the summer in warm locations. Sometimes people can choose completely their clothing for work, others must respect formality, which obliges them to wear neckties, long sleeve shirts and pants during this season. According to the website WORKSMART¹ " *In some workplaces, there may also be health and safety reasons which make the compulsory wearing of ties undesirable.*"

2.1.4 Modern HVAC

There are three fundamental points of research under this topic, which have been in development considering new problems arisen in the last decade, associated to new diseases, energy efficiency and contamination. These are:

• *Air quality:* considering the new diseases appeared on the last 10 years, the incidence of asthma and respiratory problems and contagious sicknesses have been a major

¹The text can be found on <https://worksmart.org.uk/work-rights/discipline-and-policies/dress-regulations/can-my-employer-make-me-wear-tie-work>

issue. Air treatment, must be exchanged enough to ensure healthy conditions in enclosed spaces.

- *Greenhouse gases*: this is one of newest topic of research, where a lot of scientific effort is being put on. Thus, being a critical point on the design of HVAC systems. The main reasons are related to the generation of greenhouse gases, generated through the thermodynamical processes involved in the use of fossil fuels or refrigerants used in heat pumps, which damage the ozone layer. These contaminating chemicals have been a matter of concern in norms and codes of air treatment systems.
- *Energy efficiency*: the reduction of energy used has been the most important for research, driven by economical reasons. Professionals all over the world are searching for innovative ways of decreasing energy consumption, in order to develop more efficient and effective *electro-thermo-mechanical* systems without compromising the overall thermal comfort.

2.2 Ergonomics basics

The Cambridge Dictionary defines **ergonomics** as "*The scientific study of people and their working conditions, especially done in order to improve effectiveness*"². The greatest issue of ergonomics is to deal with adverse human conditions of work. And by "adverse" should be understood not only necessarily what makes *difficult* a labour, but also the factors that diminish the efficiency of work.

For instance, the design of a chair is a classical example of this matter of study. At the moment of designing a chair, the basic requirements are related to many factors that modify the final design:

- *Mechanical reliability*: a chair needs to be mechanically capable of resisting the weight and stresses associated to its use. If these minimum requirements are not satisfied, the design is not practical and potentially dangerous causing injuries to whom may use it.
- *Economic viability*: unless the aim of the chair is just a matter of homemade carpentry or hobby, the model must be viable to produce. If the profit of selling the chair cannot compensate its variable costs, is unlikely that the designed chair will be on business until a profitable redesign has been done.
- *Ergonomic design*: it is designed for people and no other use should be given, meaning that the human component decides whether the designed chair is safe for

²Definition available in <https://dictionary.cambridge.org/dictionary/english/ergonomics>

use or not. If the model is not designed for a straight position of the back, adequate height for legs or support for the arms, it could cause damage in the health of the person who uses it constantly.

The latter point is a big matter of concern. The importance of psychological and physical health of workers is on board when it comes to heavy duty jobs, environmentally unhealthy workplaces or long and monotonic hours of work. In the *Injury Research* book, S. Wiker (2012) mentions that ” [...] *poor ergonomic design creates excessive structural or energy demands upon the body, or through degradation of perception, information processing, motor control, psychosocial, and other aspects, produces unsafe behaviors or strategies that result in accidents and injuries*”. Therefore, a *non-ergonomic* design does not only affect the person who makes use of the product, but also the people in the surroundings. For instance, bus passengers can be affected by a driver going at high speeds due to poor *thermal comfort* feeling, caused by low-quality heater.

Even if it could seem that *ergonomics* is a concept just applied at the workplace, it is not. The objective of *ergonomics* is wider, it is the evaluation and the design of the interaction between people and the systems which people interact with during their work and daily life activities[10].

2.2.1 Environmental ergonomics

There is a branch of ergonomics that concerns in much more detail the scope of this thesis, and that is *environmental ergonomics*. It addresses the problems associated to maintain human comfort, activity and health when exposed to stressful environments[8].

Its studies is more specific. In fact, it can be seen with the *chair design* of section 2.2. In that example the ergonomic analysis is related to the *physical* design of the chair i.e. features that can be controlled directly in the design process, such as height, angle of the chair back, arm supports and their correct height or mobility. An example of this is shown in Figure 2:

Environmental ergonomic variables are difficult to control during the process of design. Set up these variables for every working condition that the user wants to apply is an impossible task, and that is one of the reasons why developers and designers create different products for depending on the applications. Furthermore, in the design of environmental ergonomic products, is necessary the use of control systems in order to adapt them to the variable environment.

This results evident when considering the *economic viability* factor mentioned in Section 2.2: a fan has virtually no use if it only gives specific conditions of air ventilation. Those characteristics have no *economic viability*, because for every different use of the customer the manufacturer will need to design the product all over again for the new requirements. The previous example could seem extreme and unrealistic, but in a more



Figure 2: A chair has comfort attributes that can be directly designed, environmental ergonomics does not.

complex system, such as a bus air conditioning system, this is a matter of concern. Figure 3 shows some of the differences between the same model of air conditioner for buses. The different dimensions, heating capacities and cooling capacities gives flexibility to ensure an adequate performance of the air conditioning system: probably a 12 m bus will not use the exact same air conditioning system than a 7 m one. Even though this does not solve the problem of ensuring comfort for everyone, so in general a trade-off optimization problem must be solved.

				
AC 136 TECHNICAL DATA	AC 136 G3 I	AC 136 G3 II	AC 136 G3 III	AC 136 G3 IV
Cooling Capacity (kW/BTU)	24 / 82000	32 / 110000	38 / 120000	44 / 155000
Heating Capacity (kW/BTU)	37 / 130000	42 / 143000	46 / 157000	49 / 167000
Dimensions L x W x H (cm/in)	243 x 201 x 20	243 x 201 x 20	295 x 218 x 20	295 x 218 x 20
	95.7 x 79.1 x 7.9	95.7 x 79.1 x 7.9	116.1 x 85.8 x 7.9	116.1 x 85.8 x 7.9
Weight (kg/lb)	155 / 341.7	160 / 352.7	207 / 456.4	214 / 471.8
Evaporator Air Capacity (m ³ /h/cfm)	4400 / 2590	6600 / 3885	6600 / 3885	8800 / 5180
Total Power Input at 12/24 VDC	-/58 A	-/73 A	-/82 A	-/105 A

Figure 3: Different sizes of the same Eberspächer® air conditioning model.

2.3 Thermal comfort

Thermal environment is one of the major factors which affects human comfort, health and performance[8]. Both sensations of *cold* and *warm* are uncomfortable for everyone. The problem with both these concepts arises when trying to assess unequivocally thermal comfort. It is defined as a state of mind where the person can feel satisfaction with the surrounding thermal environment, and the ASHRAE³ states that is assessed by subjective evaluation [11].

The assessment of thermal comfort is associated to 4 variables that modify thermal equilibrium:

- Temperature
- Moisture
- Air movement
- Radiant Temperature

Human body must have a steady internal temperature of 36.9°C to accomplish its functions properly. There are two different mechanisms that the body uses to control its internal temperature:

- Variations of the metabolism level activity: the body produces heat as a consequence of the underlying biological processes involved in maintaining the correct basic living functions (breathing, cell reproduction, blood pumping, etc), but also because the inherent biological processes have an optimal temperature performance: 36.9 °. When the body is under *stress*⁴ conditions it automatically carries out process that produce heat, this is what variations of metabolism levels stand for. Metabolism rate is changed depending on the activity, health, age and sex of the individual. A young male individual has a higher limit of metabolic rate compared to a 70 year old. The commonly used units of measure for metabolism rate are the *Mets*⁵. Table 1 shows typical levels of metabolism depending on the activity. For instance, a person sitting in a still position has, in average, a metabolic rate of 1 Met.
- Variations of heat rate dissipation: as a response to a rise or drop of temperature, the blood vessels change its diameter in order to rise or diminish the heat transfer through the skin. The blood vessels act *similar* to a heat exchanger with the surrounding environment to regulate the internal temperature. These changes are not automatic, the blood vessels start gradually to dilate. Thus, one of the reasons of

³The American Society of Heating, Refrigerating and Air-Conditioning Engineers

⁴Stress should be understood as any activity different from resting state

⁵1 *Met* = 58.2 W $\frac{m^2}{m^2}$

thermal discomfort is because the blood vessels have to adapt to the actual environment and that process takes time. In fact, during cold weather if a *healthy* person stays in the outside with no tempering clothing, at the beginning the sensation will be of extreme thermal discomfort. After combining both processes of metabolism variation by shivering and diminishing the heat rate dissipation through the vessels, the person can reach higher thermal comfort but, instead, the discomfort feeling will be caused by the involuntary shivering.

Activity	Mets
REST	
Sleeping	0.7
Sitting, still	1.0
Standing up, relaxed	1.2
DRIVING	
Car	1.5
Motorcycle	2.0
Heavy Vehicle	3.2
Aircraft, regular flight	1.4
Combat flight	2.4
OFFICE WORK	
Writing	1.2-1.4
General	1.1-1.3
WALKING ON PLANAR SURFACE	
3.2 km/hr	2.0
4.8 km/hr	2.6
6.4 km/hr	3.8
DOMESTIC WORK	
Cleaning	2.0-3.4
Cooking	1.6-2.0
Washing and ironing	2.0-3.6

Table 1: Metabolism levels for different activities. Adapted from *ASHRAE Handbook* (2005)

2.3.1 Research in thermal comfort

When assessing and researching about thermal comfort, practically every single article or book related to this topic is biased towards building and houses HVAC. This is based on common needs: building and houses thermal comfort should have more importance than vehicles since people spend more time in constructed dwelling. Vehicle comfort has acquired importance in the last decades. Though, the most relevant codes of design, such as the *ASHRAE Handbook* of 2005, deal with indoor thermal comfort in normal living environments and office-type environments.

Pala & Oz (2015) reviewed the thermal comfort advances reached since 1970. As mentioned before, most of the new information retrieved is related to buildings' thermal comfort. Despite of the developments done in buildings, general knowledge of this affair that could be applied in wider areas has been made:

- Clothing: models of clothing resistance and insulation to take into account the heat transfer in analytical models. Also a research in the asymmetry of clothing insulation and quantification of different types of clothing to assess the evaporative resistance of clothing.
- Body heat transfer: thermal models that assess the overall heat transfer coefficient of the body as well as thermal resistances. Also, body mechanisms of heat transfer through division in different particular segments and a deep research in the body core temperature that maintains thermal comfort was made.
- Energy Balance Models: *Fanger's Model* (1970), *Gagge's Model* (1971) and the *Berkeley model* (2010). Fanger's model is a steady state model which considers no heat storage in the body. On the other hand Gagge's model does consider storage in the body core or the skin of the modeled human. Figure 4 shows a the *Gagge et al.* model, based in a cylindrical body core with concentric cylinders of skin and clothing that interact with the surrounding environment. Finally, the most new model is the *Berkeley model* or *Advanced human thermal comfort model*⁶, which was developed for automobiles. This model is highly sophisticated, since considers the non-uniformity of body parts, thus using the body not only as resistances which let heat pass through them, but also taking into account the thermal comfort in different segments of the body, leaving aside the simplicity of *Gagge's* model which considers unidimensional heat transfer.
- Vehicle comfort: studies carried out include driving performance in warm, thermo-neutral and cold environments, passenger's thermal comfort under severe winter conditioning and human thermal comfort in highly transient conditions, are just some of the **general vehicle**⁷ purposes research that have been investigated. Section 2.3.2 will cover in more detail this topic.

2.3.2 Thermal comfort in vehicles

Throughout the research in literature regarding thermal models to assess cabin thermal comfort, several studies were carried out with the existent tools available to analyze human

⁶A basic summary of the research and history of the model available in <https://cbe.berkeley.edu/research/advanced-human-comfort-model/>.

⁷Again, as mentioned before, no bus thermal comfort apart from the research done by *Pala & Oz* in 2015 was found.

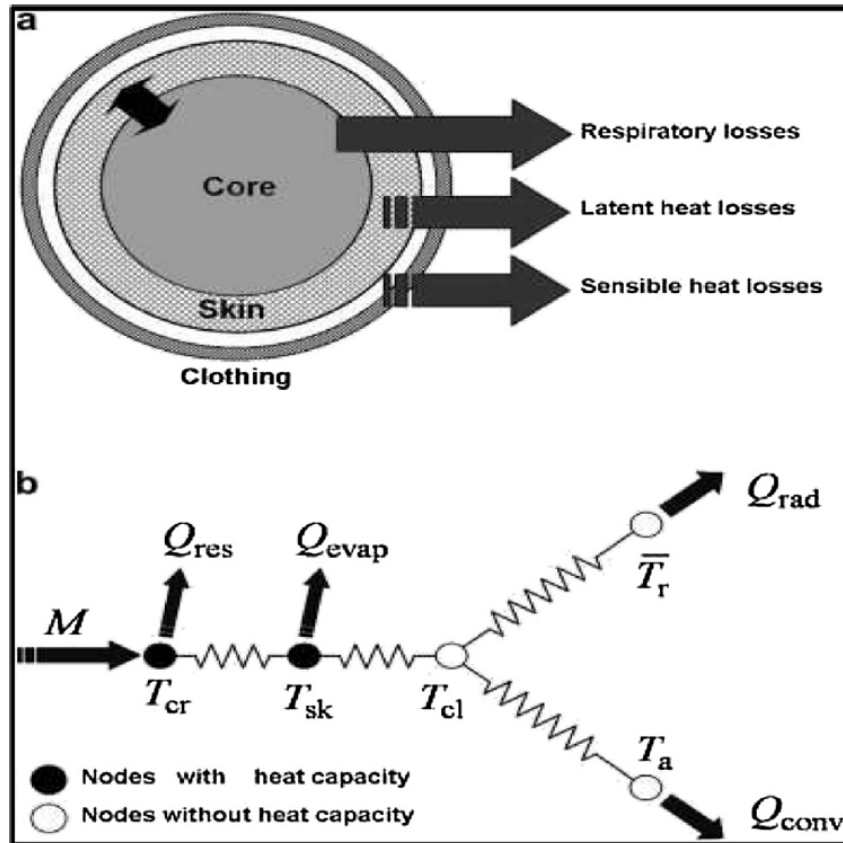


Figure 4: Gagge's thermal model of the human body[12]

body. These tools are mainly analytical, such as correlations and empirical values for clothing and general modeling of heat and mass transfer through resistances and sweat, respectively. Of course, since thermal comfort inside a vehicle is a transient process, the *Advanced human thermal model* must be mentioned because of its new feature models in comparison with the previous ones (Fanger and Gagge), such as segmentation of the body and added complexity of the human structure.

On the other hand, both heating and cooling processes in vehicles have been investigated. In the early 90's *Burch et al.* carried out an experimental study of passenger thermal comfort in an automobile under severe winter conditions[12]. In the same decade, an analysis of thermal comfort inside a car was followed through by *Chakroun and Al-Fahed* to assess thermal comfort in a car parked under the sun during summer in Kuwait.

Furthermore, driving performance in cold and warm environments was an important topic to research. *Daanen et al.* took care of this topic, since at that moment it was proven by previous research that high environmental temperatures deteriorate driving performance, but there was no investigation regarding cold environments. As a result, they discovered that both selected extreme ambient temperatures have a profound impact on human skin temperature. Moreover, during high temperature tests (35 °C) the driving performance dropped 13% in relation to the thermoneutral conditions (20 °C). On the

other hand, cold environment had a decrease in 16% of driving performance, probably due to shivering and fine dexterity loss according to the authors[14]. Table 2 shows the main results obtained from this study, which led to the conclusion that driving performance is indeed affected by thermal variables.

Variable	Cold (5 °C)		Neutral (20 °C)		Warm (35°C)		
	Mean	s.d.	Mean	s.d.	Mean	s.d.	Sign.
Leg Temperature(°C)	18.5	3.8	28.1	1.3	36.6	0.7	*
Head Temperature (°C)	24.9	1.2	28.4	1.9	30.8	3	*
SDLP (cm)	118	32	102	29	115	31	*

Table 2: Results of Daanen et al., adapted from *Driving performance in cold, warm, and thermoneutral environments*, (2002)⁸

Related tests to measure thermal discomfort and diseases such as hypertension were accomplished at Belo Horizonte, Brazil. The test results were clear to correlate the hypertension and thermal discomfort in warm climates for drivers who classified as "disturbs a lot" or "unbearable" the thermal sensation. [15].

As it can be seen, almost no work has been implemented in the ambit of bus comfort. The previous research of bus thermal comfort is mainly related to the consequences of a *bad thermal comfort*, rather than modelling the actual thermal conditions in a bus. In fact, the following authors are the only ones found in the literature who treated this topic:

- **Pala** and **Oz** in 2015: both developed a general mathematical model with an experimental procedure for the use of automotive HVAC engineers on thermal comfort. This work was particularly scoped to buses.
- **Velt** and **Daanen** in 2017: a work related to energy efficiency in electric buses, where the main concern is to maximize driving autonomy while maintaining comfort functions. Their work was indeed useful to assess the need of lower inner bus temperature from 22.5°C to 20.9°C, considering that the overall opinion of the passengers was that the bus was "slightly warm", thus 20.9°C is the aimed temperature for a neutral thermal sensation and improvement in efficiency of an electric bus.
- **Scurtu** and **Jurco** in 2019: their article consisted mainly in a *Computational Fluid Dynamics*(CFD) simulation of a bus using an existing CAD geometry. The main achievements of this simulations were related to optimization of internal bus features by using air deflectors to improve thermal comfort. They also concluded that CFD simulation offers the optimal solution in fluid volume flows[16].

⁸SDLP stands for standard deviation of the lateral position, whereas the asterisk under the Sign. column indicates that there are significant differences between tests.

2.4 Computational Fluid Dynamics

In Sections 2.1 and 2.2, various topics that will be treated in this thesis were explained. When talking about **HVAC** the main objective was to introduce heating and ventilation systems, which of course are easily related to ergonomics, in particular to **thermal comfort**. At the ending of both these subsections, general and particular research scope was done and an easy relationship could be established between both of them. The difficulty of relating these topics to Computational Fluid Dynamics⁹ will be discussed here. Furthermore, it will be argued the reasons why CFD has not been taken into account in modeling buses thermal behaviour.

Generally speaking, when talking about CFD, most people who are not familiarized with the subject tend to think in high velocity airflow systems. It is easily noticeable when looking at cover pages of CFD books: almost all of them have typical coloured streamlines around supercars, aircrafts, turbine blades, helicopters or drones. This is mostly a *neuromarketing*¹⁰ process rather than a representation of the real attainments of CFD.

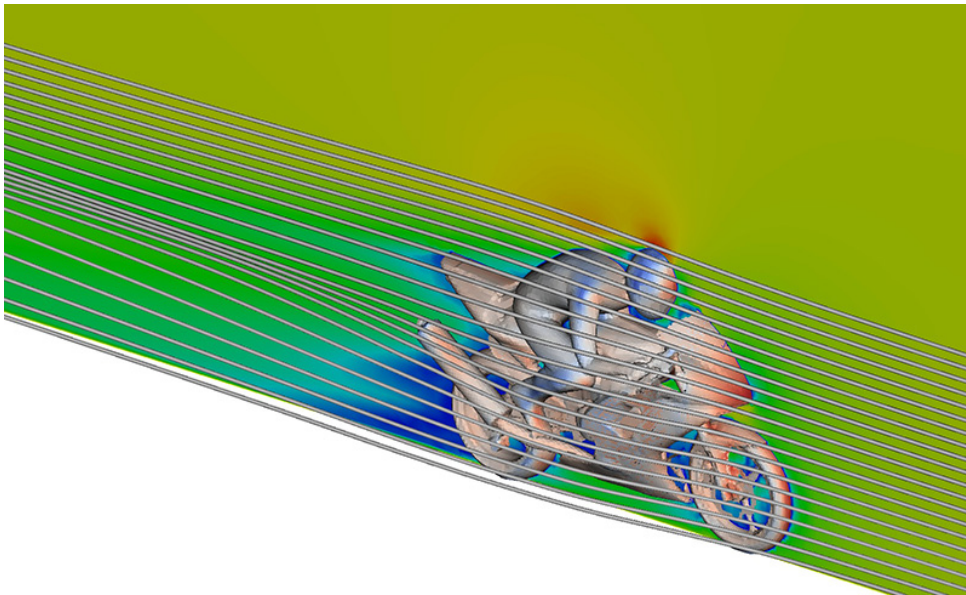


Figure 5: Colorized OpenFOAM simulation of motorbike external airflow.

As stated before, CFD is largely scoped for high velocity airflow, such as one of the base tutorial simulations of `OpenFOAM` which is shown in Figure 5. Nevertheless, the aim of CFD is wider than external flow with high *Mach* or *Reynolds* numbers. Just to enumerate some of them:

⁹From now on, the acronym CFD will be used for brevity

¹⁰People get more attracted to a certain attribute depending on what does stimulate on them. Sensation of velocity, for example.

- Flow through pipes
- Liquid metal injection modelling
- Near-coast sea waves
- Chemical reactions
- Hydraulic design of dams
- Conjugate heat transfer
- Refrigeration cycles
- Multiphase flows
- HVAC

The list could continue indefinitely because the limits depend on the necessity of the user. The most common fluids in industry are air and water. Even though, CFD has an extremely wide range of applications which involve complex systems as liquid metal flow, non-newtonian fluids or mixed-fluid flow.

Even if CFD is a sophisticated tool, it has lagged behind other CAE¹¹ tools, such as stress analysis codes. The main reason is the complexity of modeling fluids, due to the underlying chaotic behaviour. But the problem is not how to model the behaviour by itself, in fact, there are works and research that model the most tricky and entangled feature of CFD: *turbulence*. The actual difficulty is the time and computational resources needed to obtain "perfect details" of the flow. The process of simulating real *turbulence* is time consuming; **Kolmogorov scales** require unpractical computation resources to be used in practice. However, with new *turbulence models*, industrial CFD has become an actual possibility and a cheaper way to stress fluid flow expected outcome without using a physical test.

¹¹Computer Aided Engineering

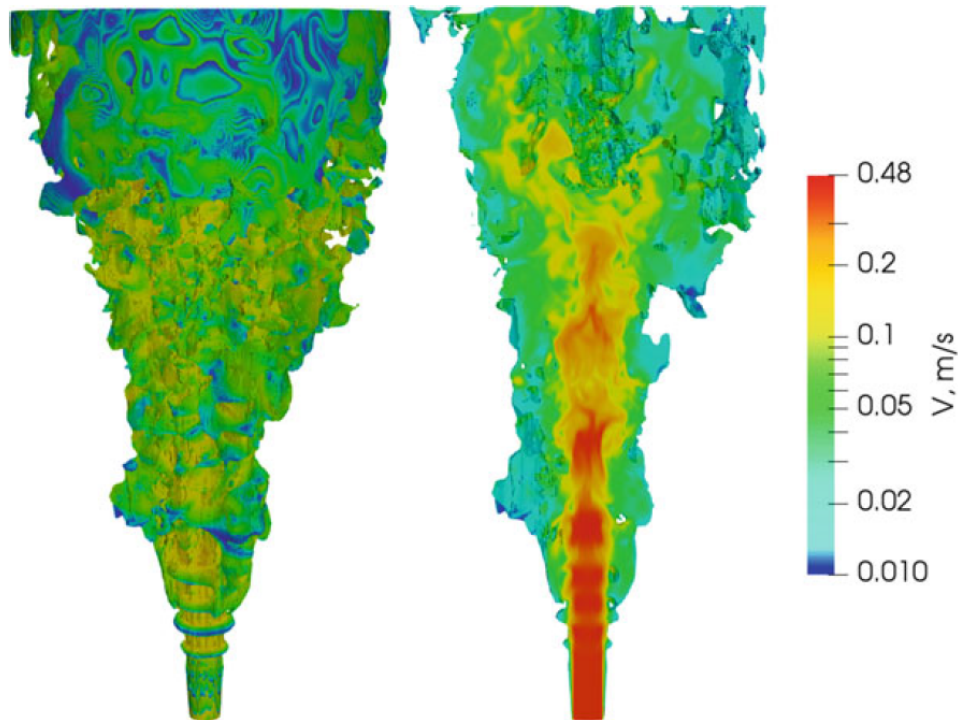


Figure 6: DNS of jet flow against gravity. On the left 3D jet, on the right cross section. Retrieved from Rodriguez, S. (2017). *Applied Computational Fluid Dynamics and Turbulence Modeling* (No. SAND2017-13577B). Sandia National Lab.(SNL-NM), Albuquerque, NM (United States).

The investment in CFD could be high, indeed. The minimum cost of hardware in 2007 was between £5,000 and £10,000. Perpetual licenses in the same year were around ranges of £10,000 to £50,000 [20]. Figure 7 shows different server's features that could lead to different prices according to each server capability of storage, processing and multiprocessing. These pricing values have changed since 2007 with adjustments of CPI¹² and new technology enhancements that allow more computing in smaller processing units.

There are different solutions also for CFD softwares. Evidently, the comparison will depend mostly on the user needs, objectives, budget, deadlines, to name some. Differences that could be found are that a particular software is pressure based rather density based, pricing of the license, additional features, type of GUI¹³ (if existent), operative system compatibility, post-processing additions and so on. CFD solvers are (just to name some): Simcenter Star-CCM+, ANSYS Fluent and CFX, COMSOL Multiphysics, OpenFOAM, Gridgen, PHOENICS, TACOMA.

There is no doubt that simulations can be costly, both in time and money, but the payoff of doing such an investment can be quite rewarding compared to do solely experiments. There are advantages that are inherent of doing CFD, instead of a scaled experiment, that can largely support the inversion in CFD equipment in short and long

¹²The so called *Consumer Price Index* in economy

¹³Graphical User Interface



(a) Dell server with 3.3 GHz, 8 GB of RAM and 4 cores.



(b) Lenovo server with 2.1 GHz, 8 GB of RAM and 8 cores.



(c) Fujitsu server with 3.5 GHz, 16 GB of RAM and 4 cores.



(d) HP server with 1.7 GHz, 16 GB of RAM and 8 cores.

Figure 7: Different server type solutions

term time frames [20]:

- Lead time reduction and costs of new designs for each experiment.
- Capability of studying quite difficult systems, that experimentally could be impossible to perform.
- Ability of studying systems under extreme or hazardous conditions without damaging a real experiment implement (e.g. a manikin exposed to high temperatures).
- Theoretical unlimited level of detail of results, limited only by computing capability available.

2.4.1 CFD basics

The main idea is not to overextend into the details of CFD processes, there is vast literature for that. The intention is to explain the main processes that lead to make a simulation from beginning to end. In this work, these steps will be indeed performed exhaustively in the following Sections. Yet, this section is a brief insight for general and historical purposes in CFD development.

The process of CFD *coding* has three main parts, according to Versteeg and Malalasekera (2007):

- **Pre-processing.** The first part of generating a CFD code related to a particular problem is to create a CAD¹⁴ of the fluid domain i.e. the region where the fluid to model will flow.

After the creation of the 2D or 3D fluid domain, the next step is to create a grid with the fluid domain already designed. The set of all control volumes created by this subdivision is commonly named **mesh**, where the **cells** are the small control volumes created from the mesh. This process is the most time consuming in a CFD project[20].

When the so-called *meshing* process is over, the definition of the system must be implemented into the software, either the meshing software or the solver itself (or partially both), being the fluid properties, thermo-physical models and boundary conditions the ones to define prior to the next step. This will be clear in the next sections.

- **Solver.** One of the major steps in the solving process is translating all the information gathered previously and inserting it into the software in the "solver's language". Strictly speaking, there is no need to understand every single mathematical feature that is beneath the solver's code. For relatively simple simulations is enough to know some rough classifications of the methods and schemes, such as *diffusive, time consuming, accurate, unstable, spurious oscillating* and so on. But at the same time, the knowledge of what the solver is actually doing can save much more time while *debugging* or doing a *crash* analysis.

Nevertheless, the basic equations solved by commercial codes are the **Navier-Stokes** equations in its different forms. The intricate description of how to solve these equations is out of the scope of this text. A basic description will be provided, but of course it summarizes lots of research done about this topic throughout history. The Finite Volume Method is a conservative way of discretizing the Navier-Stokes equations. The cells mentioned in "pre-processing", are the hierarchical minimal structures where the conservation equations are solved. When discretized and interpolated, are transformed into algebraic equations. Computing processing units do not deal with *calculus-like* syntax, but instead can read matrices and solve linear systems of equations, either by direct methods or iterative ones. The latter ones are preferred in large-sparse matrices. Prior to run the simulation, the solving attributes must be chosen: matrix solvers, interpolation schemes, gradient schemes, number of

¹⁴Computer Aided Design

inner-loops, time step and general control parameters for the solver. After all this setup is ready, the simulation can start.

- **Post-processing.** The final step is to convert raw data output of the solver into a graphic and user-friendly visual output. It could seem an unnecessary task to post-process the solver's output, but is a powerful tool considering that in an engineering project there are two types of people who will need to visualize the information:
 - Simulation Engineer(s): the output files of the solvers are floating numbers hard to interpret. This output can be revised in a plain text file, but this is an unpractical and time consuming process. If the simulation engineer needs not one single value of the data, but thousands output values of the simulation, the logical choosing is to plot the results. Even more, graphic-colored data is useful to determine critical points and to detect visually a *GIGO*¹⁵ simulation.
 - Non-simulation Engineer(s): engineering projects involve more disciplines, and graphical output is an extremely powerful tool to communicate ideas to a person who has no knowledge in the area. Vector plotting, particle tracking, streamlines can be useful for someone who does not understand the raw data output.

With this summary of CFD process, is possible to get an insight to the final subsection of this chapter: internal environment modelling of a vehicle. Different CFD objectives were mentioned at the beginning of Section 2.4. The matter that concerns this study is the heating of a bus. The next section is an outline of what has been found in literature regarding bus heating simulations with CFD.

2.4.2 The absence of thermal simulations in buses

Heating analysis in vehicles is of major importance, particularly in cold weather zones. Analysis of the thermal comfort of car cabins, buses, aircraft, trains and so on have wide importance. Nonetheless, CFD HVAC analysis of vehicles, without being a new tool in the industry, is not widely spread over all types of vehicles. Significant importance has been given to mainstream car simulations. Not only in HVAC systems, but also in external aerodynamics, combustion chamber or battery cooling. The number of papers about these topics, where automobiles are analyzed, is not comparable to any other vehicle. This is not a coincidence, the classic rule of "start with easy, end with difficult" also applies here: simulating a bus, which is almost 3 times larger, is a difficult task to achieve with accuracy. Mainly because the simulation engineer has to deal with a *trade-off* of choosing a precise and realistic solution considering the time that it could consume with the computational resources available.

¹⁵Garbage In Garbage Out

Even though, turns out to be quite surprising the fact that, during this research, only two CFD model references of HVAC were found for bus simulation. After all, buses are not a new fancy engineering machine and neither are CFD models. Probably, is related to the complexity of such a vehicle. It requires a considerable amount of cells in the mesh to obtain accurate results. Furthermore, the cost is highly increased when simulating it with humans and their body thermal characteristics.

Walgama, Fackrell, Karimi, Fartaj and Rankin (2006) gave a first approach of general thermal comfort in several cabin comfort types, including different models. In their review, they mention that CFD simulations from the 1990s started to be adequate for reasonably time frames and made a research of the cabin simulations achieved at that moment, where they evaluated:

- Vehicle used
- Solver
- Buoyancy effects
- Radiation accounting
- Thermal process (cool down, warm up, steady, transient)
- Mesh size
- Boundary conditions applied
- Comfort evaluation method

Is worth noticing the advances accomplished in that period. Initial meshes of 50,000 cells in 1989 evolved to 2 million hexahedral cells and afterwards the possibility of using tetrahedral meshes appeared. In general, the early simulations included transient calculation, rather than steady-state processes. At the same time, buoyancy is not included in the majority of the solvers which use steady-state simulation, the reason will be clear in next sections.

Despite of Table 3, Murakami et al. made a basic cabin simulation with a virtual thermal manikin, treating its surface boundary in 2 different ways: constant heat transfer and constant surface temperature. Another study was made using *Stolwijk's thermal model* in order to represent mathematically the boundary conditions of humans in a car cabin. According to Walgama et al. the results of combining thermophysiological models and CFD provide good results. It is also remarkable noticing the difficulty of creating a thermal manikin (virtual or physical) that could actually model thermoregulatory processes and evaluate not only the body thermal comfort as whole, but rather the local comfort of each body part.

Reference	Process	Boundary conditions	Mesh
Han 1989	Cool-down implicit, $\Delta t = 1 s$, 5 min	Air velocity and temperature at AC outlets. Isothermal walls	$39 \times 29 \times 45$
Currie 1997	Winter, steady	Ambient temperature	2 million hexahedral cells
Aroussi and Aghil 2000	Steady	Uniform velocity profile at the manifold inlet area, with turbulence intensity and hydraulic diameter	260000 tetrahedral cells

Table 3: Extract of numerical simulation summary for passenger thermal comfort. Adapted from Walgama, C., Fackrell, S., Karimi, M., Fartaj, A., & Rankin, G. (2006). Passenger Thermal Comfort in Vehicles - A Review. *Proceedings of the Institution of Mechanical Engineers, Part D: Journal of Automobile Engineering*, 220(5), 543-562.

On the other hand, the paper written by *Danca et al.* (2017), developed a thermal CFD simulation for the cockpit of a commercial city car. They evaluated thermal comfort based on the PMV¹⁶ and PPD¹⁷ metrics in local areas of the body. Using both CFD results and experimental measures, they concluded that CFD and experimental values have good agreement in air velocity, temperature and thermal indexes evaluated according to ISO7730. Nevertheless, they also claim that PMV and PPD are poor indexes to evaluate comfort at the interior of a vehicle. This due to the high velocities while conditioning such environment, unlike ISO14505 which describes comfort conditions at lower air velocities at the internal of an enclosed space[18].

¹⁶Predicted Mean Value

¹⁷Predicted Percentage Dissatisfied

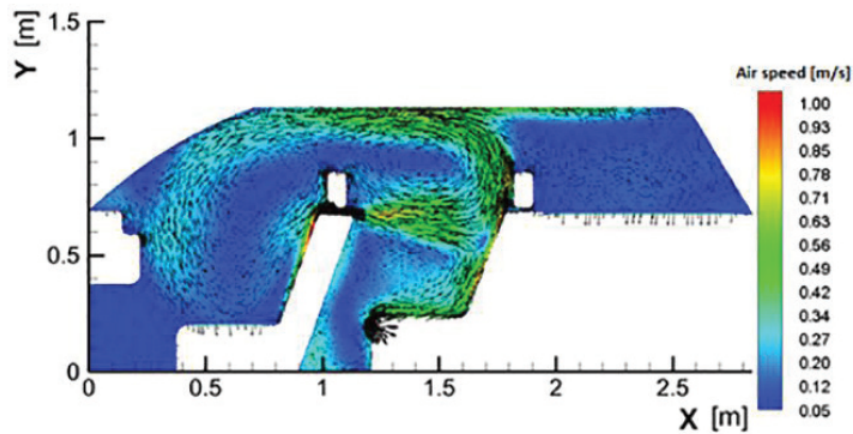


Figure 8: Velocity magnitude obtained by *Danca et al.* in the co-pilot plane of the car. Retrieved from Danca, P., Bode, F., Nastase, I., & Meslem, A. (2017). On the Possibility of CFD Modeling of the Indoor Environment in a Vehicle. *Energy Procedia*, 112, 656-663.

Special mention must be given to the work carried out by Scurtu & Jurco (2019). It is mentioned in this section again because it has a close relationship with the objectives of this research. The most remarkable fact of this work is the combination of several disciplines in an attempt to assess thermal comfort in a bus. The fact that the authors have taken into account various thermophysiological variables as inputs to model the thermal environment of a bus, is a remarkable milestone. The combination of computational fluid dynamics with psychrometrics and thermal indexes for the particular case of a bus has been seen few times in literature. The same authors mention just 2 sources where they could retrieve bus CFD thermal analysis. Those mentions are quite recent (2014 and 2018).

To summarize, in the previous sections a review of the current works and development in HVAC, thermal comfort and CFD was provided, to introduce the topic to be treated in the subsequent sections. The absence of bus thermal comfort evaluation throughout the literature is surprising, having in mind the vast literature with regards to numerical modelling of other vehicles. The next sections aim to fulfill part of this void by joining both CFD and thermal comfort applied to a bus.

3 Geographical context

Considering that the simulation will be performed based on Turin's climate, a brief review of Italy's geographical context is provided. A deeper insight will be given about the particular weather variables that dominate Turin's meteorology.

3.1 Turin, Italy

Italy is an European country located in Southern Europe between latitudes 35° and 47°N, and longitudes 6° and 19°E. Most of the Italian limits consist of sea, since in the North limits only with four countries: France, Switzerland, Austria and Slovenia. Also, it is partially delimited by the Alpine watershed.



Figure 9: Map of Italy and its border countries.

Most of Italy's limiting areas are sea, being the Tyrrhenian, Mediterranean and Adriatic seas the ones which most cover Italian water territory. Nevertheless, the northern part is mainly composed of mountainous landscapes.

Turin is in the northwest part of Italy, making part of the Piedmont Region. It is surrounded by the Alps in the northern and western front. On the eastern part has high hills which are the natural continuation of Monferrato's hills.

The Po river crosses all northern regions of Italy: Piedmont, Lombardy, Emilia-Romagna and Veneto. The Po river is born in the Cuneo region, near the French-Italian borders. It enters the Turin province passing through Carignano, La Loggia and the city of Moncalieri, where it receives four different streams of water. Comes across Turin starting from the south, with a channel 200 m wide and a mean flow of $100 \text{ m}^3/\text{s}$. As a natural source of water, it regulates the air temperature by capturing heat and transporting its thermal energy through water.

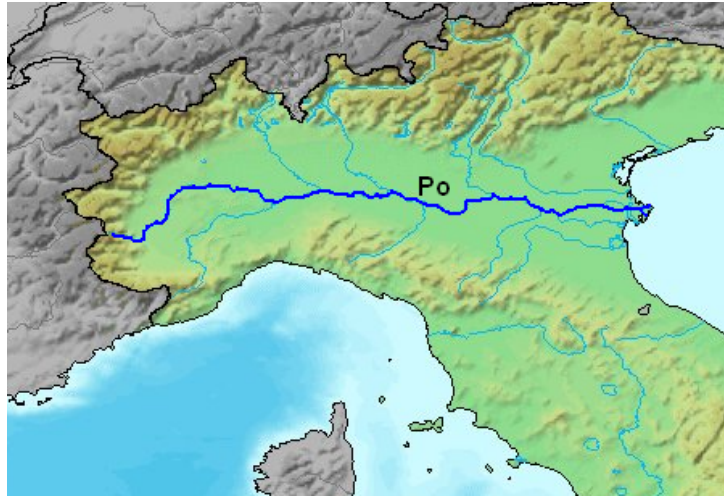


Figure 10: The Po river crosses completely the north of Italy, with several confluent flows in its path.

3.2 Climate and temperatures

According to the Köppen–Geigen classification, Turin's climate is pointed as "humid subtropical climate" (Cfa), as most of the northern part of Italy [19]. Generally speaking, winter seasons are mostly cold and dry. On the contrary, summers are usually hot in plain terrain, produced by accumulation of heat due to the mountains and hills covering the fronts of Turin.

With regards to the weather in Turin, the average annual temperature is 11.6°C . In the warmest months the average high temperatures are 24.7°C , 27.6°C and 26.5°C for June, July and August, respectively. Contrarily, the average lowest temperatures in cold months are -2.3°C , -3.3°C and -1.1°C for December, January and February, respectively.

The CFD code will consider only winter months, to test extreme conditions of cold. Therefore, the thermal variables relevant for the simulation are those retrieved from December, January and February. In particular, the data to be collected is the Average Low Temperatures and Average Relative Humidity on those months. Table 4 shows the mentioned variables average in the last 30 years which are on record. Also, shows wind speed and daily solar radiation, which are variables that affect thermal comfort.

	DEC	JAN	FEB
Average low temperature (°C)	-2.3	-3.3	-1.1
Average relative humidity (%)	80	75	75
Average wind speed (km/h)	16	14	6
Average daily solar radiation (MJ/m^2)	4.6	5.7	9.1

Table 4: Average values for winter months in Turin.

Even if the average wind speed could be useful to compute the mass flow rate at the outlet of the heat pump of the HVAC system, it will not be used. The energy delivered to the fluid by the heat exchanger is mostly transformed into enthalpic energy and changes in kinetic energy are negligible. This will be explained with more detail in case setup related sections. Plus, daily radiation will not be considered in this case, due to the difficulty to assess this parameter in a radiation model CFD code.

4 Bus case setup

Buses have not only a variety of sizes and shapes, but also different layouts related to their purpose. For instance, they can be designed as tourism buses with seats in the rooftops. They also might be coaches for passenger transport among cities, having two floors or just one. In addition, some can be used for urban transport along the metropolitan zone of the city or the suburban part.

In-city buses have variable length. Its main objective is to optimize the number of passengers to be transported within their lifespan. A reduced length of it implies the acquisition of additional buses to comply with the demand of transport in the course of the bus. On the contrary, a large bus which spends most of its trip path empty is a needless investment. When the expected number of persons that will travel in the bus is unknown, the risk is to buy an oversized bus.

CLASIFICACIÓN DE BUSES DE TRANSPORTE DE PASAJEROS EN METROS DE LONGITUD Y CANTIDAD DE PASAJEROS	
Microbús 6 m a 7 m 10 a 19 pasajeros	
Buseta 7 m a 10 m 20 a 30 pasajeros	
Busetón 10 m a 11 m 20 a 30 pasajeros	
Autobús 11 m a 15 m 30 pasajeros en adelante	
Articulado 17 m a 19 m Alta cantidad de pasajeros	

Figure 11: Types of urban city buses.

Figure 11 summarizes most type of buses used in urban zones. These vary in their length and passenger capacity. Depending on the design, the layout of the seats can vary a lot: seats in floor height, over the axles of the bus wheels, inverted seats or lateral-view seats. However, these also vary in number of windows and the possibility to open them. The same occurs with bus doors, where some of them just have one unique entrance and exit or many doors.

Most of the urban buses are represented in Figure 11 which are 7-10 m, 10-11 m and 17-19 m long. Microbuses of 6-7 m tend to be used in suburban zones rather than urban. Similarly, autobuses are generally long-distance bus types, meaning that their main use is related to intercity applications. Autobuses are sometimes used to transport private groups, such as people from the same company or university. The previous classification does not consider 12 m or even more bus types for urban use, suitable for medium-large cities with high number of inhabitants.

The first step is to define a base model for the simulation, because all the dependent features of the CFD code rely on this.



Figure 12: K9 electric bus in Turin.

As a model for the next sections, the K9 BYD® bus of the electric bus fleet of Gruppo Torinese Trasporto (GTT) will be chosen, since they provided access to this bus model in their bus depot. In Figure 12 is depicted a photo of the bus where the external main features can be seen. The base characteristics that must be beared in mind are the three door layout; two of them are exits and one is an entrance, and the size of the bus, which is 12 m long¹⁸.

4.1 Bus CAD geometry

In order to accomplish the simulation, there are two main options to obtain the geometry where flow of air parameters will be computed:

¹⁸Information available on https://www.just-auto.com/news/turin-takes-first-byd-electric-buses_id178758.aspx

- The first one is to model completely the bus interior through an appropriate CAD software. This option is complex to achieve, since the features of the bus must be measured from a real bus on-the-site and with particular tools. Besides, it would require to know *a priori* which are the features to be measured and draw a sketch to be designed in the CAD software. This choice is not viable. In fact, the modeling of a vehicle is a complex task which is normally fulfilled by specialized mechanical designers.
- The second one is to use a **pre-model of the CAD**, searching for similar features that produce similar results with regards to the original K9 bus model. These features to be looked for are the number of doors, dimensions, number of seats, position of seats and so on. This alternative has the issue of finding a suitable bus in free-for-use CAD webpages. However, there is no doubt is a more manageable choice, recalling that some paper authors have done it (Scurtu and Jurco in 2019).

Obviously, is virtually impossible to find a bus which is *exactly equal* to the one depicted in Figure 12. Most of the existent designs are of public use and, as such, they rarely represent all the features of a brand bus, whose design is copyright protected. As aforementioned, there is a trade-off when choosing the correct model. The main scope is to maintain the principal aspects of the bus, in order to have a representative simulation, but also consider the computational limits. In some CAD designs just the external design is depicted, rather than the complete interior design, which is the usable space for the meshing process.

Buses shown in Figure 13 are some of the models that were evaluated to determine whether they are viable and representative for the case study or not. Each model had advantages and disadvantages for the next processes:

- Figure 13a bus is really accurate in the general design, since it has three doors, comparable number of seats and similar length with the K9 bus type. However, the entrance and exit stairs, the highly agglomerated seats and the elevated seats located on top of the wheel axes do not exist.
- Figure 13b bus is evident that such a design is not suitable, since there is no interior volume for the meshing process.
- Figure 13c bus has excellent attributes for a two door bus. It has a classical interior design of a city urban bus of 10–11 m. Nonetheless, the CAD model shown has less doors so it does not represent the actual heat flux through the boundaries of the bus.
- Figure 13d displays a 12 m intercity bus. Since the modelled bus is an urban one, this design is not applicable.



(a) Three door bus with entrance step.



(b) Toy-based bus. No interior design for seats.



(c) Two door bus design with high rear seats.



(d) Intercity 12 meter autobus. No interior design.

Figure 13: Examples of possible bus CAD designs.

The previous description depicts the general process of evaluation the use of certain designs. The selected bus is not expected to be an exact replica of the K9, but must comply with characteristics that modify as less as possible the simulation outcome. Naturally, more bus types were to be evaluated by means of the same judgements. The main web-pages to this purpose were: *Free3D*¹⁹, *GrabCAD*²⁰, *CADblocksfree*²¹ and *Autodesk Online Gallery*²². At the end, a bus which complies with most of the internal bus characteristics was chosen from *GrabCAD*. This bus agrees with most of the required features in its interior and in the boundary, being the most important seat distribution, number of doors and length of the bus. This is shown in Figures 14 and 15, where the outer and inner designs are shown.

¹⁹<https://free3d.com/3d-models/>

²⁰<https://grabcad.com/library>

²¹<https://www.cadblocksfree.com/en/3d-cad-models.html>

²²<https://gallery.autodesk.com/projects/>

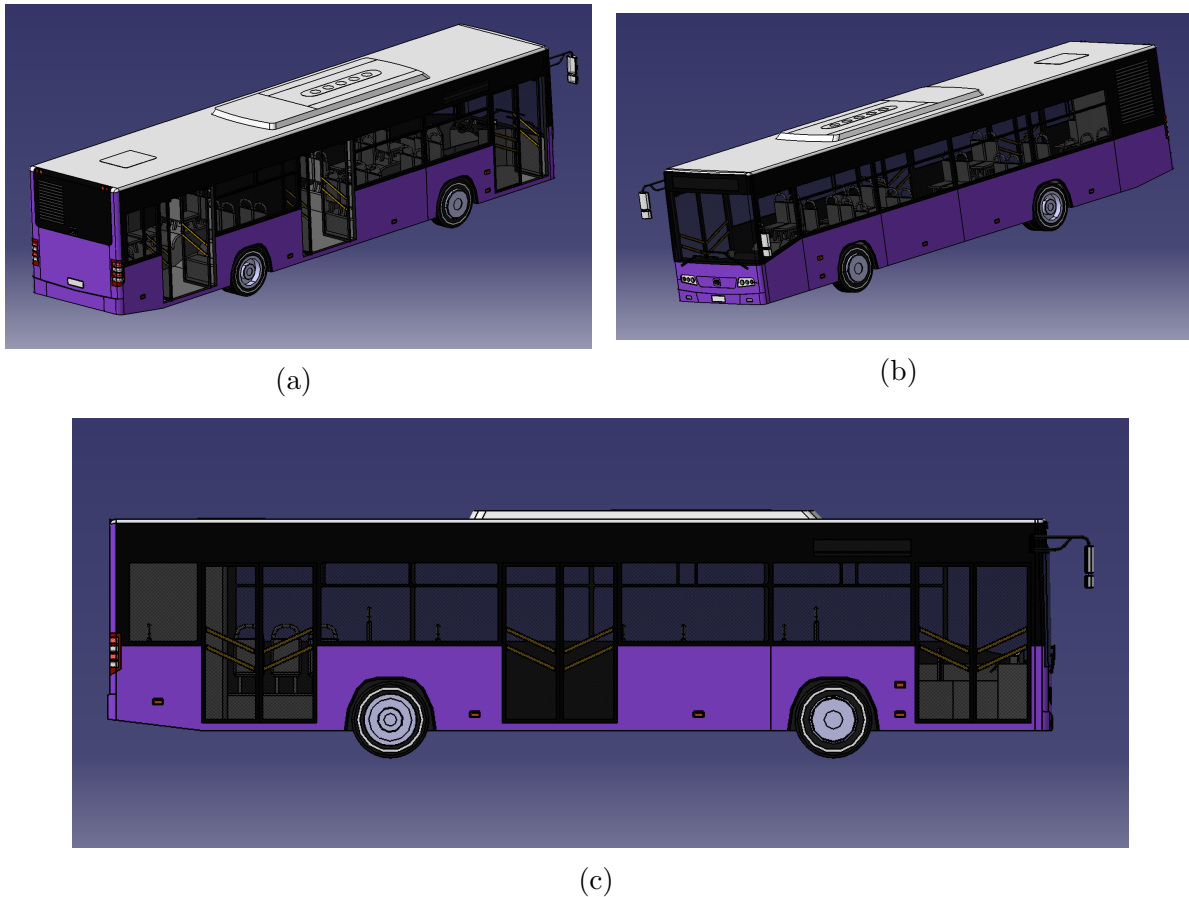


Figure 14: Different external views of the selected bus

Figure 15 shows an isometric view of the interior of the bus with its main features. The original bus of Figure 14 has been disassembled to illustrate the interior. External body, wheels, doors and windows are not needed for the consequent processes (at least not by themselves). From this iso-view, many advantages can be identified related to the K9 bus design.

- The seats position is mainly the same. Indubitably, there are different number of seats, the seat distribution is not equal, but the rear seats layout and the elevated seats are similar.
- The geometry is easily modifiable. This is a CAD assembly and unneeded parts can be deleted.
- There are no handrails or hand holders. At first sight this could be a disadvantage because it left aside a real component. Contrarily, it makes easier the meshing process because these type of geometries need *small cells* to be correctly defined. In the Bus simplification Section this will be argued in more detail.

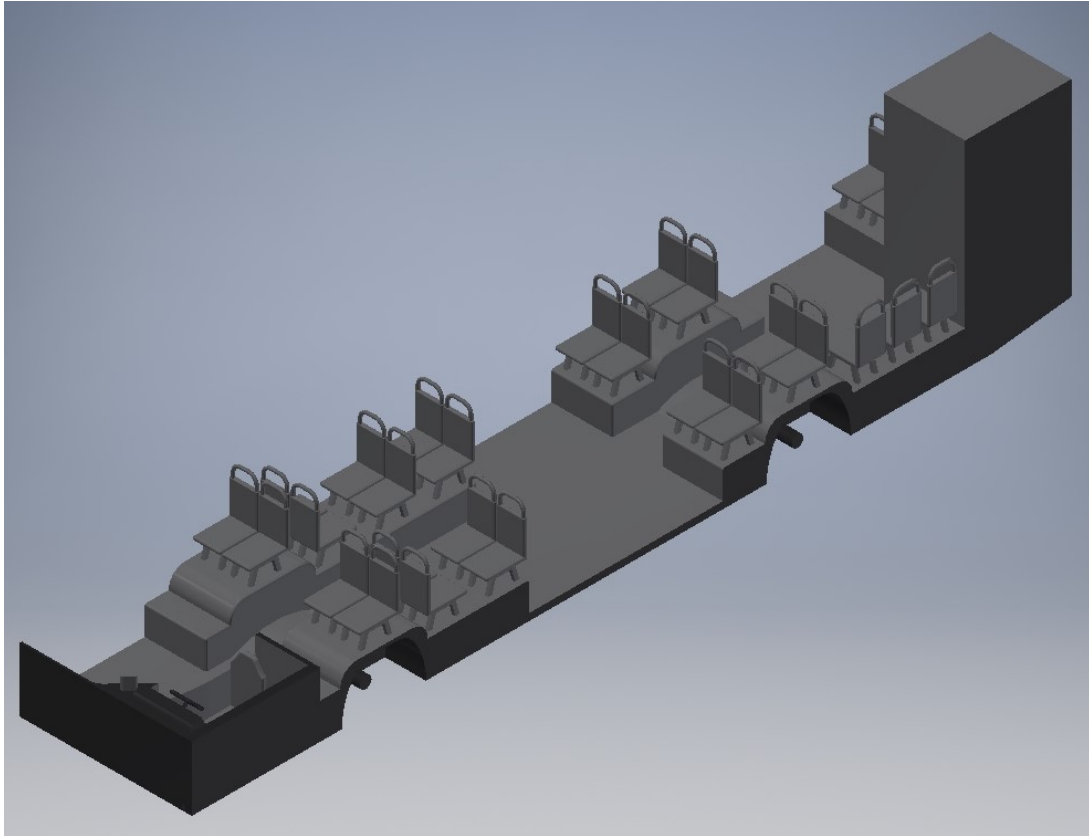


Figure 15: First interior isometric view.

4.2 Bus simplification

4.2.1 Computational resources and geometrical implications

The need of simplifications is related to the time frame for satisfactory simulations. CFD codes solve high dimension matrices in an iterative way. There are parameters that imply higher computation time. In this section, these parameters will be mentioned to understand the reasons why it was decided to modify the geometry.

First, the processing and memory capabilities available must be clarified, since these are the most limiting resources for the CFD code. The simplifications are mainly geometrical features that make the computer take longer times to resolve the matrices and even compute poorly the variables of interest. The simulation will be executed in a **MSI GS63 7RD Stealth** laptop with with an **Intel Core i7-7700HQ CPU, 2.8 GHz, 4 cores, RAM 16 GB** and it will be performed in a **Linux Ubuntu Virtual Machine**. Thus, the CFD simulation will be restricted in geometrical ways, aiming to maintain the relevant features.

The reason to simplify them is straightforward. Basically, by solving the Navier-Stokes equations, the algorithm of the solver requires more memory and processing capacity in order to solve the linear system equations. As the number of cells grows so does the

computational effort, since each cell has an additional time contribution to the number of iterative calculations in the solution method. Adding cells is not harmless for the solver, in general. If these cells have *bad* properties, the solution is likely to be more time consuming to converge or, even worse, it will diverge after some iterations.

There are geometrical features that are undesirable in order to create a computationally reliable mesh for this case. Small chamfers, highly curved surfaces, sharp angles, detailed features and complex geometries make the cell count number to increase or to create *bad* quality cells. But that is not the only problem; other mesh features make the solver "crash": high *aspect ratios*, *non-orthogonal* cells and high *skewness*²³ in cells are some of the parameters that could jeopardize the performance of the simulation.

Figure 16 highlights two problematic geometries. The lower red circle shows that the leg has an angle and is very thin. This obliges to refine the mesh in the boundaries near the legs. The issue is not related to refine the mesh itself; the actual problem is that since each chair has four legs, the refinement must be done four times. The consequence is to create high aspect ratios in the cells near the legs, which is not desirable, even more considering that the legs are thin, implying a more refined mesh. On the other hand, the upper red circle shows a chair back handrail; this is also an undesirable geometry since the meshing software will define poorly the mesh in the curved zones of the cabin. There are more features that must be modified or deleted in the chair, those will be shown in the next section.

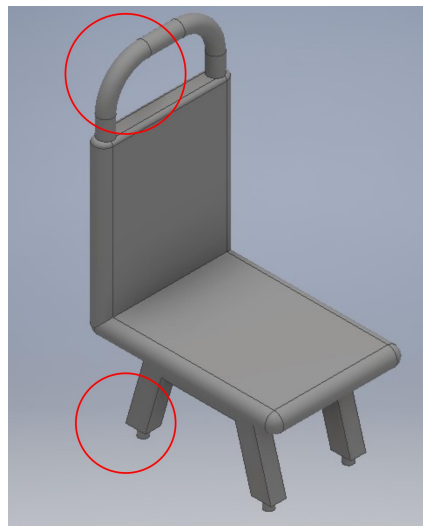


Figure 16: Original seat geometry.

²³These three concepts; aspect ratio, non-orthogonality and skewness, are expected to be known by the reader. Even though, when the mesh process is explained, a brief description of these concepts will be provided.

4.2.2 Simplifications

The last section explained why simplified geometries is a must for the bus design. Here, images of the simplified features will be provided, to end with a display of the overall simplified design. The CAD software used is Autodesk Inventor 2018, where the feature deletion and creation of simplified parts will be carried out. There are three main bus interior parts that must be modified:

- **Steering wheel.** The geometry of the steering wheel is highly complex, and has several small features. Basically, is a torus with several spline curves which give an *aesthetic* design. The shaft connecting it with the dashboard has a small diameter. This is shown in Figures 17a and 17b.



Figure 17: Isometric views of the original wheel.

Complex features will be removed and a new *simplified wheel* is provided. General dimensions are maintained: external diameter of the wheel, wheel thickness and tube length. However, most tridimensional curved features were transformed to *planar* features.

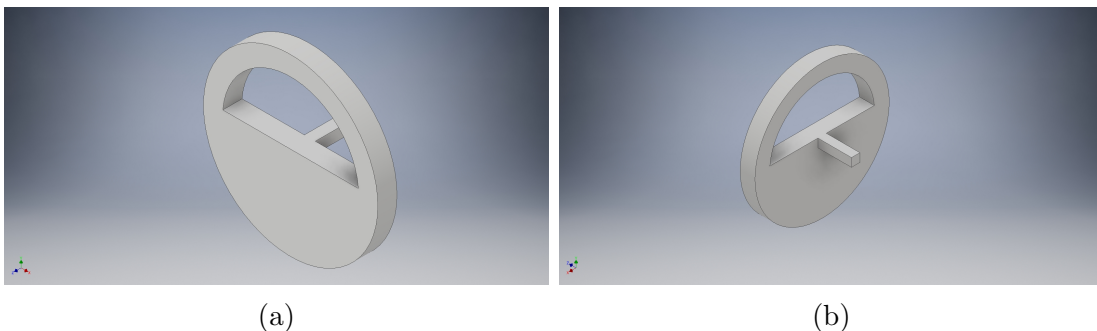


Figure 18: Isometric views of the simplified wheel.

As it can be seen, this is not a *functional* steering wheel: the shaft is a rectangular prism. However, its area and volume are similar to the original one, thus it is expected that the outcome does not change significantly. Plus, it must be considered

that thermal comfort for the bus driver will not be evaluated; their compartment has its heating system.

- **Seats.** The design is provided in Figure 19.

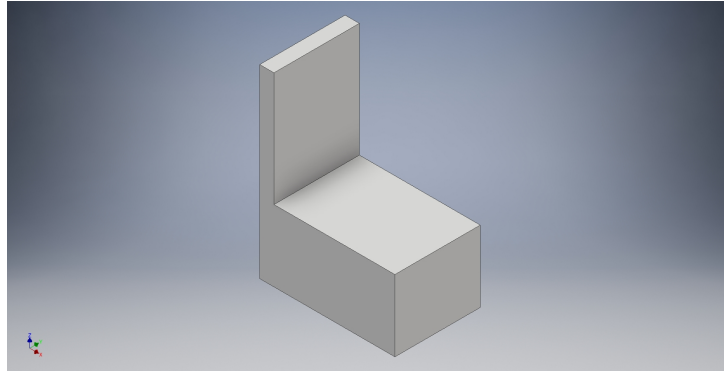


Figure 19: Simplified chair model.

It was mentioned that the seats' legs and back-handrails must be modified. The width of seats has to be changed, since it makes the space between the bus bodywork and seat too small, which will create small cells during the meshing process. In addition, every corner and chamfer was transformed into an orthogonal angle between colliding surfaces to avoid curved features.

- **Bus base.** This is the most complex geometry, since it encloses most of the design. Summarizing, the most important geometry simplifications are:
 - Planar dashboard. The original design had buttons and radars with much detail. Therefore, a deletion of these features by flattening was done in Figure 20.

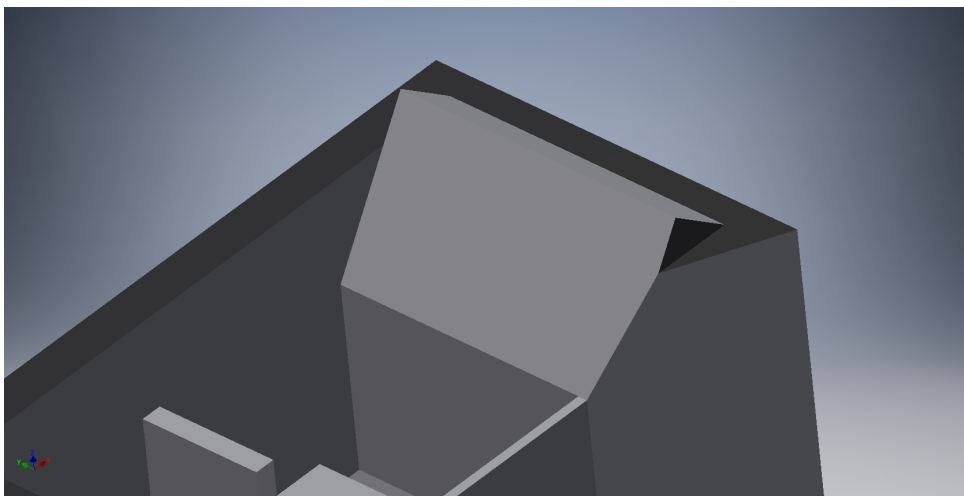


Figure 20: Dashboard flattening.

- Chamfer and hole deletion. Figure 21 shows the difference between two elevation steps of seating. Holes where the seats are fixed were erased and chamfers were left is right angles.

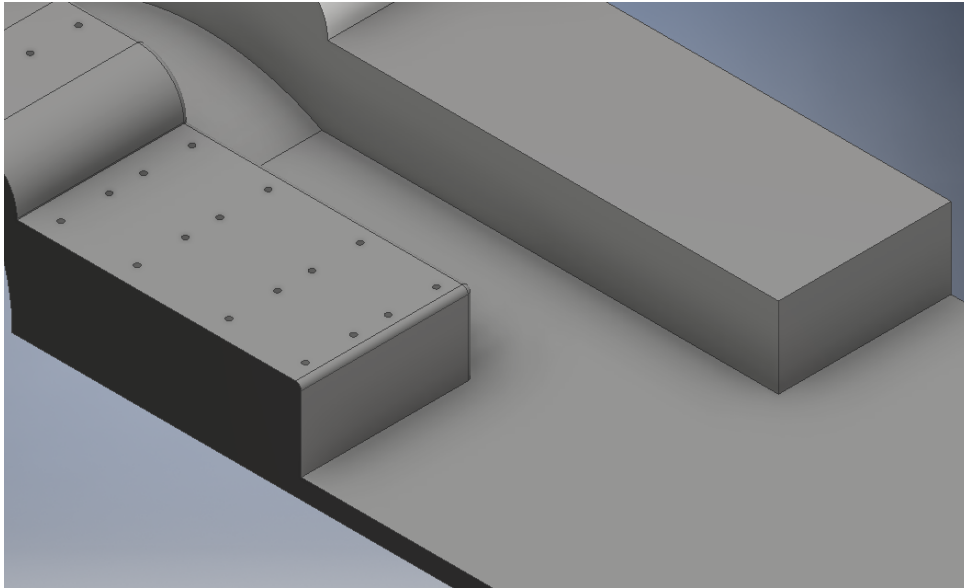


Figure 21: Chamfer and hole deletion.

- Entrance totem deletion. The totem is expected to have null influence in the simulation results. Considering that additional geometry adds complexity, this feature was deleted.

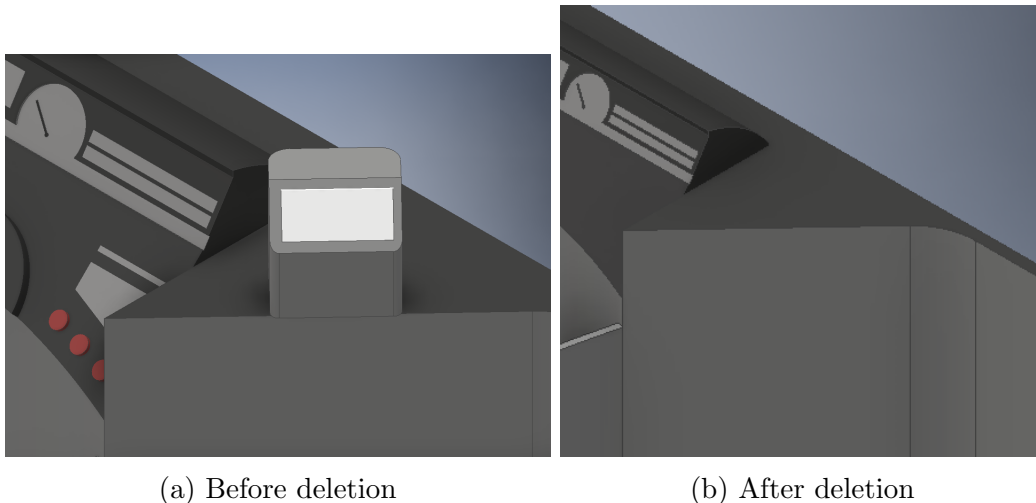


Figure 22: Totem deletion.

Additional features were deleted due to geometry compatibility or non-desirable surfaces. The final bus interior geometry is shown in Figure 23 with all the needed parts assembled. It must be noted that the doors and bus walls are not being designed at the

moment. The modelling of these structures will be done in the meshing software. *Walls*²⁴ and other boundaries are more manageable while doing the meshing, because certain *cell blocks* could cause issues in the final simulation.

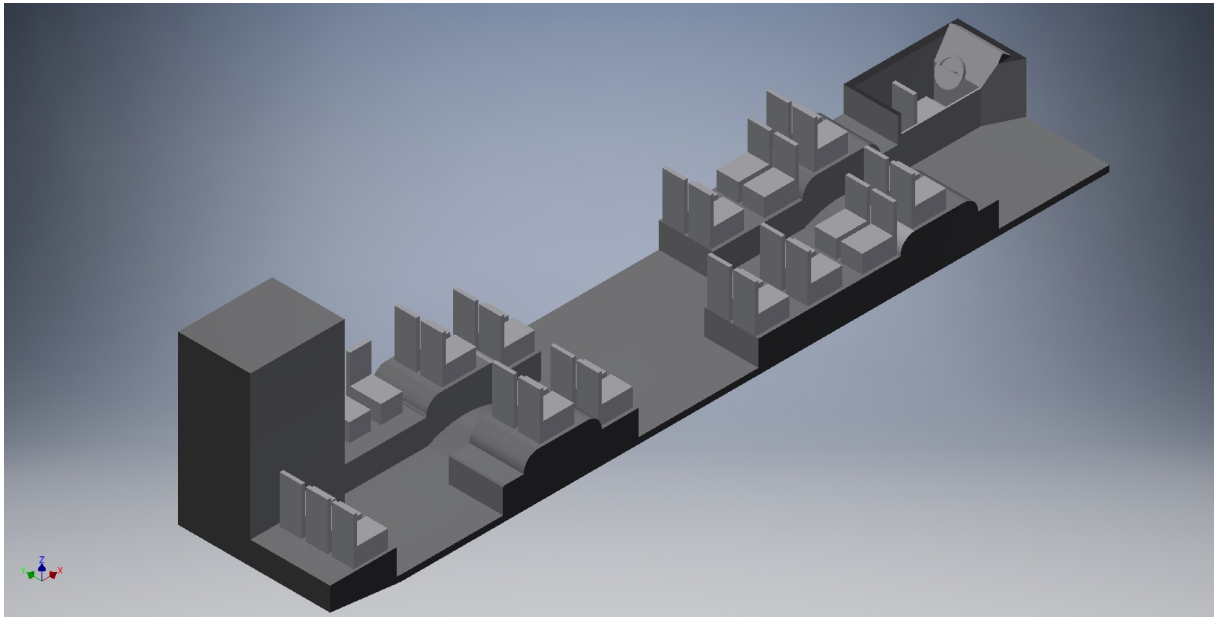


Figure 23: Simplified final bus interior assembly.

A final word of caution regarding Figure 23: this last CAD model is not a definitive one. Modeling and meshing processes are iterative, and as such are prone to changes related to the input that has been given. Meaning that, even if complex geometry has been already deleted, it does not mean Figure 23 is "bulletproof". This can be only assessed by testing the geometry, doing the mesh and simulating. Nonetheless, one of the two steps that come after the geometry design could fail: the mesh could not comply with the number of elements size requested caused by small geometries or either the simulation process has a strange behaviour due to bad quality cells that happen to modify the results in a *chaotic* way. This can only be seen by testing and monitoring the partial results on the fly.

4.3 Heating system definition: test bus²⁵ and scope of simulation

It must be stated that the step-by-step process described here is a reference to the real process that will be fulfilled during the final simulations. The steps followed here can be

²⁴In this case, by referring to walls it is intended all the boundary features of the fluid domain, excluding the roof AC inlets and the outlets.

²⁵The test is related to the intricacies of carrying out a simulation "blindfolded", meaning that no prior knowledge of the outcome is known, not even the input data. For instance, by testing a boundary condition of `zeroGradient` at the outlet and concluding that it is a better option to use an `inletOutlet` boundary condition for stability.

extrapolated to the final bus geometry, mesh and setup. This has to be mentioned, since from now on it will be assumed that these processes are known and the specific details of the final simulation will be left aside to provide information related to the thermal comfort, rather than the geometry, meshing and CFD specifics.

This section is devoted to a major topic in the CFD simulation. In fact, two important boundary selections change the entire simulation outcome. The first one is the condition of the recirculating air outlets and extractor fan i.e. the **outlet boundary conditions**. The second one is the selection of the heating system state i.e. the **inlet boundary condition**. Thus, a thoughtful selection of the heating system conditions must be accomplished, otherwise the risk is to obtain an *useless* solution. Though, with the simplifications, it is not expected a highly accurate final outcome for each variable, but an erroneous choosing of the input parameters will ensure a *bad* solution.

The simulation to be executed is a steady type one. There is a large debate among researchers about the validity of steady state simulations. The major concern with non-transient simulations is that time is a variable that cannot be disregarded, because fluid motion is a time dependent phenomenon. Certainly, steady simulations are an economical way of retrieving the fluid variables and get an overview of the process to be studied. Continuous movement devices (i.e. a turbine), can be modeled as such, but only if the temporal derivatives of the fluid equation are negligible, and this only occurs after elapsed time is large enough to disregard changes in time. The debate is found in this topic, because by neglecting time it is being disregarded how long takes to reach steadiness. In this particular case, by doing a non time-dependant simulation, the time for reaching this state is an unknown; it could be seconds, minutes or months of maintaining the heating system turned on.

The objective is not to deal with time, but rather to evaluate the capability of providing thermal comfort in steady conditions. The given boundary conditions are the real capabilities of the bus, meaning its maximum heating capacity and flow rate must be taken into account. Thus, **the scope is to determine if thermal comfort is accomplished in the K9 bus during winter in steady state.** This statement defines the scope in a large scale, but almost immediately the question on how to assess thermal comfort arises. ASHRAE-55 standard has a guideline to evaluate thermal comfort but anyway the *state* of the bus is the bigger unknown to evaluate. It could be long debated the conditions to simulate, but there are two extreme cases that suit as possibilities.

- Fully used capacity, where heat is transferred to the environment through sweating, convection through clothes and heat generation through respiration processes. This analysis has many drawbacks. The geometry is completely changed: the body geometries at the interior would have a major impact in the overall result. Addi-

tionally, these bodies act as heat sources, so it could turn out that instead of heating the bus, it could be needed to cool it.

- Single passenger, where a unique person is located randomly in any seat or standing position. This is a more adequate approach, since heat sources coming from persons can be disregarded and univocally the bus must be heated rather than cooled (even if in winter). This is the approach chosen for this thesis. To this aim, several key locations will be probed in the bus to assess if thermal comfort can be achieved in general.

The geometry shown in section 4.2.2 even if simple is not a really good one for testing different possible boundary conditions and numerical schemes. Furthermore, the visualization process will be more difficult since there are several features that must be mentioned, such as different wall heat flux boundary conditions for bodywork parts of the bus and glass parts. With this in mind, a bus test case is provided for didactic purposes; this is not the bus used for the final simulation, but the simplicity of the geometry provides an easier way to test volumetric flow rates, inlet temperatures, turbulent conditions and so on in order to do a crash analysis. Of course, it maintains the relevant features and dimensions of the geometry shown in 4.2.2 so that the conditions applied to the original geometry are, at least, similar to the ones used in the test case.

4.3.1 Bus test case overview

As previously stated, the main objective is to show a *Bus Test Case*, which hopefully provides a better insight of the layout of the HVAC system and general features. The base layout system used to design the actual geometry is shown in Figure 24.

The previous image shows a much more simplified version of the bus, with a reduced number of seats, trimmed geometries, same height for every passenger seat, non-curved features and no frontbox for the driver. Also, it shows several lines in pale green and dark purple, which will define the geometry features of the bus. In particular, these define the windows, bodywork, doors, inlets and outlets. These features will be displayed in a clearer fashion within the meshing software.

The lines shown in the geometries have two main purposes: to aid the meshing process and to separate domains where different analysis will be carried out. For instance, it is expected to estimate the heat losses through bodywork walls of the bus, windows, roof, front window, and others with certain wall heat flux functions implemented as boundary conditions. On the other hand, the narrow pale-green rectangles on the roof are the inlets of the cabin, which will consider both the mixing of the recirculated and fresh air and the heating through the roof unit. In the above figure the 14 inlets are shown. The number of inlets selection is rather an heuristic choosing which takes into account the expected distribution of seats, expected velocity of the inlets considering the inlets' area and the reference Figure 24 of a real bus HVAC system. The same applies for the extractor fan, where a visual inspection was made in order to get approximated dimensions for this air exit. Finally, the recirculation outlets, which are at the floor level of the seats, have the a similar size of that of the inlets. Again, this process is an heuristic which considers only the available and accessible data. The Table 5 shows some general dimensions of the bus features.

Feature	Dimensions	Quantity
Overall Bus	$12\text{ m} \times 2.33\text{ m} \times 2.16\text{ m}$	-
Inlets	$33\text{ cm} \times 8\text{ cm}$	14
Recirculating Outlets	$26.4\text{ cm} \times 6.5\text{ cm}$	14
Extractor Fan	$33\text{ cm} \times 45\text{ cm}$	1
Doors	$1.5\text{ m} \times 2.17\text{ m}$	3
Non-door side window height	1.49 m	-
Door side windows height	1.08 m	-

Table 5: General dimensions for the test bus. These are similar to the ones to be used in the final simulation.

Is worth noticing that there is a difference in the dimensions of the inlets and the recirculating outlets. Two main reasons support this choice:

- The first is that the inlet flow is expected to have the same velocity as the outlets, but here are 15 outlets, the 14 recirculation outlets and the extractor fan, which has a larger area. On the other hand, there are 14 inlets, but with a higher width respect to the outlets. This could help to maintain stability related to the high velocities that could be found as a difference of inlet-outlet sizing.

- The second one is related to avoiding big draft values at the ankle levels, which cause discomfort. For instance, wider recirculating outlets allow higher flow rates at the ankle levels instead of the extractor fan, thus increasing the speed, which can generate unpleasant thermal sensations.

4.3.2 Meshing of the test bus

With the geometrical features clear, the next logical step is related to the meshing process. This is the most time consuming procedure related to a CFD simulation, particularly for an `OpenFOAM` user. The software has restrictions related to non-orthogonality, skewness, use of pyramidal cells and so on. Most of the rules that should be respected in order to get a usable mesh are the following:

- Maximum included angle: cells with extreme angles tend to be a source of instability due to non-orthogonality and skewness. `OpenFOAM` recommends using values $< 170^\circ$ to ensure capability of running properly.
- Volume ratio: its ideal value is 1, but given that is not a critical parameter for `OpenFOAM`, it is not completely necessary to struggle to get a value of 1. Moreover, `OpenFOAM` accepts volume ratios up to 30, which is very permissive.
- Skewness: it is highly recommended to get low values of skewness, since they affect the way gradients are computed. In `OpenFOAM` the target value for skewness is less than 0.85, to ensure that the **skewness error** is minimized. Nevertheless, there are different methods that can overcome high skewness when computing gradients, such as the `leastSquares` gradient option and the `pointLinear` gradient schemes. These are quite handy when trying to simulate in skewed meshes, but both of them are computationally expensive than `linear gradSchemes`, since the Least Squares and the Gauss Node-Based methods both require to evaluate variables at faces and nodes of the cells.
- Non-orthogonality: this is, in fact, the most critical parameter which has to be monitored while meshing, because `OpenFOAM` unlike `ANSYS Fluent` or other CAE solvers, will crash with highly non-orthogonal meshes. The maximum valued allowed by default when using the `checkMesh` utility is 85° . However, it is strongly recommended to modify the mesh as much as possible to get low non-orthogonality values. After all, non-orthogonality plays a major role in two aspects of the simulation:
 - First, if a non-orthogonal mesh is used, it will be mandatory to use more non-orthogonal correctors in the loops, both for avoid losing accuracy and stability due to defectively computed gradients.

- Second, the implications of using these non-orthogonal corrections imply more pressure-solving iterations, consuming more time in order to obtain a converged solution. For the purposes of this thesis, it will be established that the maximum value for non-orthogonality will be 70° , so that the simulation can run in a smoother way and get more accurate results. In a steady simulation, non-orthogonality plays a major role not in the number of non-orthogonal corrections, but in the time of convergence of the SIMPLE loop.
- Aspect ratio: this is also a parameter that must be monitored closely while meshing. In general, `OpenFOAM` accepts large values for the aspect ratio. However, it is a good practice to maintain it close to one. High aspect ratios affect gradient computations in cell faces. In addition, in cells where the flow has sharp gradients instabilities will appear. However, it is allowed to use greater values in cells where the gradients tend to be high in the direction of the shortest side of the cell but low in the direction of the longest side²⁶. This is the case of the inlets and outlets of the bus, where high gradients are directed to the center of the inlets and outlets but they are lower in the flow direction. Nevertheless, in the first section of the inlets and the last section of the outlets, the cells must have an aspect ratio ≈ 1 , having consideration that the flow has to develop through the pipe.
- Triangular surface meshes: the use of triangle meshes is related to the processing of `OpenFOAM` at the moment of treating with pyramids. When a *quad* form is present as a surface, the tridimensional structure that will be generated as a cell is either an hexahedron or a pyramid. Even if a *hex* is created, sooner or later a pyramid will be created, since the extruded *quad* will have base and top surfaces composed by *quad*. Of course, this is a characteristic of PointWise. Other meshing softwares allow to create polyhedral cells from a *quad* surface. An example of this is `snappyHexMesh` of `OpenFOAM`. Even though, it is acceptable to use some hexahedral cells, which are high quality cells, while maintaining controlled the number of pyramids in the mesh algorithm.

With the previous concepts in mind, the preliminary mesh can be constructed in order to test the boundary conditions to be applied. Figure 26 shows a general overview of the mesh to be used as *test case*. Two types of blocks were generated in the mesh: structured blocks for the inlets or outlets of the bus, and one big unstructured block for the body of the bus.

²⁶This is easier to imagine in hexahedral cells

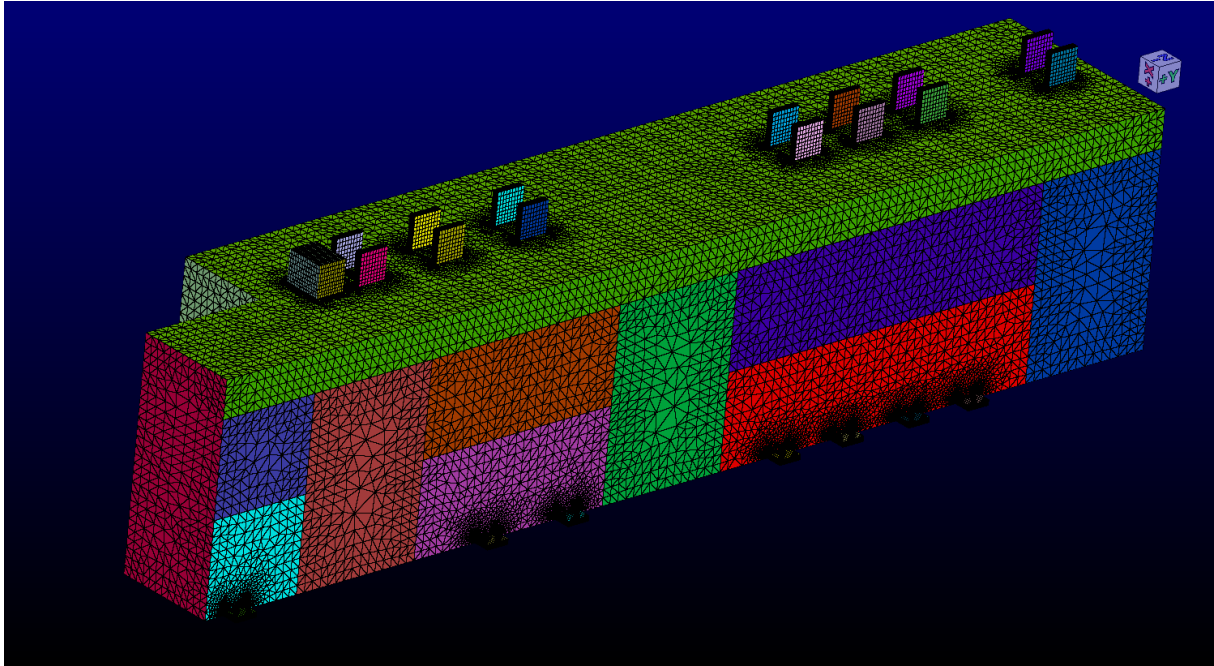


Figure 26: Test bus mesh

Some key features can be acknowledged from the figure:

- The different colored surfaces. First, is an easier way of visualizing each feature of the bus. Second, it also helps to recognize the diverse boundary conditions to be applied, since even if most of them will have a basal `wall` type boundary condition, the outward heat flux will be computed.
- Structured blocks for inlets and outlets were meshed using extrusion of structured blocks; hexahedral cells can provide high accuracy and stability, taking in consideration that in these cell blocks high velocities and gradients will be computed. Is important to obtain them accurately, otherwise the risk is to propagate errors into the control volume. The inlet and outlet blocks are shown in Figure 27.

On the other hand, unstructured blocks were adopted for the rest of the bus to comply with the need of triangular surfaces to avoid pyramids in `OpenFOAM`. This is shown in Figure 28, which displays both the exterior and interior meshing of the body surface of the bus.

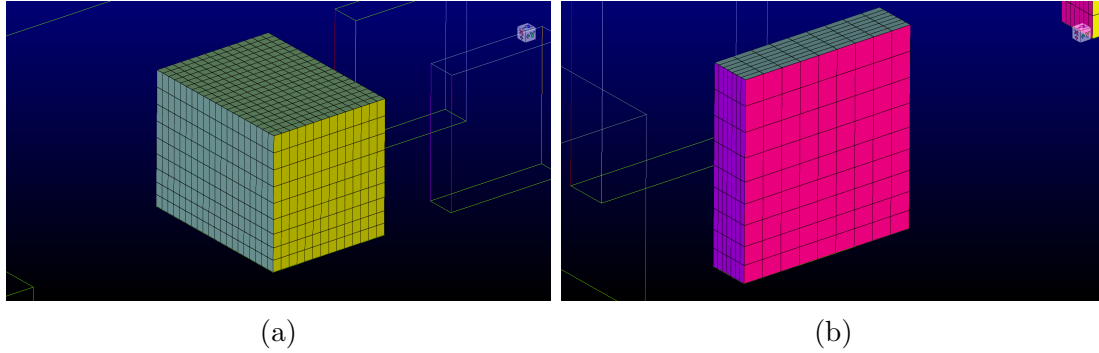


Figure 27: Extractor (a) and inlet (b) views.

- The unstructured surfaces were meshed using an *Advancing Front Ortho* algorithm. The algorithm places points in the surface in order to maximize the number of right triangles in the mesh. It was used for all the surfaces that will hold `wall` boundary conditions (or similar).
- Extruded inlets and outlets are artificial structures²⁷ (shown in Figure 27), and its main objective is to maintain stability due to high gradient boundary conditions. Velocity and temperature need flow development through the pipe to generate an appropriate profile; otherwise, if a flat inlet or outlet is meshed as a surface, the simulation in `OpenFOAM` tends to be likely to crash.
- Separation bus boundary structures are needed for computing heat losses through windows, doors, roof, bus bodywork, etc. The non-door side of the bus has two divisions: the bodywork and the glass structures. The door-side has several separations for the bodywork, doors, windows, and upper structures. Also, the frontbox is separated in glass and bodywork parts. The roof is assumed completely as a bodywork part, with exception of the extractor and inlets walls.

²⁷They do not exist in a real bus.

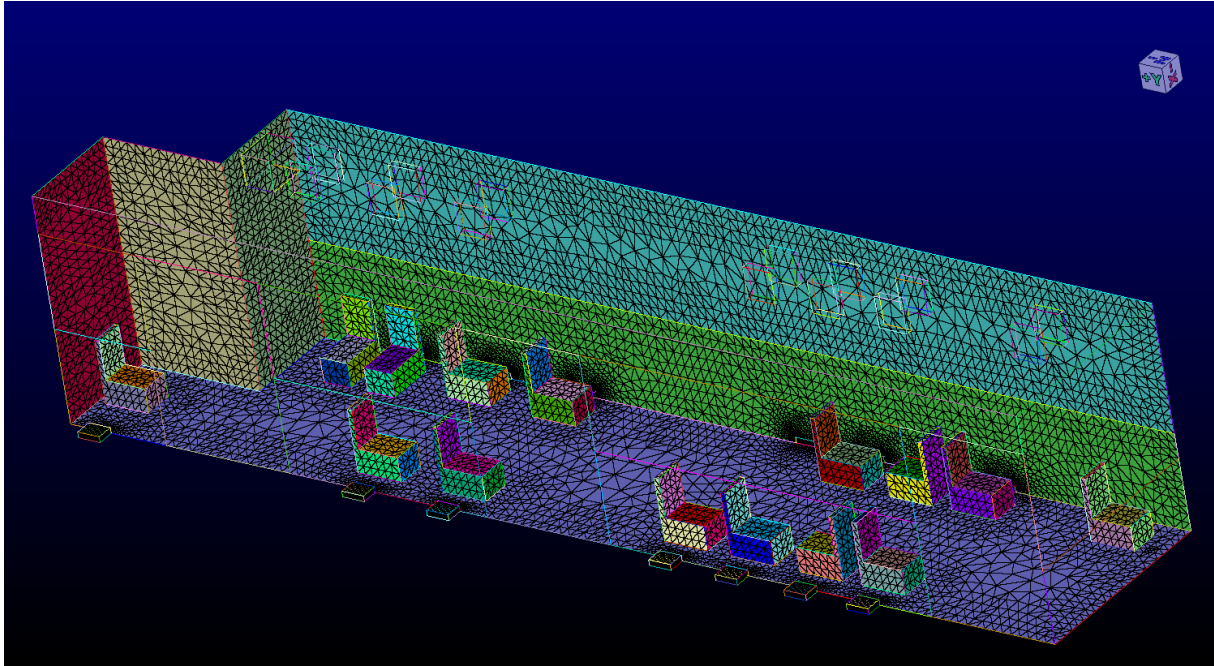


Figure 28: Interior mesh of test bus.

At the moment, only a surface mesh has been constructed, now it must be initialized in order to generate a tridimensional cell structure. PointWise does this process with many input parameters, such as the algorithm to use (Delaunay or Voxel), type of cells, edge length, maximum angle, and several characteristic and sophisticated features to improve the algorithm of mesh construction. Only the main ones are mentioned as a reference, but the rest are used without any further mention.

A summary of the type and number of cells of each type can be found in the next table, where pyramids represent less than 1% of the total cells.

Cell type	Quantity
Tetrahedra	255,748
Pyramids	2,044
Prisms	-
Hexahedra	18,396
Total	276,188

Table 6: Cell count for the test bus case.

Delaunay's algorithm was used, which generated tetrahedral cells in most of the volume but pyramids at the body-inlet, body-outlet and body-extractor interfaces, given that inlets and outlets were constructed with hexahedral cells in a structured block. Most of the remaining features were left as `default`. The resulting mesh can be seen partially in Figure 29. The cut displays a color map of an XZ plane, which goes from blue to red, indicating low and high non-orthogonality, respectively. As it can be seen, there are

≈ 400 cells that have high non-orthogonality. This number is acceptable as long as the total number of cells is much larger than the non-orthogonal cells.

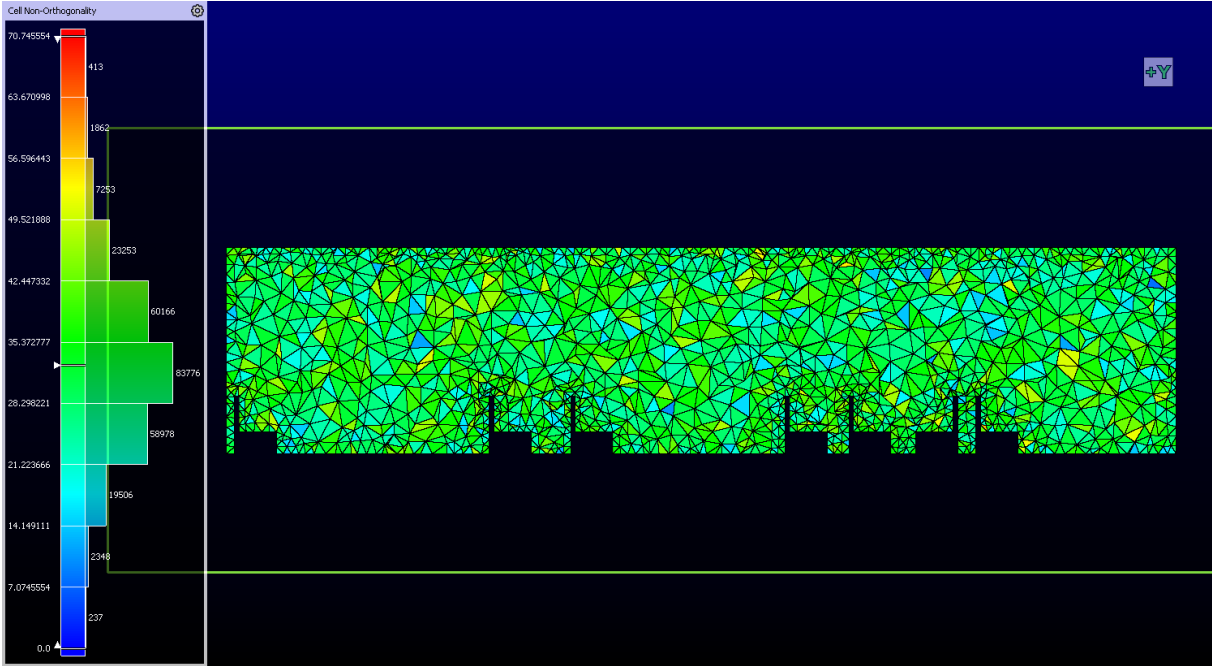


Figure 29: Non-orthogonality cut in an XZ plane.

The red dots in Figure 30 show the location of cells with high non-orthogonality. Almost every non-orthogonal cell tends to be near inlets or outlets, which is probably related either to the pyramid cells or the uneven size of the grid points near duct structures.

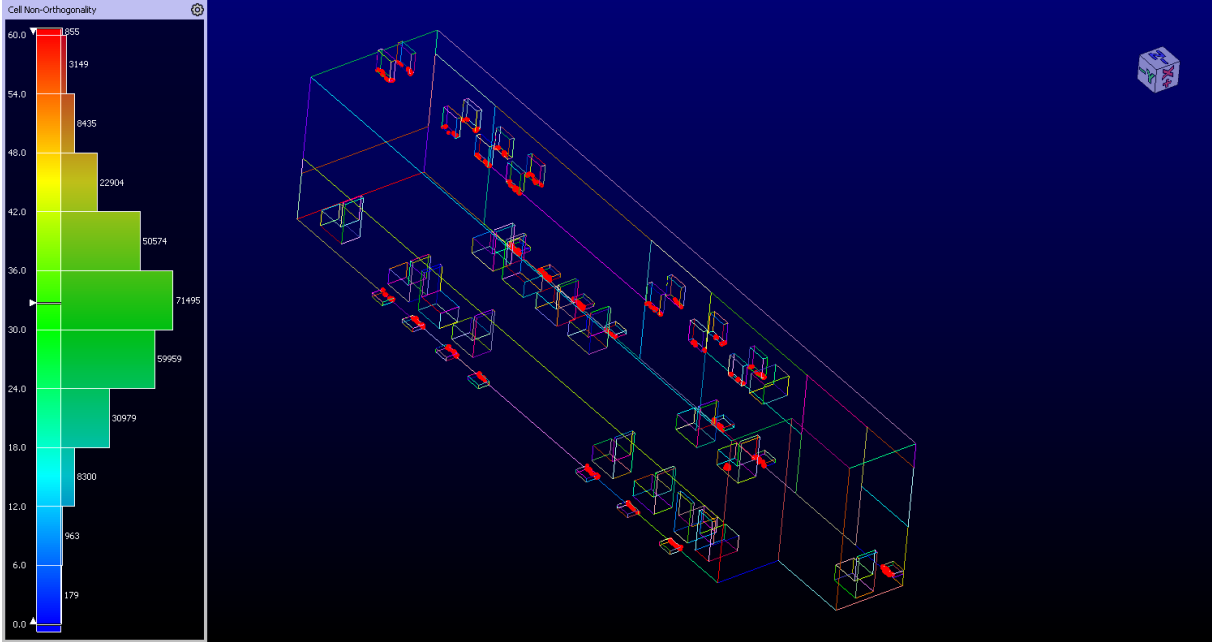


Figure 30: Highly non-orthogonal cells located at the inlets and outlets.

In any case, the number of cells with non-orthogonality higher than 60° is low compared to the total number of cells. It barely represents 0.3% of the total. Nonetheless, it does not mean that the mesh is precise and can be used without caution. Clearly, inlet and outlet values might be computed poorly. Thus, a *correction* will be added to avoid instabilities and decrease the error. Indeed, the mesh should be able to represent the physical phenomena, but for this particular mesh the main goal is to test boundary conditions, numerical schemes, relaxation factors, cell types and geometries that could be problematic for accuracy, instability and convergence in the final bus.

The same analysis can be done for the centroid skewness, volume ratio and maximum included angle. The maximum included angle is shown in Figure 31. From the histogram, no cell has a maximum included angle higher than $\approx 160^\circ$. Whereas the maximum volume ratio found is around 21, the centroid skewness is 0.77 at its maximum. Thus, this mesh suffices the basic requirements for `OpenFOAM`. Below is shown the same cut but this time the coloration is associated to maximum included angle.

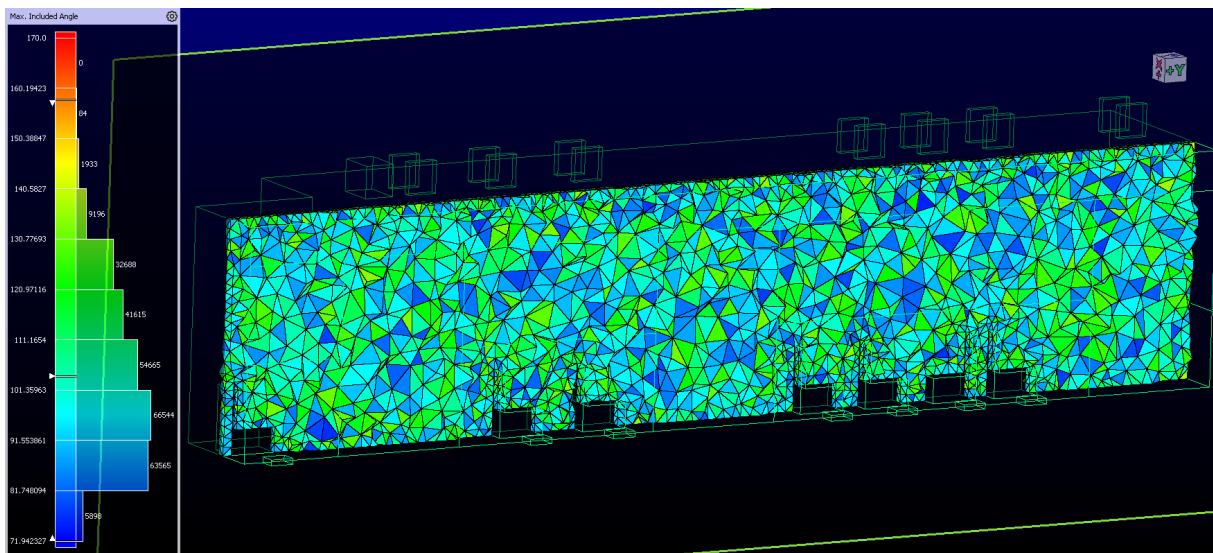


Figure 31: Maximum included angle cut plane.

To end the meshing process, surface boundary conditions (and volume conditions, if needed) must be set. These are non-physical boundary conditions, but the definition of the type of surface that is being analyzed, i.e. `inflow`, `outflow`, `wall`, `cyclic`, `wedge` and so on. In `OpenFOAM` the existent boundary conditions accepted are `patch`, `wall`, `symmetryPlane`, `empty`, `wedge`, `cyclic` and `faceSet`. The bus case will use only the `patch` and `wall` boundary types. The `wall` boundary type is self-explaining; it defines a solid surface of the control volume, where mass transfer is not possible. On the contrary, the `patch` type is a general boundary condition that defines a different physical boundary, but is mainly used to represent mass flow crossing the borders of the control volume, thus it can represent the inlets and outlets of the HVAC system. It must be

noted that the `wall` boundary type does accept heat transfer by means of conduction and surface convection, but has no mass crossing its boundaries.

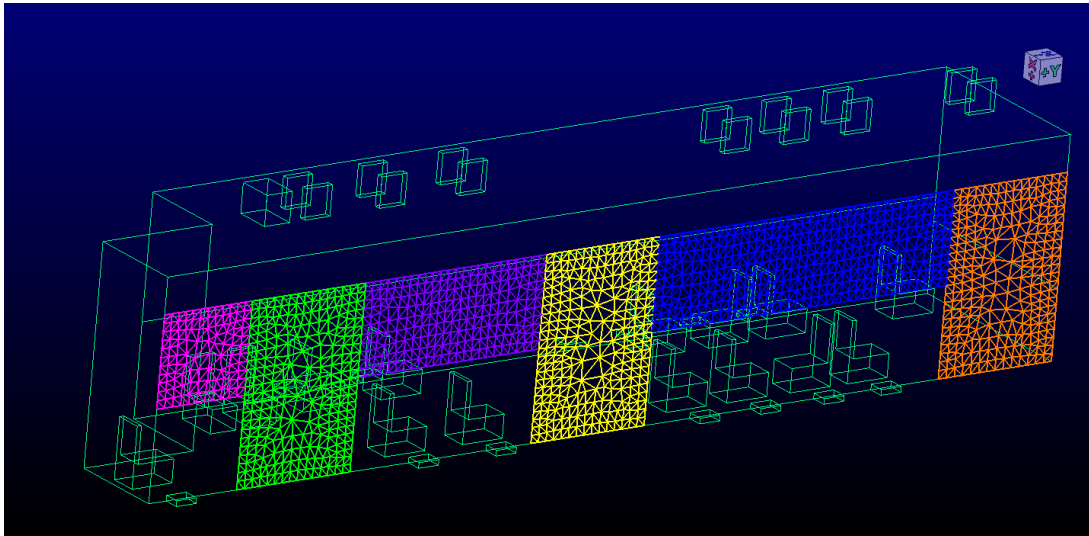


Figure 32: Doors and windows boundary conditions for the right side of the bus.

In Figure 32 the colored surfaces represent doors and windows of the right-side of the bus. PointWise also allows to set names for the boundaries, so they can be easily recognized while assigning the physical boundary conditions. By doing so, is possible for the user to plot certain key values using features of `pyFoam`, which is a package for the **Python** programming language. By assigning names to these it will be possible to plot the heat losses on-the-fly using `regExp`²⁸. The `patch` boundaries will be assigned to all the flow sections, which are shown in green, purple and orange in Figure 33; instead, the remaining surfaces will be assigned a `wall` boundary condition.

²⁸`regExp` stands for "regular expressions", which is a computational syntax for recognizing repetitive patterns and use them as needed. `pyFoam` uses `regExp` to identify floating point numbers in the output files that the user desires to plot during the simulation.

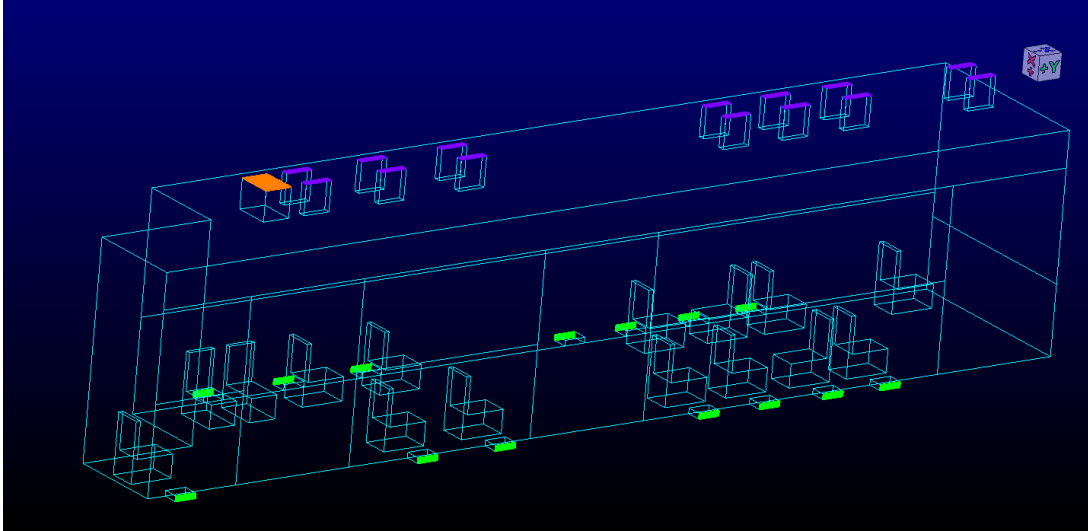


Figure 33: Mass flow crossing boundaries is allowed in the colorized structures.

4.3.3 Test bus simulation setup

Now, the setup the bus for the simulation in `OpenFOAM` must be accomplished. Prior to this phase, the characteristics of such a simulation must be clarified:

- **Steady-state simulation:** the reason to perform a steady-state simulation is related to the available computational resources mentioned in Section 4.2.1. Considering that no servers or supercomputers are being used, a transient simulation could be hard to achieve with reliable results. Courant's number must be controlled and maintained below 1. This would have impacts in the simulation; first, if the transient is of real importance, the Courant number should be controlled and actually below ≈ 0.5 to get relatively reliable results. Implying that the simulation will have a small time step. This is time consuming because each PISO loop will advance slowly in time, so obtaining some seconds in the simulation would take several hours, and finding the "steady section" of the simulation turns to be unpractical.
- **Thermophysical models and dynamics of air:** important physical properties must be clarified how will be calculated beforehand.

Density (ρ): there are many gas models for determining the density, depending on the thermodynamical variables. One of the most widely used is the *perfect gas* model, that has as inputs both pressure and temperature, and as a parameter its own gas constant.

$$\rho = \frac{p}{R_{air}T} \quad (1)$$

Where p, T and R_{air} ²⁹ are the pressure, temperature and perfect gas constant of the fluid, in this case air. There are also other models for calculating ρ , such as poly-

²⁹For air the constant is defined as $R_{air} = 0.287 \frac{kJ}{kg \cdot K}$

nomial models, `Boussinesq`, `incompressiblePerfectGas`, and several additional models. The one to be used is `incompressiblePerfectGas` or `Boussinesq`, since for HVAC applications it is widely used. Furthermore, Ferziger & Perić (2002) state that `Boussinesq` has an error expected to be lower than 1% for air HVAC applications. The `incompressiblePerfectGas` is a useful model since it is more stable than its counterpart `perfectGas`, because it is not a function of pressure but only of temperature. In addition, it is more stable than the `Boussinesq's model`, because its calculation is smoothly non-linear rather than linear.

Boussinesq's approximation for calculating the density is:

$$\rho = \rho_0 [1 - \beta (T - T_0)] \quad (2)$$

Where ρ_0 is a reference density, β is the coefficient of thermal expansion and T_0 is a reference temperature.

The incompressible perfect gas model is:

$$\rho = \frac{p_{ref}}{R_{air}T} \quad (3)$$

Where p_{ref} is a value to be set by the user, which is a reference value of pressure. An important characteristic of this model is its usability where small pressure changes are present, such as an HVAC application.

Buoyancy adds instability to the solution. Additionally, this effect can lead to un-converged solutions, particularly in a steady-state simulation. Flotage is inherently a transient phenomenon, which involves convection currents due to differentials of density. By not considering buoyancy, the solution will lack of a real component, but this choice will increase the probability to actually find convergence. There is a *trade-off* relating convergence and accuracy. Buoyant effects can be eliminated by setting gravity $\vec{g} = \vec{0}$ in the simulation, and this decision will be evaluated by comparing buoyant and non-buoyant simulations.

Heat capacity c_p is a variable that depends on thermodynamical and psychrometric properties, but temperature and humidity ratio are the most relevant ones. Nevertheless, moisture changes will not be considered to assess c_p , since variations caused by moisture content are negligible ($\approx 1\%$). Temperature changes can have a major impact in heat capacity, but only if these changes are of considerable magnitude, which is not the case in most HVAC applications, where the fluid temperature changes within the order of 40 °C.

- **Transport model:** viscosity μ can be implemented in different ways. It can be used as a constant value or a viscosity model included in `OpenFOAM` can be adopted. Recalling that the Navier-Stokes equation must be solved in a Reynolds Averaged formulation, the term that is modified is the stress tensor, by means of the viscosity in the shear stress. In particular, the model chosen changes the way the viscosity is computed in the $\nabla \cdot \bar{\tau}$. Two models should be mentioned, since both are available in `OpenFOAM`, and are commonly accepted in literature.
 - Constant μ : this is the simplest way of computing shear stresses. It also simplifies quite a bit the momentum equations, since the Laplacian term does not interpolate the μ values and assumes it is a constant throughout the simulation.
 - Sutherland’s law: one of the equations that models the behaviour of the viscosity depending on temperature is Sutherland’s law. It is defined as:

$$\mu = \frac{C_1 T^{\frac{3}{2}}}{T + S} \quad (4)$$

C_1 is a constant defined as:

$$C_1 = \frac{\mu_{ref}}{T_{ref}^{3/2}} (T_{ref} + S) \quad (5)$$

The coefficients are shown in Table 7

Gas	$\mu_0 \left[\frac{kg}{ms} \right]$	$T_0 [K]$	$S [K]$	$C_1 \left[\frac{kg}{ms\sqrt{K}} \right]$
Air	1.716×10^{-5}	273.15	110.4	1.458×10^{-6}

Table 7: Sutherland’s coefficients

Sutherland’s model is recommended in NASA’s webpage³⁰, if should the $k - \omega$ *SST* model is used. Particularly, in thermal applications it is highly recommended to use either the $k - \epsilon$ model or the aforementioned, being the former more adequate for heat transfer applications. Even though, the **ASHRAE** standard of 2001 relies more on the $k - \epsilon$ because at that time the $k - \omega$ *SST* model was not deeply studied. The main difference with the constant viscosity model is that the solver will interpolate the μ values between cells when computing the Laplacian terms, since Sutherland’s law is a temperature function.

- **Turbulence modelling:** one of the most difficult parameter for a simulation to be reliable is the turbulence modelling, because its nature is still an unknown and under research. However, turbulence models provide quite reasonable outcomes for

³⁰<https://turbmodels.larc.nasa.gov/implementrans.html>

commercial purposes. OpenFOAM has implemented models for turbulence in its source code: `kOmegaSST`, `kEpsilon`, `kOmega`, `spalartAllmaras`, `kEpsilonRealizable` and so on. In the previous item, two of the common possibilities were mentioned. There are some reasons to choose the `kOmegaSST` rather than the `kEpsilon` or the `kOmega`, but the most important one is that the `kOmegaSST` model "includes" in its code both models. This is implemented by using blending functions that modify the scalar transport equations of the turbulent kinetic energy k as well as the turbulent viscosity μ_t .

With all the generalities associated to the process of presetting clear, now the actual setup will be chosen. This implies setting boundary conditions, numerical schemes and all the relative parameters for the solver. Striving to provide details of the code has no point, since there are many variables to control and the essence of the CFD code fades if each one is described. Even though, some will be mentioned with brief descriptions to give an insight of the chosen parameters.

The solver to be used in OpenFOAM is `buoyantSimpleFOAM`³¹, which solves the equations for a steady-state fluid using the **SIMPLE** algorithm. A list that summarizes the turbulent related variables is provided in Table 8.

Variable name	Symbol	Near-wall treatment	Inlet treatment	Outlet treatment
Turbulent thermal diffusivity	α_t	<code>alphatWallFunction</code>	Calculated from other variables	Calculated from other variables
Turbulent kinetic energy	k	<code>kqRWallFunction</code>	<code>fixedValue</code>	<code>zeroGradient</code> or <code>inletOutlet</code>
Turbulent kinetic viscosity	ν_t	<code>nutUSpaldingWallFunction</code>	<code>fixedValue</code>	<code>zeroGradient</code> or <code>inletOutlet</code>
Specific turbulence dissipation	ω	<code>omegaWallFunction</code>	<code>fixedValue</code>	<code>zeroGradient</code> or <code>inletOutlet</code>

Table 8: `buoyantSimpleFOAM` input turbulent parameters required for a `kOmegaSST` type simulation.

Most of the wall treatments shown in Table 8 are standard. A variety of wall functions is available and is a matter of testing them to choose the most suitable for the user's purpose. A special mention must be given to `nutUSpaldingWallFunction`. Unlike other wall

³¹This code is aimed to solve buoyancy in fluids. When the simulation is run with gravity, the momentum equation will change adding a source term associated to the Boussinesq approximation or the incompressible perfect gas model, depending on the choosing. Otherwise, the solver has no change in the momentum equations and solves it with no source term.

functions, Spalding’s function is a continuous one, whereas others are blendings between viscous sub-layer and log-law layer functions. The advantage of Spalding’s function is related to its versatility, since it works reasonably well even in the buffer layer. Other wall functions give poor results if the first cell height if the near wall coincides with the buffer layer, leading to low accuracy results for the shear stress computation.

In addition to the inputs shown in the previous table, three variables must be given: **pressure**, **temperature** and **velocity**. The treatment applied for the boundary conditions will not only depend on the wall, inlet and outlet basis; it also considers the *type* of wall being analyzed or if the outlet is a recirculating one, etc. The treatment changes mainly for the temperature boundary conditions, as it will be shown:

- Temperature (T): temperature boundary conditions vary in inlets, outlets and walls. But depending on the wall it also varies, since heat losses can be computed with unidimensional heat transfer with `OpenFOAM`, and this of course depends on the surface area, type of material and thickness of the layer. That is the actual reason why the bus structures were divided as shown in Figure 32. At the moment of the simulation, some assumptions were to be made due to the lack of data regarding the real thicknesses and sizes of windows, doors and bodywork layers. Indeed, this is not expected to be of high importance, since this is only a test of numerical stability and adjustments are likely. Before starting with the complex boundaries, the inlets and outlets boundary conditions will be given:
 - Inlet temperature: the inlets will have the same temperature of 300 K . This is an heuristic guess that will be explained in more detail in the next chapter, but basically it is associated to the temperature that could be thermally comfortable for all the occupants of the bus, in conjunction with the velocity expected. Thus, in `OpenFOAM` there will be a `fixedValue` boundary condition with an `uniform 296.6` value.
 - Outlet temperature: the boundaries associated to outlets are the extractor fan and the recirculating exits. Both have differences since the extractor goes to the exterior ambient and the recirculating pipes are maintained at the "bus interior" by passing the air in the condenser again and re-heating the air that was circulating at the bus interior. It will be used a `zeroGradient` condition, due to stability but also to represent the physics involved at the interior in a proper way. By setting the outlets as `zeroGradient` it is being set that no thermal diffusion occurs in two consecutive layers of air at the exits.
 - Glass walls: this comprises both windows and door wall boundary conditions. In these structures heat loss is of major importance. The `wallHeatFlux` boundary condition receives four parameters, namely the convective coefficient `h`, the conductivity of the layers that compose the wall `kappaLayers`, the thickness

of those layers `thicknessLayers` and the external temperature (typically the symbol T_∞ is assigned in 1D conduction) that is assigned to the parameter `Ta`. The external temperature was described in section 3, for Turin the temperature to be used is -3.3°C , the value of κ_{glass} will be $0.7 \frac{W}{m \cdot K}$ from *Incropera's* table of materials for glass, and the thickness of the glass will be used as 1 cm. Of course, these values can be further modified for more precision in next simulations.

Finally, the most difficult value to assess is the \mathbf{h} convective coefficient, since it is calculated in general from correlations depending on the Reynolds value, Prandtl value, characteristic length and so on. Further, it depends strongly on the type of flow: laminar and turbulent flows have different correlations for \mathbf{h} and also depends on the shape of the surface to be analyzed. To simplify this process, for the relevant parts, i.e.: the roof, bus sides and frontbox, the same correlation of **parallel plate for turbulent flow** will be used. Cengel (2007) recommends using the following correlation for mixed boundary layer.

$$\text{Nu} = \frac{hL}{\kappa_{fluid}} = (0.037Re_L^{0.8} - 871) \text{Pr}^{1/3} \quad (6)$$

Where Nu is the Nusselt number, Re_L is the Reynolds number with characteristic length L and Pr is the Prandtl number. For this calculation, it will be assumed that the bus travels at an average velocity of $36 \text{ km/h} = 10 \text{ m/s}$, the characteristic length will be taken as $L = 12 \text{ m}$, the maximum bus length which is parallel to the flow, and from Incropera's textbook the Prandtl's number for the range of temperature analyzed will be $Pr = 0.707$. With the data, the convective coefficient leads to:

$$h_{external} = 21.3 \frac{W}{m^2 K} \quad (7)$$

- Bodywork walls: the walls are composed of steel, plastic and insulating material inbetween these layers. Table 9 shows the conductivity, and thickness of each material modelled for the heat losses through bodywork. The values were obtained from Cengel's textbook (2007). Additionally, the same average value for Nusselt and convective coefficient calculation shown in Equation 7 will be used for the bodywork heat flux calculation.

Material	Thermal conductivity (W/mK)	Thickness (mm)
PVC, vinyl	0.1	2
Steel	50	3
Polystyrene	0.004	70

Table 9: Thermal layers of bodywork.

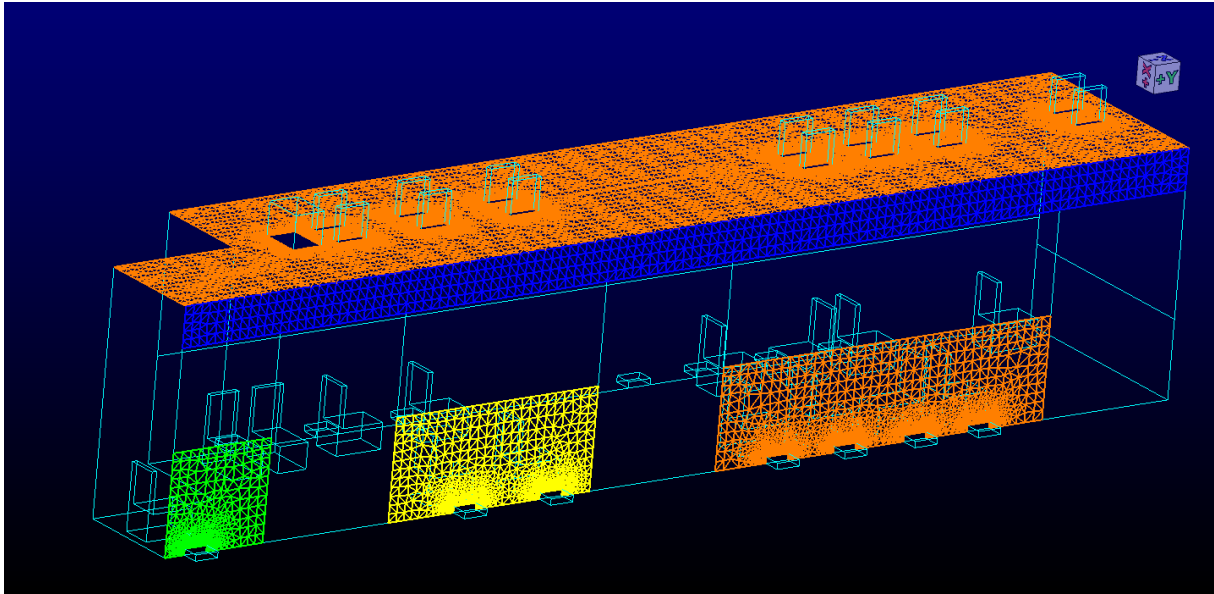


Figure 34: Bodywork surfaces (only the right side is shown).

- Remaining items: seats, floor, artificial walls for the inlets-outlets and the rear part of the bus will have an adiabatic boundary condition assigned. The inlet-outlet structures must be adiabatic, since they do not represent physical structures. On the other hand, seats, floor and rear bus have adiabatic boundaries only to neglect heat transfer through these walls. This is due to the high complexity of the geometry that makes difficult to assign an h value plus the difficulty to model a wall thickness for all of them. Even though, these are thick structures, so heat losses can be neglected.
- Velocity–Pressure coupling: this is one of the foremost choice that must be made in the system, since it modifies the stability of the solver. In general, the data sheets of heating systems carry two information types; first, the maximum heat power that the heating system installed can deliver; second, the flow rate that can be impelled through the condenser (or the evaporator). The latter datum is given as maximum available volumetric flow rate, divided in fresh air and recirculation air capacity. **OpenFOAM** is able to receive as input the volumetric flow rate as a "velocity boundary condition". Thus, by examining some data sheets of commercial use, it can be seen

that the maximum capacity can be up to $9000 \frac{m^3}{h}$. The data sheet of the BYD K9[®] bus of GTT sets a maximum value of flow rate as $6000 \frac{m^3}{h}$, where $1500 \frac{m^3}{h}$ is the maximum air that can flow through the recirculation system. Therefore, the limits are equivalent to $1.667 \frac{m^3}{s}$ for the maximum flow rate and $0.417 \frac{m^3}{s}$ for the recirculation air. However, these maximum values are seldom reached in practice.

A test value of $900 \frac{m^3}{h}$ will be used. The choice is based on the inlet velocity that this implies, so that no extreme velocities are found in the cabin. It must be noticed that $900 \frac{m^3}{h}$ is much less than the $6000 \frac{m^3}{h}$ available to deliver. Even though, the amount of heat power used is more than a half of the heating capacity of the HVAC system. This makes mandatory the use of the recirculation system.

Regarding the boundary conditions, in Table 10 common combinations are shown in order to maintain stability. The most stable one is the Volume Flow Rate and Static pressure system ³².

	Inlet		Outlet	Stability
Volume flow rate	<code>flowRateVelocity</code>	Static pressure	<code>fixedValue</code>	Excellent
Total pressure	<code>totalPressure</code>	Total pressure	<code>totalPressure</code>	Very good
Total pressure	<code>totalPressure</code>	Static pressure	<code>fixedValue</code>	Good
Static pressure	<code>fixedValue</code>	Static pressure	<code>fixedValue</code>	Poor

Table 10: Common velocity-pressure systems in OpenFOAM.

The boundary condition assignment can be summarized as in Table 11.

Boundary Condition			
Variable	Inlets	Outlets	Walls
U	<code>flowRateInletVelocity</code>	<code>inletOutlet</code>	<code>noSlip</code>
p	<code>fixedFluxPressure</code>	<code>fixedValue</code>	<code>fixedFluxPressure</code>

Table 11: Pressure and velocity assignment.

With the boundary conditions, thermophysical properties and dynamics models set up, it is possible to advance to the numerical set up. To not overextend this chapter,

³²<https://www.openfoam.com/documentation/guides/latest/doc/guide-bcs-common-combinations.html>

the numerical schemes and matrix algorithms used will not be described exhaustively. Rather, a brief insight will be provided on how to make the solution converge and/or be accurate.

Obtaining convergence and accuracy is a matter of trial and error. Nevertheless, sometimes it is possible to tune the parameters on-the-fly to obtain both of the aforementioned characteristics. This will depend mainly on the problem and mesh quality.

The basic concept in mind is that, for the numerical schemes, the `divSchemes` variable associated to `U`, `k`, `h` and `omega` will be initialized with a first order scheme: `upwind`. After several iterations, when stability is reached and the residuals are also stable, the `divSchemes` will be changed to a second order scheme, beginning by the most stable ones and ending with the most spurious variable. Particularly, during these tests it has been seen that `omega` is the most spurious and "exploding" variable, similar to the enthalpy `h`. During the course of this thesis, two accurate schemes were preferred: `linearUpwind`, being a second order scheme, and `limitedLinear 1` as a TVD scheme. Nonetheless, during the tests, the first order schemes and very limited gradients/laplacians were preferred, due to impossibility to find convergence with other accurate schemes.

For the matrix solvers, in the density case a diagonal solver was used since it only implies back-substitution from the incompressible perfect gas equation. For pressure the `GAMG` solver has proven to give good results as well as the `PCG` solver, but the former will be used because it tends to be faster. For the rest of the variables, i.e. energy, velocity and turbulent variables a bi-conjugate gradient solver will be implemented, ideal for non-symmetric matrices. Finally, the relaxation factors are key for maintaining stability and finding convergence, since they improve diagonal dominance in steady-state simulations. The relaxation factors shown are the result of a trial and error to find convergence without losing the quantities of interest. Table 12 summarizes the final values used, as well as the residual control as a criteria for convergence in each variable.

Variable	Relaxation factor	Residual control
<code>p</code>	0.5	1e-4
<code>rho</code>	0.05	1e-3
<code>U</code>	0.3	1e-3
<code>k</code>	0.3	1e-3
<code>h</code>	0.7	1e-3
<code>omega</code>	0.4	1e-3
<code>nut</code>	0.7	1e-3
<code>K</code>	0.3	1e-3

Table 12: Simulation control.

The domain decomposition for parallel computation will be in 4 different domains of analysis, by dividing it with the decomposition method `scotch`, which optimizes the

number of cells and shared faces in the overall computational domain. A maximum of 9000 iterations will be set to find convergence, otherwise the simulation will stop with the last 10 iterations saved for post-processing. Additionally, several graphs related to residuals, heat flux through walls, some probe values for temperature and velocity in a passenger seat will be plotted on-the-fly. Next, the file of the **fvSchemes** is shown, where the on-the-fly tuning was essential to monitor convergence.

fvSchemes file setup used for finding convergence

```
ddtSchemes
{
    default                steadyState;
}

gradSchemes
{
    default                cellLimited Gauss linear 0.9;
    grad(U)                cellLimited Gauss linear 0.9;
    /*high limiters, and diffusive*/
}

divSchemes
{
    default                none;
    div(phi,U)             bounded Gauss upwind;
    div(phi,k)             bounded Gauss upwind;
    div(phi,h)             bounded Gauss upwind;
    div(phi,K)             bounded Gauss upwind;
    div(phi,omega)         bounded Gauss upwind;
    div(((rho*nuEff)*dev2(T(grad(U)))))) Gauss linear;
    /*first order schemes for stability*/
}

laplacianSchemes
{
    default                Gauss linear limited 0.1;
    /*limited laplacians*/
}

interpolationSchemes
{
    default                linear;
}

snGradSchemes
{
    default                limited 0.1;
}
```

It must be noted that the accuracy of the solution is low: limited gradients and laplacians, diffusive limiters and first order schemes will give as output a diffusive solution. This is expected for a coarse mesh, which cannot capture well the numerics of the problem, but the setup that was made is a powerful tool for finding convergence in the next steps, where the time frames are much larger.

To determine whether convergence has been found, not only the residuals must be monitored, but also quantities of interest. To this purpose, three important types of quantities of interest were additionally evaluated when dealing with on-the-fly plots.

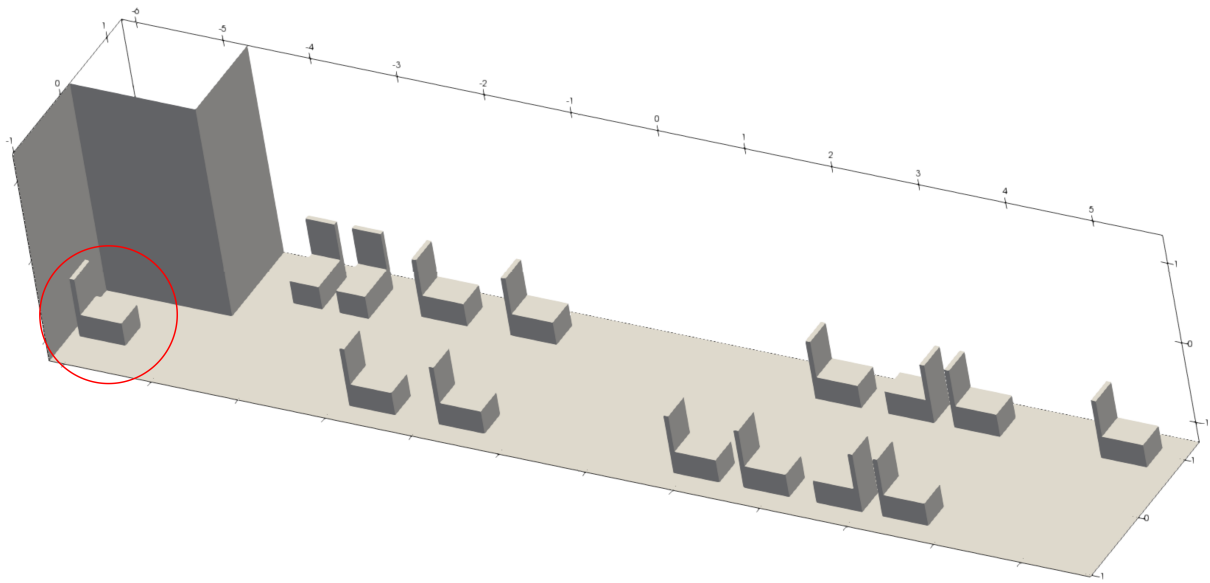


Figure 35: Bus seat chosen for sampling.

- Velocity magnitudes: three probe points were selected for evaluation. These were sampled in approximate body locations where ankle, waist and head levels are located, according to **ASHRAE-55** standard. Considering that the input-output is time consuming and computationally expensive in the solving process, a few probes must be done. In this case, only one passenger seat was sampled, since this location is the most prone to be uncomfortable, but also to be unsteady given the location of the inlets. In Figure 35 is depicted the seat where the probes were placed. The height levels used are "Seated" according to the table shown in Figure 13.

State	Height Level (m)		
	Ankle	Waist	Head
Seated	0.1	0.6	1.1
Standing	0.1	1.1	1.7

Table 13: Average temperature measuring according to **ASHRAE-55**.

Velocity magnitudes plots are shown in Figure 36. The simulation stopped at ≈ 6000 iterations, even if at 4000 iterations the three quantities of interest were almost converged. The reason can be seen by looking at the residuals plot shown in Figure 41, recalling that for p the convergence demanded is 10^{-4} . However, it is clear that after 4000 iterations a spurious behaviour in the three curves appears. Nonetheless, the order of variations is small for the purposes of thermal comfort assessment, since changes of velocity of $\pm 0.05 \text{ m/s}$ are considerable. In this case, the variations found after 4000 iterations are less than 0.005.

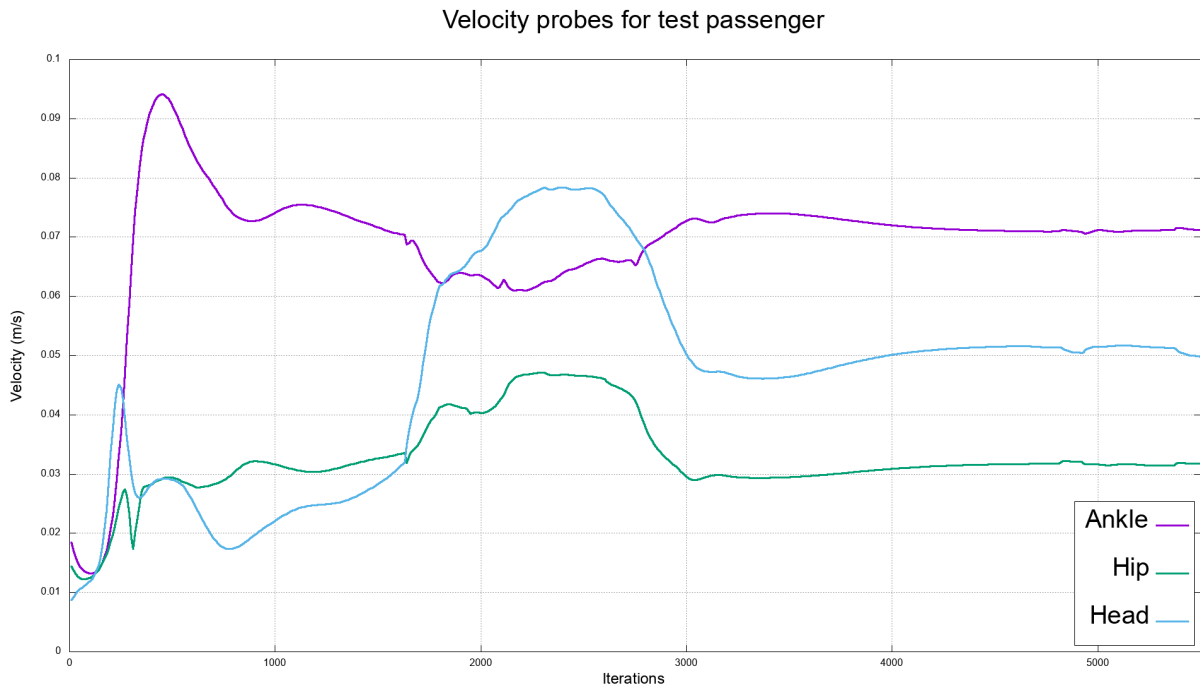


Figure 36: Velocity probes convergence for test passenger.

- Temperature: the same applies for temperature, where the samples must be taken according to the standard shown in 13. Data must be averaged and, in conjunction with the average air speed, will define the usage of the **PMV-PPD** model for thermal comfort.

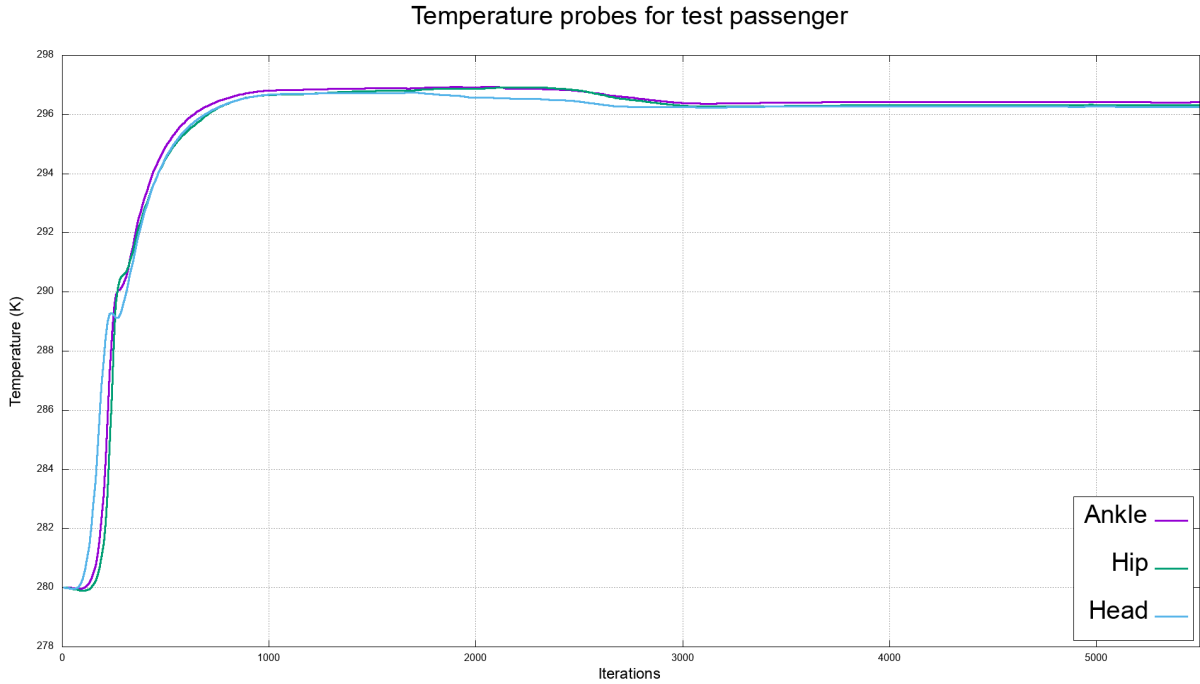


Figure 37: Temperature probes convergence for test passenger.

In the above Figure, the convergence of temperature probes is shown. During the first 1000 iterations, a "transient" behaviour can be seen for the three curves. Even though, the temperature values through iterations is quite similar for the three height levels, with a convergence temperature of $\approx 296 K = 23 ^\circ C$. It must be noted that, even if the temperatures are quite similar visually, in thermal comfort the order of magnitude for temperature can be as low as $0.01 ^\circ C$. So the temperature probes must consider at least 2 decimal digits.

A summary of both the temperatures and velocity magnitudes are depicted in Table 14, where the average temperature and velocity were computed.

	Level			Average
	Ankle	Waist	Head	
Velocity (m/s)	0.072	0.031	0.049	0.051
Temperature (K)	296.42	296.32	296.27	296.33

Table 14: Velocity and temperature probes summary.

Additionally, the average values for each variable were computed, since those are input parameters for the **PMV-PPD** model described in the **ASHRAE-55** standard. The values given here, in addition to some characteristics are the inputs to assess thermal comfort through the Predicted Mean Value function. For this particular case it will only be calculated as a demonstration, even if it has no particular

meaning at the moment.

$$PMV(clo, met, wme, T_A, T_R, V_A, \phi) \quad (8)$$

Where the variables in the PMV function stand for:

- **clo** represents the clothing insulation of the person analyzed.
- **met** is the metabolic rate of the person, where Table 1 can be used as reference for standard activities.
- **wme** is the external work exerted on the person, generally it is taken as 0.
- **T_A** stands for air temperature, which is taken as the average value obtained with the height levels shown in Figure 13.
- **T_R** is the mean radiant temperature, which depends mainly on the location of measurement.
- **V_A** represents the air velocity, which is taken using the same averaging method mentioned in the T_A point.
- **ϕ** is the so called relative humidity of air, which represents the content of moisture in air with respect to the saturation level.

Table 15 shows the values used for estimating the PMV value of the test passenger. These values represent a seated passenger, relaxed, with winter clothing and no external work applied on him/her. It must be noted that the relative humidity was chosen as 0% just as a critical value, since extreme values of relative humidity tend to augment discomfort. Additionally, the mean radiant temperature was used equal to the air temperature, since generally this parameter is measured *in situ*. As a reference the PMV value must comply with

$$-0.5 \leq PMV \leq 0.5 \quad (9)$$

in order to declare as "thermally comfortable" a location.

clo (clo)	met (met)	wme	T _A (°C)	T _R (°C)	V _A (m/s)	ϕ
1	1	0	23.18	23.18	0.051	0

Table 15: Test passenger values used for PMV estimation.

The shown values lead to a **PMV_{test passenger} = -0.35**, so that the test passenger can be classified as a comfortable one. The previous computations for thermal comfort have two intentions: to exemplify and give an insight of the PMV method and

to determine an approximate value of inlet conditions (air velocity and temperature) that provide thermal comfort in a passenger located in a potentially critical position.

- Heat fluxes: in addition to the former quantities, heat fluxes must be monitored in order to represent convergence. Indubitably, depending on the surface where heat transfer is analyzed, the convergence could be uncertain. That is why every surface will be plotted in a single graph. This kind of monitoring allows to visualize the heat flux data through the body of the bus and to compare surface with different magnitude orders of heat flux.

In the graph displayed below, all the heat losses were plotted against the number of iterations. It is evident that around iteration 1000 convergence is almost reached. Around 2000 iterations were used for stating complete convergence. On the other hand, most heat losses are negligible compared to the *Left window* heat loss. However, the area of this window covers all the bus length.

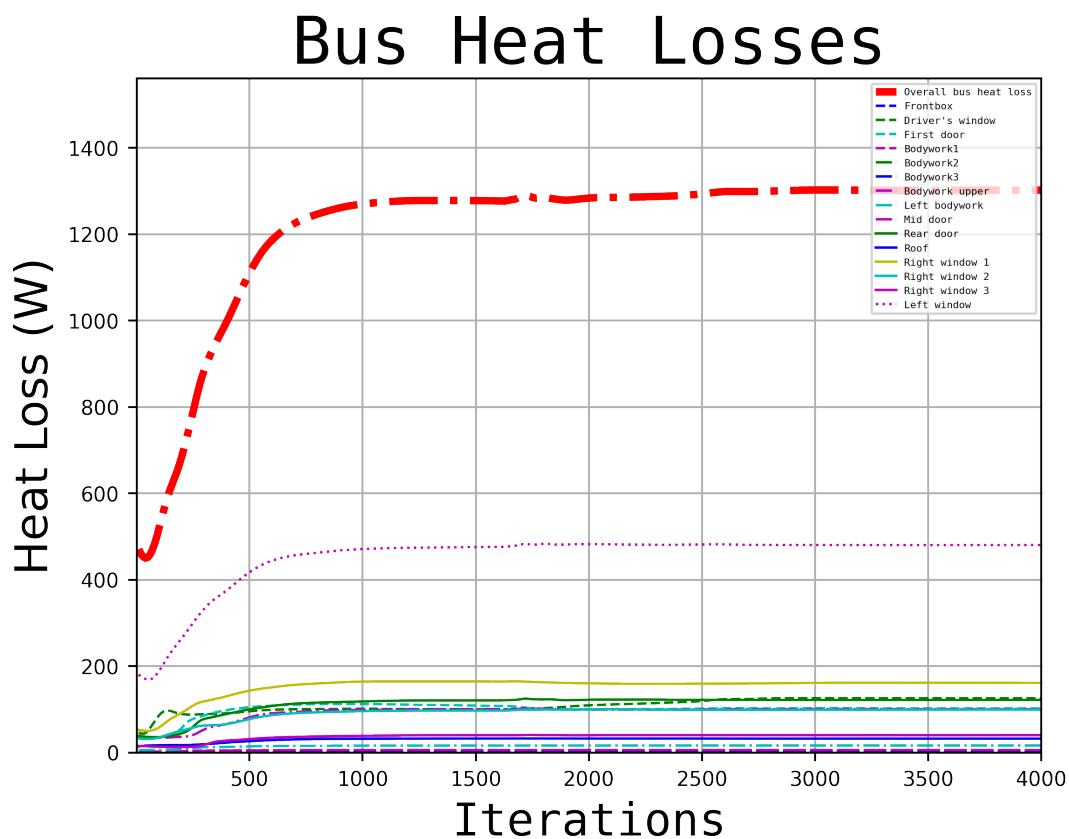


Figure 38: Heat loss through bus.

Nonetheless, conclusions can be made with the next two plots, which isolate the bodywork losses and the glass losses. The former plot is shown in Figure 39, whereas the latter is depicted in Figure 40.

Bodywork Heat Losses

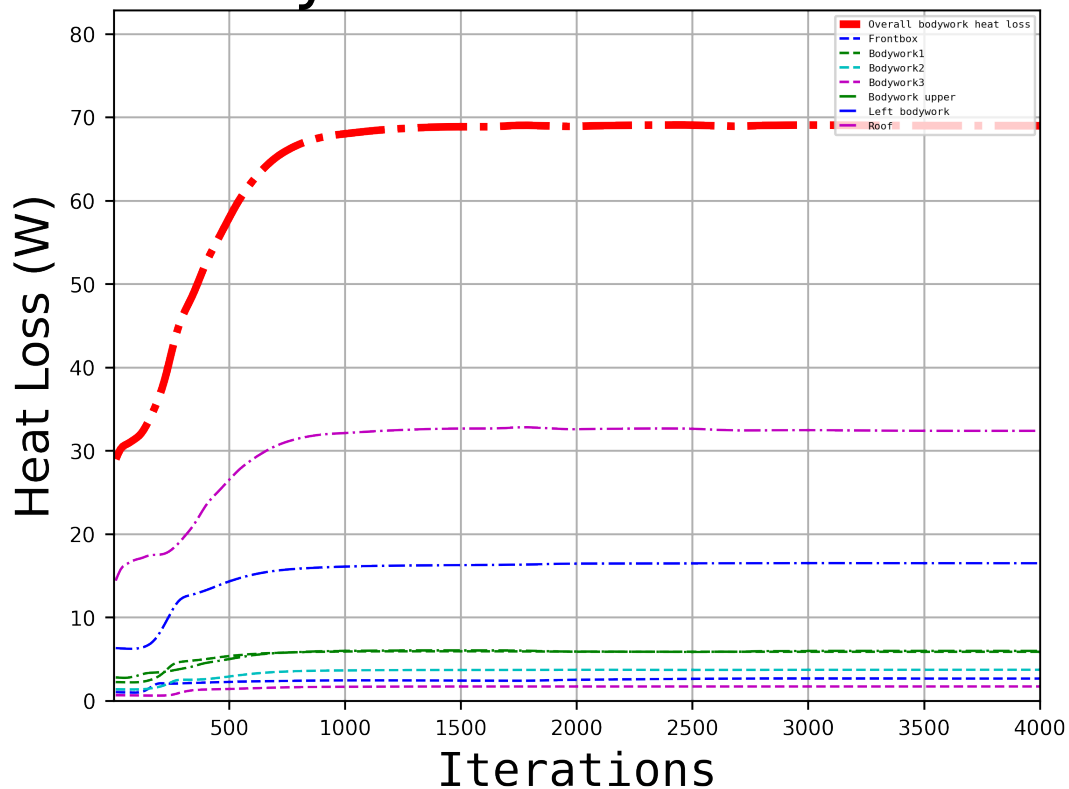


Figure 39: Heat loss through bodywork.

It must be noted that for bodywork and glass heat loss, the surfaces were oversimplified. For instance, the roof may have irregular layer thicknesses depending on the place where it is analyzed: several structures, such as the battery compartment or inter-layer cables, can act as insulating or conductive heat resistances. The same occurs for the bodywork panels, where wires and internal functioning structures can be present inbetween the steel external panels and the PVC internal panels.

Glass parts, such as windows and doors were simplified: plastic frames of both windows and doors were not considered for the analysis. Even though, in a worst-case scenario it is expected to overestimate the heat loss through windowed surfaces in a small quantity.

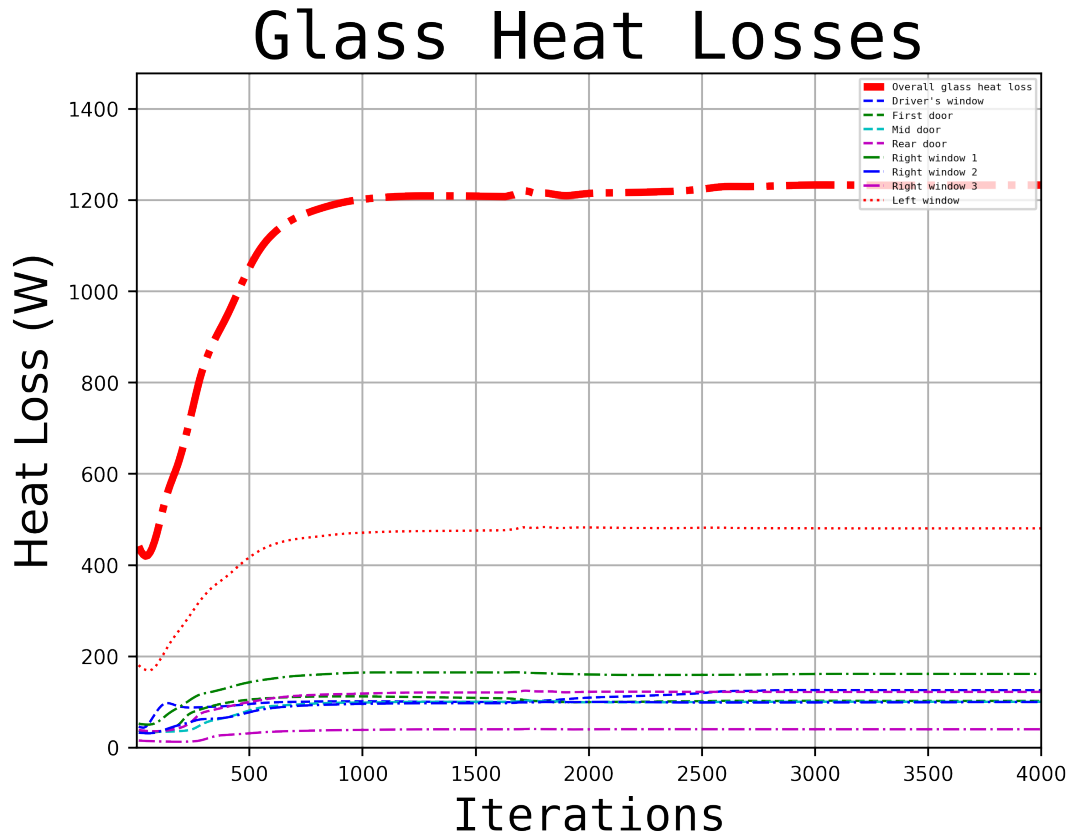


Figure 40: Heat loss through glass surfaces.

The order of loss magnitude is much higher through glass, compared to the bodywork heat loss converged value. Glass heat losses are almost 20 times higher than bodywork losses. This is expected, as the thermal resistance of the bodywork is composed of three layers, where one of them is an insulating material with an extremely low conductivity, whereas glass surfaces are much thinner. Even if glass does not have a high thermal conductivity, it cannot be considered as an insulating material.

Table 16 summarizes the heat losses in the converged solution, after 5700 iterations. It is clear the magnitude difference between isolating layers and glass. Glass heat losses are quite similar, the only exception is the *Left window* which has a larger area. Nonetheless, by comparing it with the sum of the *Right windows* a difference of $\approx 180\text{ W}$ can be found. The overall loss value obtained will be used for an energy balance confirmation.

Finally, the residuals were plotted for each variable. It must be noticed that at several points some peaks were found. This is the result of the on-the-fly tuning. Generally speaking, most of the parameters changed were the relaxation factors. Nevertheless, the spurious peak depicted between iteration 1600 and 1800 is due to the change in the `laplacianSchemes` from 0.1 to 0.4, afterwards this value was returned to its original value

Surface	Heat loss (W)
Bodywork	
Frontbox	2.7
Bodywork1	5.9
Bodywork2	3.7
Bodywork3	1.7
Upper bodywork	6.0
Left Bodywork	16.5
Roof	32.4
Total bodywork	69.0
Glass	
Driver's window	125.8
First door	102.5
Mid door	100.3
Rear door	121.9
Right window 1	161.3
Right window 2	99.3
Right window 3	40.1
Left window	480.0
Total glass	1231.2
TOTAL OVERALL	1300.1

Table 16: Heat loss through surfaces

of 0.1 since the chaotic behaviour did not stop. Most of the time, the relaxation factors of p_rgh , U , k and ω were the tuned ones. In general, p_rgh and U were the foremost tuned which led convergence:

- p_rgh was adjusted between 0.2 and 0.5, with better convergence using 0.5, but with higher values the initial residual does not decrease.
- U was tuned within a range of 0.3 to 0.7, with values near 0.3 giving convergence towards 10^{-3} . Lower values tend to slow down noticeably the convergence.
- k and ω both were also maintained between 0.3 and 0.7 but when changing those relaxation factors they tend to show better convergence related to those variables, rather than general convergence. Nonetheless, if ω grows without limit by means of a wrong choosing of relaxation factor, it will tend to increase all residuals of the variables, showing a volatile behaviour.

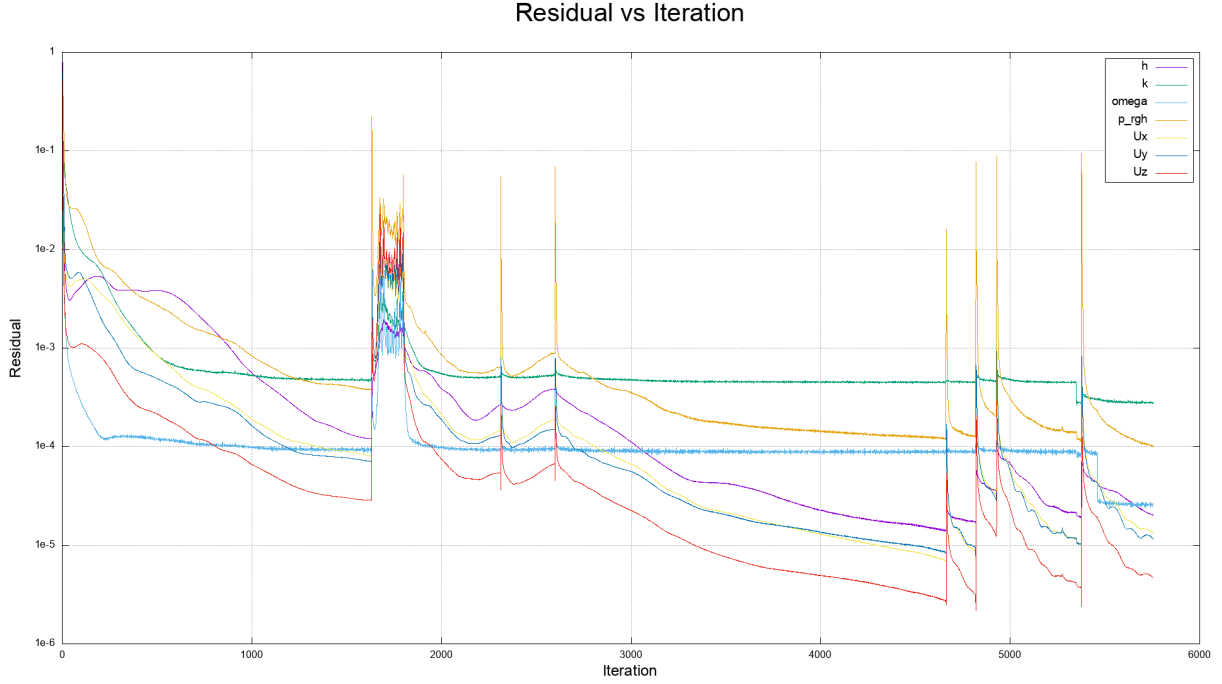


Figure 41: Residuals plot for each analyzed variable.

To confirm the validity of the simulation, the energy conservation in the bus control volume was executed. This type of confirmation is useful to find additional errors in the solution. Theoretically, the method is conservative, but round-off errors could apply. The equation for the energy conservation³³ relates the enthalpy of the fluid entering and the forms of energy going out of the control volume, i.e. outlet enthalpy of the flow and heat loss through solid walls of the bus:

$$\dot{m}_{inlet} \cdot h_{inlet} = \dot{m}_{outlet} \cdot h_{outlet} + \dot{Q}_{walls} \quad (10)$$

The last term was already calculated when dealing with wall heat losses. For the other terms, OpenFOAM has several post-processing features to calculate the inlet and outlet enthalpy. One of them is calculate the weighted sum of each inlet, with the weights ϕ , the local flow rate, and weight value h , the specific enthalpy. The specific enthalpy can be expressed as:

$$h = c_p \cdot (T - T_{ref}) \quad (11)$$

where c_p is specific heat capacity of the fluid at constant pressure, and T_{ref} is a reference temperature. In practice, the reference temperature has no influence in the results, since the important characteristics are computed as differences of variables, thus cancelling the T_{ref} value. The values assigned were:

³³Equation 10 is a simplified form of expressing the divergence theorem through the control volume. The real equation involves surface integrals representing the inflows and outflows, and the addition of the first law of thermodynamics, relating heat and work.

- $c_p = 1010 \frac{J}{kgK}$

- $T_{ref} = 0 K$

According to Incropera’s textbook, c_p for dry air is $1007 \frac{J}{kgK}$. The reason to use $1010 \frac{J}{kgK}$ instead is to consider air humidity, which depending on the humidity ratio changes its value. Variations are almost negligible, with changes within the order of $\approx 0.5\%$. With the previous remark, by evaluating the enthalpy flow through boundaries:

	Value (W)
In	
Roof AC	89113.340
Out	
Recirculation	56042.310
Extractor fan	31771.040
Surface exchange	1300.143
Error	-0.153

Table 17: Overall energy balance.

The difference in energy balance is less than $0.2 W$, which compared to the minimum order of energy flow magnitude through the control volume (surface heat exchange) can be neglected without further caution. Therefore, the error in the simulation is fairly low.

5 Real bus simulation

5.1 Geometry

In the previous sections, a description of the complete simulation process, from beginning to end, was provided. The relevant items of the real bus used will be described in this section. Of course, it will be done with much less detail, since it is less relevant and is virtually identical to the procedure of making the *bus test case*.

The geometry was provided by Gruppo Torinese Trasporti (GTT), whose personnel handed over all the available datasheets at the moment of development of this research. Additionally, GTT personnel fixed several appointments to analyze, take photos and measure all the bus structures, to get as much real data as possible. There will be, indeed, differences with the bus shown in the latter pictures and the simplified geometry made in the CAD software: the position of seats, its number, level of detail in all features (windows, seats, driving wheel, etc) are contrasting.

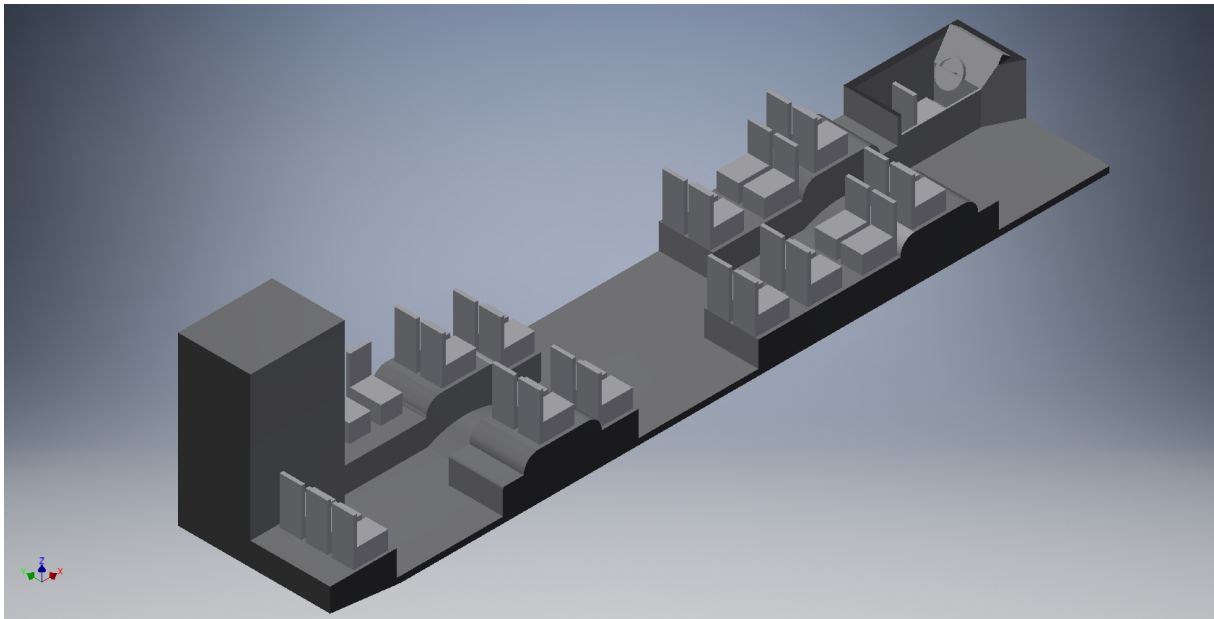


Figure 42: Bus base geometry.

Here, the main structures that must be re-designed with respect to the test case will be shown and described, as well as the assumptions that will be made due to complexity of geometries. The first structures to be analyzed are the inlets: the location of these are unlike their original position in the test case. Figure 43 shows the grilled structures that define the actual inlets found in the GTT bus.



Figure 43: Grill inlets of BYD K9® bus.

The dimension of these grill holes is $0.7\text{ cm} \times 2.5\text{ cm}$ and each blue-grill structure has a total of 35 holes, placed cyclically throughout the grill. Furthermore, these have an even placement along the bus, as it can be seen in Figure 44.

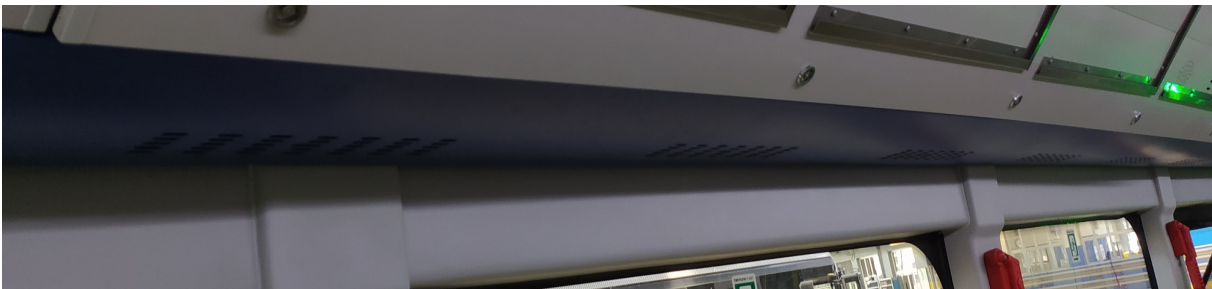


Figure 44: Blue inlets are evenly distributed throughout the bus length.

There are additional bus grills that can be considered. In Figure 45 two additional types of grills that can be used as inlets are shown. Both the oval-shaped and rectangular grills are to be used if additional inlets are desired, but they only change the distribution of air flow rate rather than the amount of hot air delivered to cabin. This can be understood by looking at Figure 46, where the direct air ducts that connect the rooftop unit are shown.



Figure 45: Oval shaped and rectangular shaped grills.

The image below is an horizontal view of the air ducts found when opening the grills case. The ducts point downwards to the air distribution compartment, where air is distributed along the blue and grey grills, if they are open. The rooftop AC unit is found at the mid-rear length of the bus, as well as the ducts shown in Figure 46. These ducts are **not** distributed through the entire length of the bus, but only in the top mid part of the casing.



Figure 46: Air ducts connected to the rooftop AC unit.

Yet, for the purposes of this research, the grey vents will not be considered. The reason is because of the added complexity that is carried with these kind of vents. Both the oval and rectangular grills point in non-straight angles, so that they do not deliver air vertically nor horizontally into the cabin. At the moment of measuring the bus *on the field*, the instruments needed for gauging angles were not available for use. Additionally, GTT personnel stated that generally those vents are closed, and they are

open when high flow rate is being used for the thermal regulation in the cabin. Thus, only the blue vertically-oriented grills will be utilized as inlets.

The number of blue inlets is 25: the non-door side has 14 inlets, whereas the door side has 11, because upon the doors there are no inlets. The modeling of this structure will be carried out with an equivalent area, to maintain the average velocity of delivered air. Thus, the vent areas will be approximated as rectangles with the following dimensions:

$$0.7 \text{ cm} \times 2.5 \text{ cm} \times 35 \text{ holes} = 61.25 \text{ cm}^2 \text{ each inlet} \quad (12)$$

On the other hand, two types of air outlets are installed. These are the extractor fan and recirculation vents. The former has rectangular dimensions and is located on top of the rear corridor, in front of the final door. It has rectangular dimensions of $77 \text{ cm} \times 50 \text{ cm}$ and its main function is to exhaust the internal air in for maintaining stability in pressure and generate a ventilation current with the fresh oncoming air from the condenser.

The recirculation vents are very different from the ones depicted in Section 4.3.1. In reality, these are located in the middle of the bus, in front of the mid door. The differences are noticeably clear by looking at Figure 47. Instead of multiple channels located at the floor height these are two high placed ducts at the very center of the roof. Their rectangular measure is of $14 \text{ cm} \times 167 \text{ cm}$ and they are placed symmetrically on top of the main corridor.

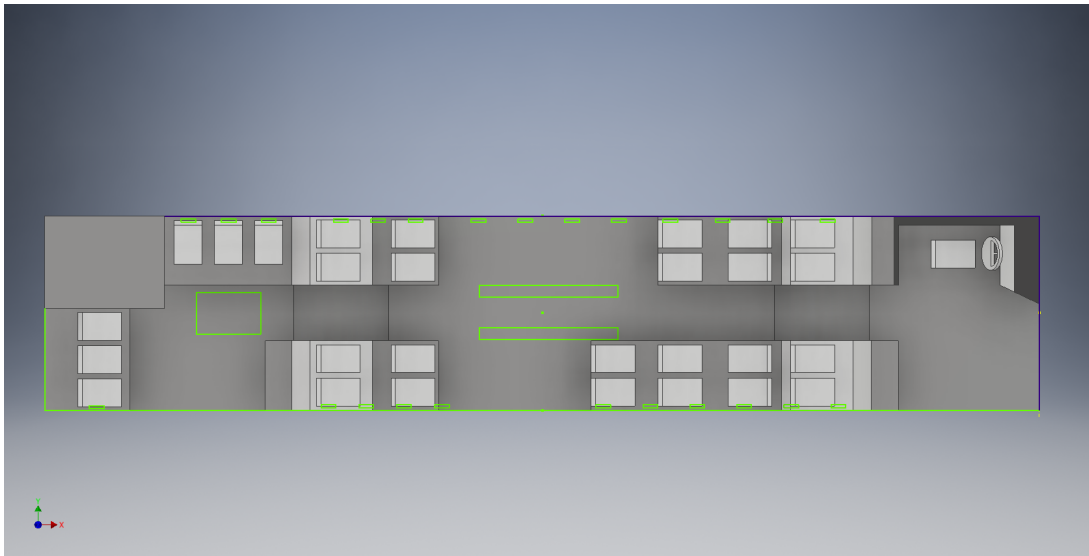


Figure 47: Upper view of the geometry.

5.2 Mesh

The final mesh needs to be more accurate in order to have reliable results. But the trade-off to be faced is the time frame that would take to develop and simulate a finer mesh. The bus test case had an approximate of 250,000 cells, and the convergence of the

solution takes 30 minutes with the appropriate relaxation factors and using a convergence tolerance of 10^{-3} for the pressure `p_rgh`. Even though, the required simulation time is dependent on the mesh size and the problem. There is no rule of thumb that can relate the time of computation with the mesh size. The best way to assess this is by trial and error. As a first approach it will be supposed that there is a linear relation between time of computation and mesh size. In that case, for a simulation with 10 hours of elapsing time, it should be used a mesh of $\approx 5,000,000$ cells to find convergence. An important remark is that the residuals are not the scope of analysis, it is merely a metric to be monitored and find **divergence** rather than **convergence**.

Similar to the process done in Section 4.3.2, the mesh will be composed of several blocks, being the ducts of a structured type, whereas the body of the mesh will be an unstructured one, composed of tetrahedral and pyramidal cells.

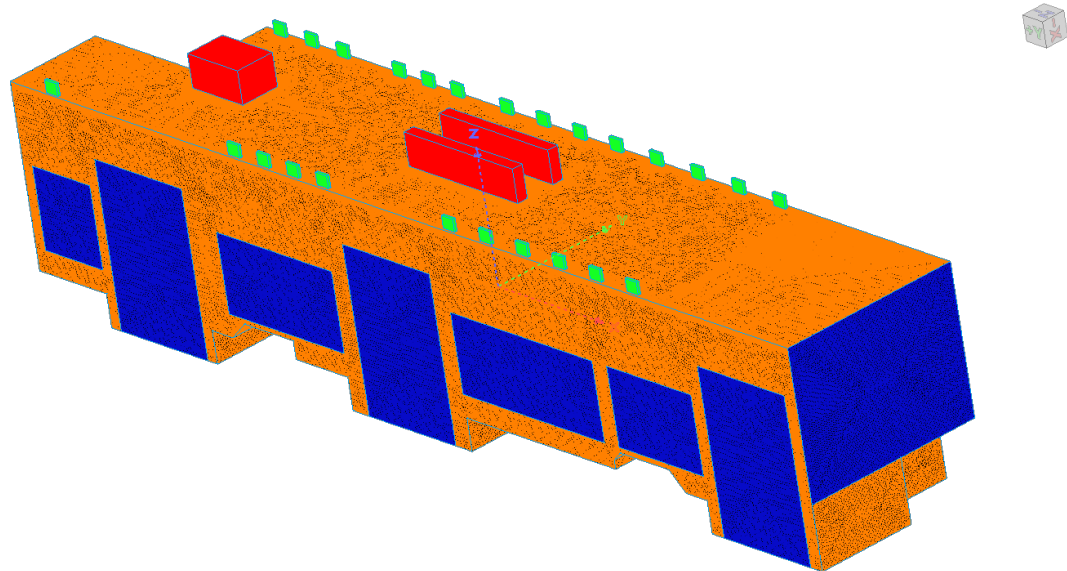


Figure 48: General view of final mesh.

In Figure 48, the mesh has been colorized depending on the structure type, where green, red, blue and orange has been assigned to inlets, outlets, glass and bus body, respectively. The same procedure for mesh initialization used in the test bus was followed, the difference now is that the mesh has been constructed with an average size of 3 cm for the 1D structures of the body. On the other hand, the inlet and outlet structured elements have an average size of 1 cm.

The roof, left and right side of the bus are near-inlet walls. The choice of meshing the body with different size to the inlets can put at risk the results of the simulation, due to the volume ratios. To compensate this difference, several key points of 1D structures were resized locally, so that near inlets a local refinement was achieved, but far from them the

mesh tends to be coarser, as depicted in Figure 49. The refinement was chosen so that the size of the edge in an inlet zone is 1.5 cm.

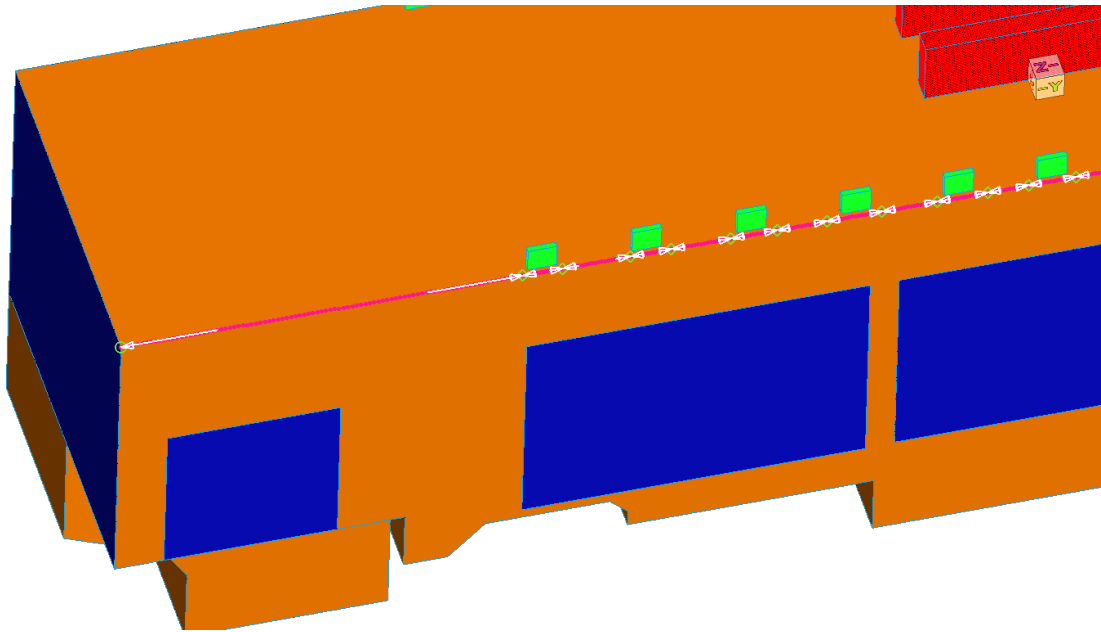


Figure 49: Breakpoints in roof's left side for refinement in near-inlet walls.

Below, a summary of the metrics for mesh quality is shown, where it is clear that every value accomplishes the requisites for `OpenFOAM`. Moreover, the mesh is of pretty high quality, so it takes less time in the SIMPLE loop and admit even higher order schemes, recalling that the test bus simulation was done with first order schemes and gradient limiters.

Metric	Maximum value
Aspect Ratio	6.625
Volume Ratio	12
Maximum Included Angle	156°
Skewness	0.65
Non-orthogonality	63.5°

Table 18: Metrics of the final mesh.

The table shows that the maximum value of skewness and non-orthogonality are fairly good. Even more considering that the non-orthogonality average has a value of 20.9°. Volume ratio and aspect ratios are quite high, but they do not represent the majority of cells, where only 12,250 have an aspect ratio between 10 and 12, whereas the rest ($\approx 5,000,000$) have a volume ratio less than 3. In overall, the mesh has good quality to try and use higher accuracy schemes. Below is shown a cut of the mesh which shows a much finer distribution in all the control volume.

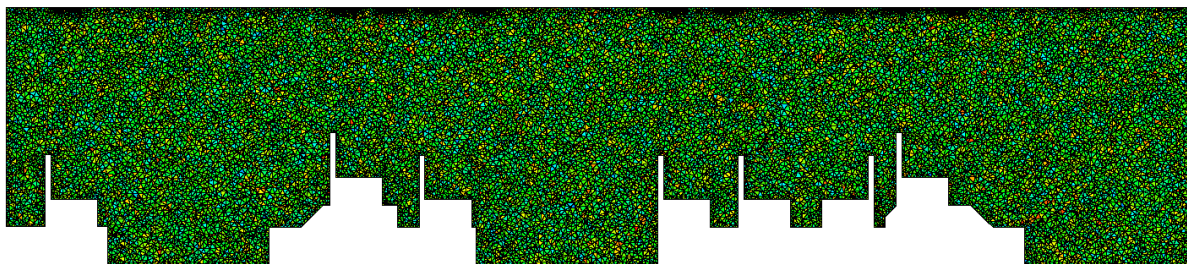


Figure 50: Cut of the mesh showing non-orthogonality color map.

Figure 50 is a cut of the right side of the bus. The doors were placed inbetween rows and inbetween frontbox and first row prior to the meshing. Figure 51 depicts the result of the refinement in near inlet spaces. In this view, the refinement of the last rear inlet is shown colorized according to the volume ratio parameter.

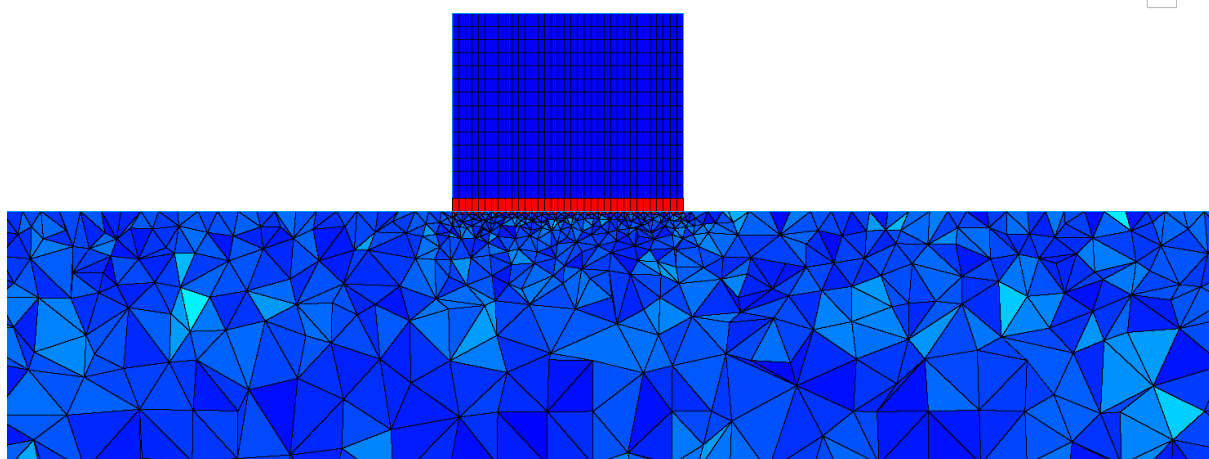


Figure 51: Volume ratio cut plane in near inlet zone.

5.3 Simulation and post-processing

The final step to finalize this chapter is the simulation and post-processing setup. The CFD code has virtually no difference with that carried out in the test case, but only the inlet temperatures to be used as input. The scope is to run two simulations, assess

thermal comfort in each one, and determine which is the best temperature for ensuring passenger's thermal comfort by interpolating (or extrapolating) the results. It even could occur that is not possible to achieve comfortable conditions for every passenger, but this will be evaluated with the post process data.

Since convergence was found using first order schemes, limited gradients and interpolation schemes, the same setup will be used here. The difference will be visible after stability is reached. When this happens, U,h and K will be switched to `linearUpwind` to enhance the accuracy of the results. In addition, the value of the gradient limiters will be lowered as well as the `laplacianSchemes`. By raising the accuracy, the obtained values will be more reliable and comfort will be less prone to over or underestimation. The following is the last code used for the schemes. It can be noticed the upgrade reached by using less diffusive schemes in the `gradSchemes` and `laplacianSchemes`. Gradient calculations are much more accurate, since the limiter was set to 0.1 and the accuracy improvement by setting the multi-direction limiter `cellMDLimited` rather than the equal-direction limiter `cellLimited`. Also, `laplacianSchemes` were bettered by rising the blending factor to 0.5.

fvSchemes file setup implemented for final iterations accuracy

```

ddtSchemes
{
    default                steadyState;
}

gradSchemes
{
    default                cellMDLimited Gauss linear 0.1;
    grad(U)                cellMDLimited Gauss linear 0.1;
    /*Low vectorial limiters, high accuracy*/
}

divSchemes
{
    default                none;
    div(phi,U)             bounded Gauss linearUpwind grad(U);
    div(phi,k)             bounded Gauss linearUpwind default;
    div(phi,h)             bounded Gauss upwind;
    div(phi,K)             bounded Gauss linearUpwind default;
    div(phi,omega)         bounded Gauss upwind;
    div(((rho*nuEff)*dev2(T(grad(U)))))) Gauss linear;
    /*Second order schemes with accurate gradients*/
}

```

```

}

laplacianSchemes
{
    default                Gauss linear limited 0.5;
    /*Stable and accurate laplacians*/
}

interpolationSchemes
{
    default                linear;
}

snGradSchemes
{
    default                limited 0.5;
}

```

During the test case simulation, when testing higher order schemes, it could be seen that sufficient convergence of the results was not achieved, particularly for the turbulent variables and enthalpy. Temperature tended to diverge or a negative Kelvin temperature was found after some iterations. To fix this issue, the `fvOptions` file allows the user to set a property to certain blocks. In the file, temperature was limited so that its computations were not able to reach values below or above the limits. The upper limits depend on the simulation, but for the lower limits the value chosen was the external temperature of the bus i.e. $-3.3\text{ }^{\circ}\text{C} = 270\text{ K}$. For the upper limit value, it was chosen the inlet temperature.

The inlet temperature was selected on the basis of the outcome of the test case. The value used was 296.6 K , which led to a rear passenger in comfort conditions. A word of caution, since the obtained result is extremely inaccurate and could lead to wrong conclusions. However, since this is the only reference, it will be used for the first simulation, bearing in mind that the outputs were satisfactory as test results. The exact same applies for the volumetric flow in the inlet: considering there is no further knowledge about "comfortable inlet flows", the value of $900\frac{\text{m}^3}{\text{h}}$ is the one to be used throughout the oncoming simulations, since the air speeds were low enough, meaning that no surplus of energy is being used for delivering tempered air into the bus. In addition, low velocities tend to be more versatile for thermal comfort because greater ones tend to require higher temperatures for ensuring thermal comfort. As an example, the range of comfort for a velocity of 0.1 m/s , in the winter conditions used in this thesis³⁴, is in the range of $21.4\text{ }^{\circ}\text{C}$

³⁴1 clo, 1 met for a seating person, $T_R = T_A + 2.8\text{ K}$ and a relative humidity of 50%

to $25.3\text{ }^{\circ}\text{C}$, whereas for a velocity of 1 m/s it is needed a temperature of, at least, $25.1\text{ }^{\circ}\text{C}$, which clearly is more energy consuming both for the air mass flow required (\dot{m}) and the higher temperatures to be reached (ΔT).

This time, instead of one probe for the presumably most uncomfortable passenger, multiple probes will be sampled at different locations. The probes will be plotted during the simulation in order to monitor convergence and, after that, smoothing will be applied to the plotted variables in case steadiness is not reached. The sampling will be done in 7 key locations, taking both temperature and air speed values at ankle, waist and head levels. The locations to be sampled are shown in Figure 52, where the choosing of passenger was based on the row and the expected tendency to be uncomfortable. This trend of discomfort is evaluated by means of density of inlets near the passenger and distance to windows or doors. For instance, passenger 1, 4 and 7 are located in highly uncomfortable zones due to the scarcity of inlets in their surroundings. Left-side seats tend to be more comfortable due to higher number of inlets and less glass surface, which reaches the lowest temperatures. Even though, front passengers have a clear lack of inlets and should have tendency to cooler thermal perceptions.

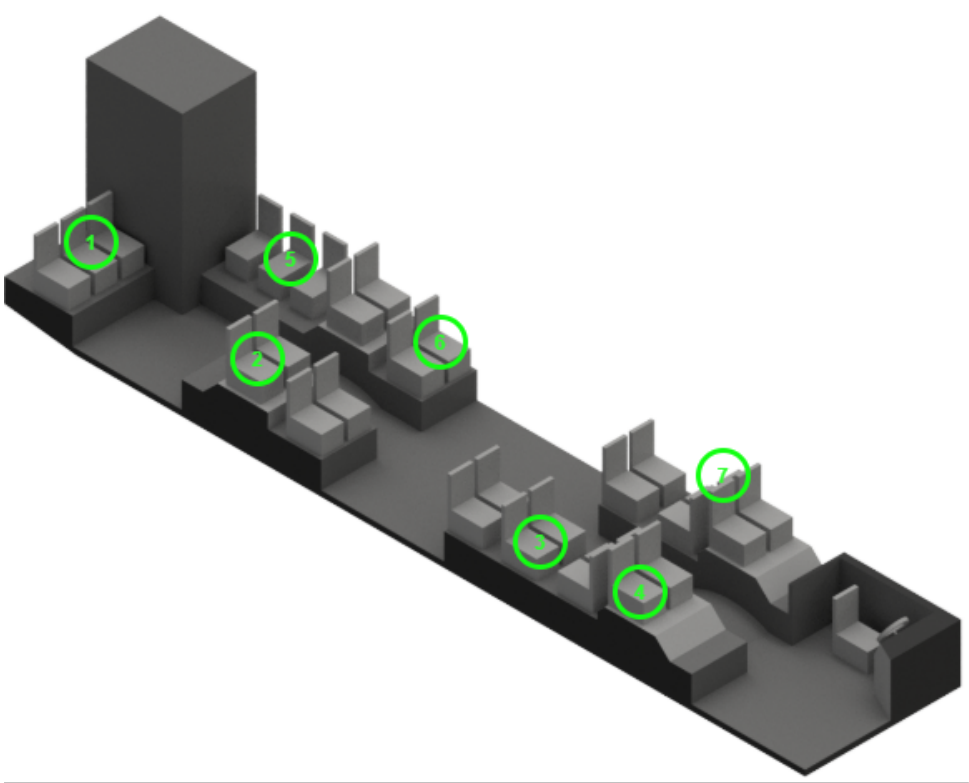


Figure 52: Sampling locations for thermal evaluation.

6 Thermal comfort assessment and results

The final goal of this investigation has a practical purpose: to minimize the energy consumption while maintaining thermal comfort in the bus cabin. With the results already obtained, there is a final tool that must be employed to complete the analysis. That is to answer the question on how to assess thermally pleasant conditions. In literature there is plenty of models to determine whether a person is in that state or not.

To retain a standardized and validated result, the **ASHRAE-55** of 2017 book for thermal comfort will be the guide text. To this aim, the relevant definitions given here by the authors are provided below, to determine which are the values of comfort with the existing heating unit with the used definitions clear.

6.1 Concepts in thermal comfort

Some of the concepts used to address thermal perception were explained in Section 4. Here, the additional notions to be known by the reader are defined in further detail:

- **Average air speed**(V_A) and **temperature**(T_A) define representative values of the velocity magnitude and temperature surrounding an occupant. The average is calculated as the mean found in three points: ankle, waist and head heights. Its calculation depends on whether the occupant is seating or standing, as depicted in Table 13.
- **clo** and **met** are the units used to express thermal insulation by clothing and metabolic rate, respectively.
- **Thermal environment** is the sum of all conditions that affect a person's heat loss through the body regulation processes.
- **Metabolic rate** is the transformation of chemical energy to heat and work in a person, in order to comply with its normal activities, per unit of surface area.
- **PMV** is the acronym for **Predicted Mean Vote**, and represents an index which measures statistically the mean sensation of a large group of persons in a thermal sensation scale. The reference sensation scale is shown in Table 19. The source code is partially provided in Annex A3.
- **PPD** as well is the acronym for predicted percentage of dissatisfied, similar to the PMV value is an index that gives a quantitative prediction of the percentage of people that would be thermally displeased with the thermal conditions calculated with the PMV equation.

PMV	Sensation
+3	Hot
+2	Warm
+1	Slightly warm
0	Neutral
-1	Slightly cool
-2	Cool
-3	Cold

Table 19: PMV sensation scale.

- **Operative temperature**(T_o) is defined as the temperature of an imaginary black enclosure, in which occupants would exchange the same amount of heat by all means of heat transfer.³⁵

The same table mentioned in Section 4 will be used. The difference here is that it will not be analyzed for only one passenger, but rather all key passengers that were on probe locations. Some values are predefined: the clothing insulation is set to 1, which is a representative value for people in winter conditions; the metabolic rate was set to 1 representing a seating relaxed user according to Table 1 and the external work was set to 0, since there is no external work influence at the bus cabin.

On the contrary, the temperatures, average speed and relative humidity must be computed from the output of the simulation, so T.D. is the acronym for "To determine" in the following table. In any case, relative humidity tends to have a minor role in the evaluation of PMV under these circumstances.

clo (clo)	met (met)	wme	T_A (°C)	T_R (°C)	V_A (m/s)	ϕ
1	1-1.2	0	T.D.	T.D.	T.D.	T.D.

Table 20: General table used for thermal assessment.

6.2 Inputs and thermal calculations

Additionally, it must be remarked that the maximum heating capacity of the roof unit is 16 kW. Thus, at the end of the simulation, heat power supplied to the oncoming air plus the recirculated air must not exceed the heating capacity. This is an important confirmation, but it is possible to modify the recirculating air percentage in order to reduce energy consumption and find a suitable value of heat power supplied. The disadvantage on increasing the recirculation percentage is due to additional humidity in air. Nonetheless,

³⁵The mean radiant temperature must be measured in-place. It will be assumed that it is equal to $T_R = T_A + 2.8^\circ$ for the sake of simplicity. This value comes from ASHRAE-55 which addresses that, under certain conditions, this value can be used if no data is available.

in the PMV model, humidity tends to change fairly low the thermal comfort sensation, so it will not be argued in further detail its influence and, rather, it will be taken as 50% assuming that the roof unit has the capability of dehumidifying up to this value.

To compute the PMV value for each passenger, all the functions involved were coded in Visual Basic, the coding language used in MS Excel. Basically, the code considers all kind of thermal parameters to finally return as output the PMV value: it receives as input the variables chosen in Table 20, and computes clothing surface temperature, as well as heat loss through skin, sweating, respiration, radiation and convection. The final result is a thermal sensation coefficient, which leads to the value of PMV and to PPD. This kind of treatment will be useful to tabulate passenger's comfort by means of identifying the critical places where a passenger could be uncomfortable, which was already explained in Section 5.3, where Figure 52 depicted the seats to be analyzed.

Two simulations were executed in **OpenFOAM** with the final refined mesh and real geometry. The first was done with an inlet temperature of $296.6\text{ K} = 23.4\text{ }^\circ\text{C}$. The result was a non-comfortable thermal environment for every single occupant, even if the test case assessed, at least, the rear passenger as comfortable. This led to the second simulation, which instead of using $23.4\text{ }^\circ\text{C}$ as inlet, the new temperature was $296.6 + 6.7 = 303.3\text{ K}$. The choice of this specific value will be clear in the next section, where the quantitative results will be shown. Basically, the most exposed passenger to cold environment has an overall deficiency in temperature of $5.8\text{ }^\circ\text{C}$ to reach comfort i.e. when the solution was found, the PMV value would have a "Neutral" sensation if the mean temperature obtained for this critical person was $5.8\text{ }^\circ\text{C}$ higher. Yet a safety factor was applied since the response of that probed position is not one-to-one. The next sections explain with more detail this resulting temperature.

6.3 Results

The results are divided in two sections: the first simulation with inlet temperature of 296.6 K , and the second one with inlet temperature of 303.3 K . Both of them had noisy unsteady curves when sampling the quantities of interest i.e. the probed temperatures and speeds. So the process of smoothing will be exemplified here to clarify the obtained values.

Three heights were probed, but in the final stage of thermal evaluation it is not important *per se* each value, but the **average temperature T_A** and **average speed V_A** . For didactic purposes it will be shown only the retrieval of Passenger 2 data that leads to a single output value for each comfort variable.

To this extent, the solver writes the output to a text file, which is converted to a comma separated value by a suitable **Python** script. These **csv** files are imported into a

spreadsheet and edited accordingly. In Table 21 is an example of the first 5 rows of the spreadsheet. This has been truncated in order to show less decimals. In any case, it uses all the available digits for calculations. It must be clarified that the sample output was written every 10 iterations, rather than sampling for all of them, due to limited storage in the virtual machine.

Iteration	Ankle	Waist	Head	Average
10	291.9	291.9	291.9	291.9
20	291.8	292.0	291.8	291.9
30	291.8	292.0	291.8	291.9
40	291.9	292.0	291.8	291.9
50	291.9	292.0	291.8	291.9

Table 21: First 5 temperature samples of Passenger 2.

The "Average" column computes the mean value of the sampled variable in three heights, which is the temperature in the previous table. With the average computed throughout iterations, the next logical step is to plot the Average values and determine a trend. In general, peaks and valleys were common when plotting these, so *noisy* curves came out as a result. In order to adjust the unstable behaviour, the moving Average was plotted. Noise tends to disappear and the trend is more defined. The number of periods chosen was 50, so each point in the Forecast curve is the average of the previous 50 data points. This method allows to visually foreseen the direction of the curve. Below the Average and Moving Average are shown in the same graph for the Temperature of Passenger 3. The moving average curve assigns the last forecast value as the steady-state solution. The reference curve for the the third passenger is shown below, where the smoothed curve has a steady behaviour after 1250 iterations. For all passenger's variables the process of smoothing averages was the same.

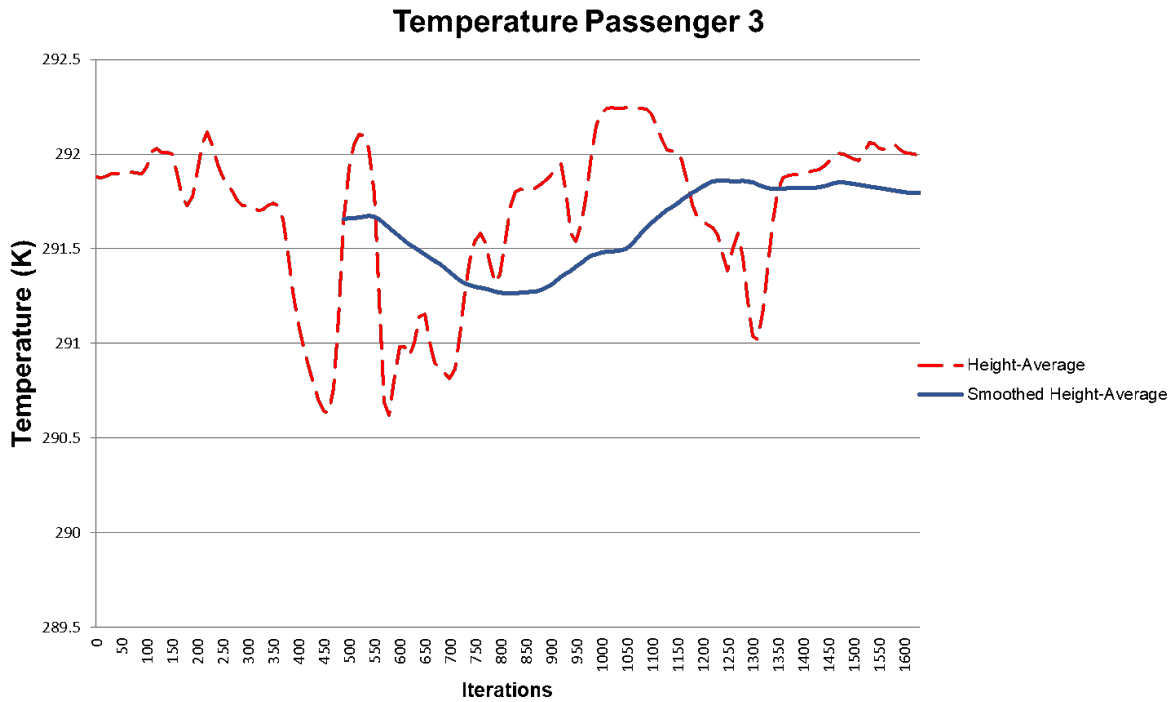


Figure 53: Average and smoothed curves used for temperature sampling of Passenger 3.

6.3.1 First simulation: 296.6 K

Prior to evaluate comfort, the energy imbalance is checked. When clear convergence is not found, the error is spread to the results, so that the difference in the energy equation could be large enough to discard the simulation output. Therefore, a brief analysis of the energy error will be presented.

Below is shown a table which summarizes the energy imbalance, calculated through enthalpy flow and heat transfer to the exterior.

	Value (W)
In	
Roof AC	88962.86
Out	
Recirculation	50789.55
Extractor fan	36537.76
Surface exchange	1668.59
Error	32.99

Table 22: Overall energy balance.

The error is larger than the test case. This could be due to the lack of complete convergence in the energy residuals. In overall, this is an expected outcome, considering that the solver had to be stopped when enough stability could be foreseen in the sampled

quantities. Even though, the error is small enough to be acceptable for results analysis, since it represents only a 2% of the surface heat exchange.

In any case, heat losses through all kind of boundaries had a steady behaviour globally. Figure 54 shows that throughout the last 1650 iterations, overall heat losses had a steady behaviour after 800 iterations. The image only shows the last 1600, but in reality an approximate of 6000 iterations were executed, where the first 3000 were carried out with first order schemes to meet an initial solution and, after convergence, the current schemes were changed for second order ones, at the same time limiters were lowered.

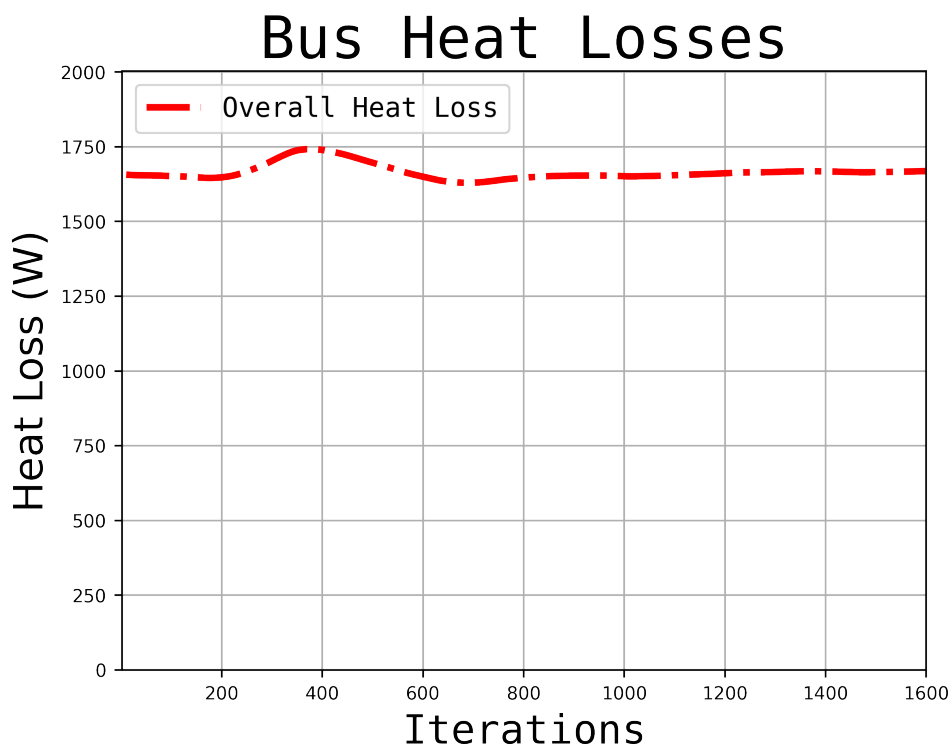


Figure 54: *Cold* simulation heat losses.

Heat losses through the right-side of the bus, where the doors are located, are greater than the losses through the left side. The latter has a global heat loss of 677 *W* whereas the right side has losses of 836 *W*. This is clearly not caused by a higher gradient of temperature in the right side, but because of the glassed surface area. The bus right side is expected to be less comfortable by two reasons:

- Less inlet ducts make obvious that lower temperatures will be present in the right side, considering that fluid is being delivered vertically to the cabin. In addition, buoyancy effects are not being considered, so buoyant currents for mixing cold and hot air do not act.
- Apart from the windows, the right side has glass doors. Both these structures tend to maintain lower temperatures in their surface. Nonetheless, it might not be so

relevant, because air motion tends to smear the conductive heat transfer through glass, but in steady conditions it creates larger gradients in near glass zones.

This prejudice agrees with the thermal comfort results. In average, left-side passengers have a higher Predicted Mean Vote. Of course, this has sense when PMV is negative, since the Neutral sensation is near 0 PMV values. Recalling that passengers 2, 3 and 4 are located at the right side and 5, 6, 7 to the left side, is evident that the latter ones have better comfort indexes.

Inlet Temperature = 296.6 K					
Passenger number	$\mathbf{T_A}$ ($^{\circ}\text{C}$)	$\mathbf{V_A}$ (m/s)	PMV	Comfortable	Sensation
1	17.6	0.11	-1.24	No	Slightly Cool
2	18.7	0.22	-1.18	No	Slightly Cool
3	17.5	0.36	-1.79	No	Cool
4	15.3	0.19	-2.13	No	Cool
5	19.0	0.11	-0.85	No	Slightly Cool
6	18.9	0.26	-1.19	No	Slightly Cool
7	16.7	0.32	-1.95	No	Cool

Table 23: Thermal comfort results for *cold* simulation

However, the table shows that all passengers are not comfortable. In fact, passengers 3, 4 and 7 have 'Cool' sensations. The outcome is very different from that found in the test case, where the rear passenger was in thermally comfortable conditions. This could have many reasons: the location of the inlets and outlets, the inaccurate schemes or the completely different layout of the bus can result in major differences between the test and the final simulations.

Table 23 shows clearly that Passenger 4 is the most uncomfortable in the bus cabin, whereas Passenger 5 is close to reaching thermal comfort. As a consequence of these results, a new inlet temperature must be set to ensure a pleasant environment for every occupant. Location of Passenger 4 is the most critical, because it has the lowest temperature. To compensate this, the minimum temperature to ensure thermal comfort in the fourth passenger was computed by trial and error. This is done by changing the mean temperature $\mathbf{T_A}$ until the Predicted Mean Vote reaches a value of -0.5, which is the lower limit for ensuring a Neutral sensation. This calculation leads to a minimum mean temperature of ≈ 21.1 $^{\circ}\text{C}$, which is 5.8 $^{\circ}\text{C}$ higher than the current mean temperature. Thus, assuming a direct *transfer function*, by rising the inlet temperature in 5.8 $^{\circ}\text{C}$, Passenger 4 should feel a Neutral sensation. Even though, the function correlating the inlet temperature and the mean temperature of Passenger 4 is not direct; by rising the inflow temperature on a certain quantity it does not imply that average temperature at that location will rise the same amount. The apparent reason of the discomfort on Passenger 4

is caused by scarcity of ducts near this location, so hot air is concentrated in other places rather than near front-door locations. This implies that the sampled zones populated with inlet vents should have a *direct* response³⁶ when changing the air temperature. On the contrary, Passenger 4 should not have high sensitivity to inlet temperature changes, compared to other seating locations.

To acknowledge the unknown relationship between the inlet temperature and passenger's average temperature, a higher temperature will be implemented as input in the so called *hot* simulation. This option is selected in view of the expected lack of response in the average temperature of Passenger 4³⁷. To this extent, the temperature will be raised 6.7 °C rather than 5.8 °C. It could be increased even more, but the scope is to find a point which is close to the limits of comfort, seeing that the Best Operating Point (BOP) of the HVAC system will be interpolated with greater precision.

6.3.2 Second simulation: 303.3 K

The quantities were obtained with the same method used before, but an unsteady behaviour arose in the overall results. Because of this instability, peaks and valleys tended to be more sharp and of greater amplitude, so instead of using a moving average of 50 sample points, a 200 sample points was plotted. This kind of treatment transformed the unsteady behaviour into a stable low sloped curve. The plotted graph in Figure 55 demonstrates the highly unsteady behaviour. However, the smoothed curve shows that the value tends to be stable around 296 K.

³⁶Their correlation must be ≈ 1 .

³⁷By rising 1°C the inlet temperature, the mean temperature increment could be barely of 0.5° C.

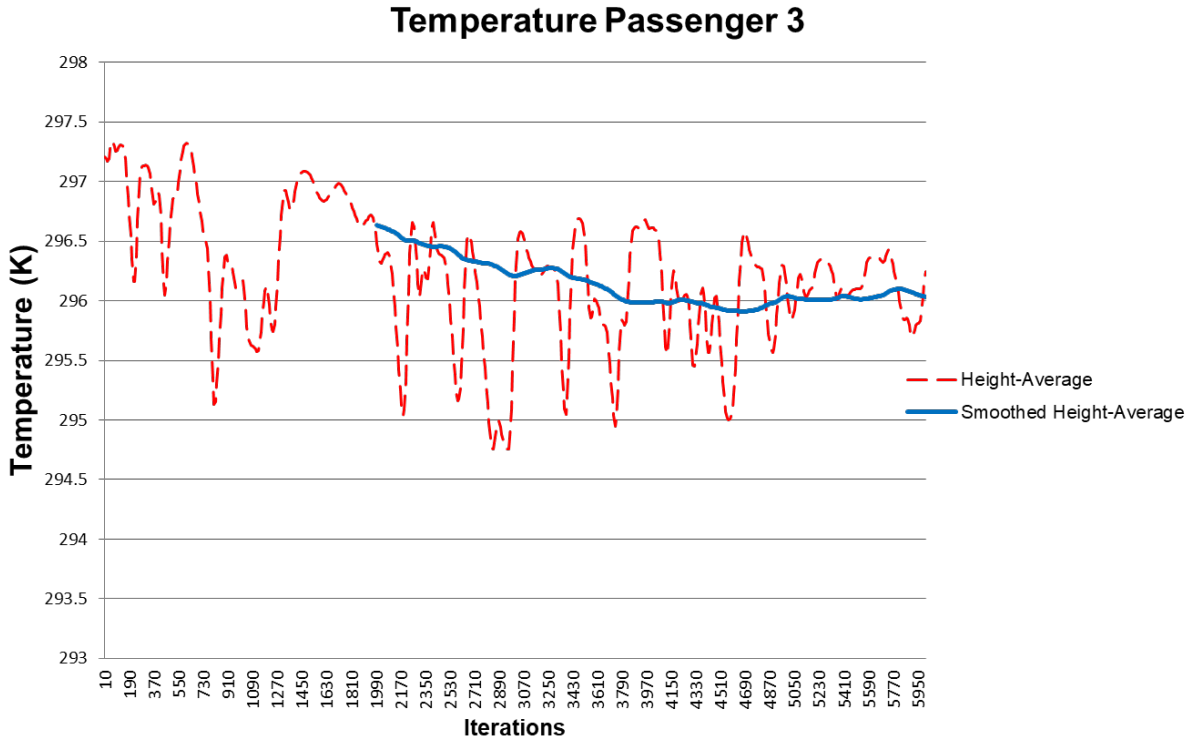


Figure 55: Passenger 3 mean temperature. The blue line represents the moving average with a sampling rate of 200 periods.

Even if it could be expected that with this new temperature comfort is achieved for every passenger, it is not the case. This is acknowledged by looking at the comfort summary Table 24.

Inlet Temperature = 303.3K						
Passenger number	T_A (°C)	V_A (m/s)	PMV	Comfortable	Sensation	
1	22.6	0.10	0.16	Yes	Neutral	
2	22.2	0.22	-0.20	Yes	Neutral	
3	22.9	0.29	-0.16	Yes	Neutral	
4	18.9	0.16	-1.04	No	Slightly Cool	
5	23.7	0.13	0.38	Yes	Neutral	
6	23.5	0.28	0.04	Yes	Neutral	
7	21.0	0.32	-0.68	No	Slightly Cool	

Table 24: Thermal results of *hot* simulation.

Clearly, the results are much better than the *Cold* simulation. Even more, these results show that comfortable PMV values are achieved for 5 out of 7 passengers. However, they are not satisfying enough; some passengers are still uncomfortable and is an unknown if this situation can be improved. In particular, passengers 4 and 7 have low PMVs, being Passenger 4 location a critical one because is not even near to comfort zone. Therefore, the outcome must be analyzed under different conditions so that thermal comfort is achieved

for every passenger, if possible. Theoretically, it should be possible by rising a fraction of degree the temperature, but the scope is to minimize energy. So the thermal conditions will be optimized to ensure thermal comfort while minimizing heating energy.

6.3.3 Optimization of inlet temperature

To begin the optimization problem, some assumptions must be made. For instance, the transfer function relating the inlet temperature and the sampled passengers is an unknown. It is assumed that the relationship between the input temperature and all mean temperatures is linear, at least in the analyzed temperature range. By assuming this, is possible to use the collected data of the simulations to draw a line³⁸ for each passenger that correlates the mean temperature as a function of the inlet temperature. So that it is satisfied:

$$T_{p,i} \approx \frac{T_{p,i1} - T_{p,i0}}{T_{inlet,1} - T_{inlet,0}} \cdot (T_{inlet} - T_{inlet,0}) + T_{p,i0} \quad (13)$$

The previous is the line equation, where the quantity expressed as a fraction is the slope of the line. The subindex i stands for the passenger number and the numerical subindexes 0 and 1 represent the *cold* and *hot* simulation.

By using expression 13, is possible to construct a nested optimization problem as follows:

- The outer optimization problem is to maximize the number of passengers that can reach comfort at the same time. To this extent, a binary value will be assigned to each passenger, where 1 is assigned to a 'Neutral' sensation passenger, and 0 in any other case. This first outer problem is expressed as:

$$\begin{aligned} \max_Y \quad & \sum_{i=1}^N Y_i \\ \text{s.t.} \quad & T_{p,i} = f_i(T_{inlet}), \quad i = 1...7 \\ & Y_i \leq \frac{|PMV(\dots, T_{p,i}, \dots)|}{0.5}, \quad i = 1...7 \\ & Y_i \in \{0, 1\}^n, \quad i = 1...7 \\ & T_{inlet} \geq 0 \end{aligned} \quad (14)$$

The function $f_i(T_{inlet})$ is the linear relation shown in Equation 13. The decision variables of Problem 14 are Y_i , the binary variables that tell whether or not comfort is achieved, and T_{inlet} the inlet temperature to be chosen.

³⁸A simple first order approximation is implemented. If more simulations were available a higher degree polynomial would be more appropriate, or even a different fitting curve.

By solving this optimization problem, the maximum number of occupants that can reach comfort at the same time will be computed. The resolution of this problem was accomplished with OpenSolver, a linear and non-linear optimization solver add-in for MS Excel. When solved, it yields to a **maximum number of comfortable passengers of 6**. The obtained value for inlet temperature yields to $T_{inlet} = 304.07 K$. Clearly, this is a non-reachable operation point, having in mind that HVAC units rarely have more than one decimal digit precision.

- The second optimization problem is solved setting the number of occupants that are comfortable to 6. The objective function is different; the scope is to minimize energy consumption, while ensuring that these passengers are in comfort conditions. So the binary variables Y_i are set to 1 for all people, except for Passenger 4, who does not reach comfort. The inner optimization problem is:

$$\begin{aligned}
& \min_Y T_{inlet} \\
& \text{s.t. } T_{p,i} = f_i(T_{inlet}), \quad i = 1...7 \\
& Y_i \leq \frac{|PMV(\dots, T_{p,i}, \dots)|}{0.5}, \quad i = 1...7 \\
& Y_i = 1, \quad i = 1..3, 5..7 \\
& Y_4 = 0 \\
& T_{inlet} \geq 0
\end{aligned} \tag{15}$$

The final inlet temperature yields $\mathbf{T}_{inlet} = \mathbf{304 K}$. A summary of the consequent results for comfort calculations is shown below in Table 25.

Inlet Temperature = 304 K						
Passenger number	\mathbf{T}_A (°C)	\mathbf{V}_A (m/s)	PMV	Comfortable	Sensation	
1	23.1	0.13	0.22	Yes	Neutral	
2	22.5	0.22	-0.10	Yes	Neutral	
3	23.4	0.30	-0.03	Yes	Neutral	
4	19.2	0.19	-1.02	No	Slightly Cool	
5	24.1	0.15	0.48	Yes	Neutral	
6	24.0	0.26	0.20	Yes	Neutral	
7	21.5	0.28	-0.50	Yes	Neutral	

Table 25: Optimized inlet temperature for thermal comfort summary.

In fact, the optimum temperature up to the fourth decimal is $T_A = 304.0004 K$. In practical applications, this has no further use due to the limits in accuracy of thermal control devices. For instance, the HVAC system installed on the BYD K9® bus has a thermal control of ± 0.5 °C.

6.3.4 Energy requirements

The final subsection determines the necessary energy to reach the optimum value and compares it with the maximum heat power that can provide the rooftop unit. After that, a recirculation curve is provided, relating heat power needed as a function of the recirculation percentage.

Assuming perfect mixing of the recirculated air and fresh air, the following relation holds:

$$Q_{HVAC} = \dot{m}_{inlet} \cdot c_p \cdot T_{inlet} - \xi \cdot \dot{m}_{inlet} \cdot c_p \cdot T_{recirculation} - (1 - \xi) \cdot \dot{m}_{inlet} \cdot c_p \cdot T_{outside} \quad (16)$$

Greek letter ξ is the mass recirculation ratio. A linear interpolation will be used to determine the recirculated air temperature $T_{recirculation}$. With the two simulations carried out in Sections 6.3.1 and 6.3.2, the outlet recirculation enthalpy can be retrieved and, consequently, the temperature of recirculation at the optimum inlet temperature. Table 26 illustrates the values obtained for the recirculation temperature.

	Inlet Mass Flow Rate (kg/s)	Inlet Temperature (K)	Recirculation Enthalpy (W)	Recirculation Average Temperature (K)	Recirculable Mass Flow Rate (kg/s)	Maximum Recirculable Percentage
Cold	0.297	296.6	50789.6	290.86	0.173	58.2%
Hot	0.291	303.3	49681.3	294.76	0.167	57.4%
Optimum	-	304	-	295.17	-	-

Table 26: Recirculating air properties summary.

The Value for the Recirculation Average Temperature in the Optimum case was obtained by extrapolation from the Recirculation Average Temperature and the inlet Temperatures from the *Hot* and *Cold* simulations. The rest of the variables will not be extrapolated, since the real nature of the output of the simulation is not known and it could spread the already inherent error of the linear approximation of 295.17 K for the Optimum case. On the other hand, both *Cold* and *Hot* simulations have a maximum recirculation percentage in the order of $\approx 50\%$. Thus, this will be set as the limit of recirculation for the Optimum case for heat power calculation. Mathematically this is expressed as $\xi \leq 0.5$. Below is shown the curve of heat power required depending on the recirculation percentage.

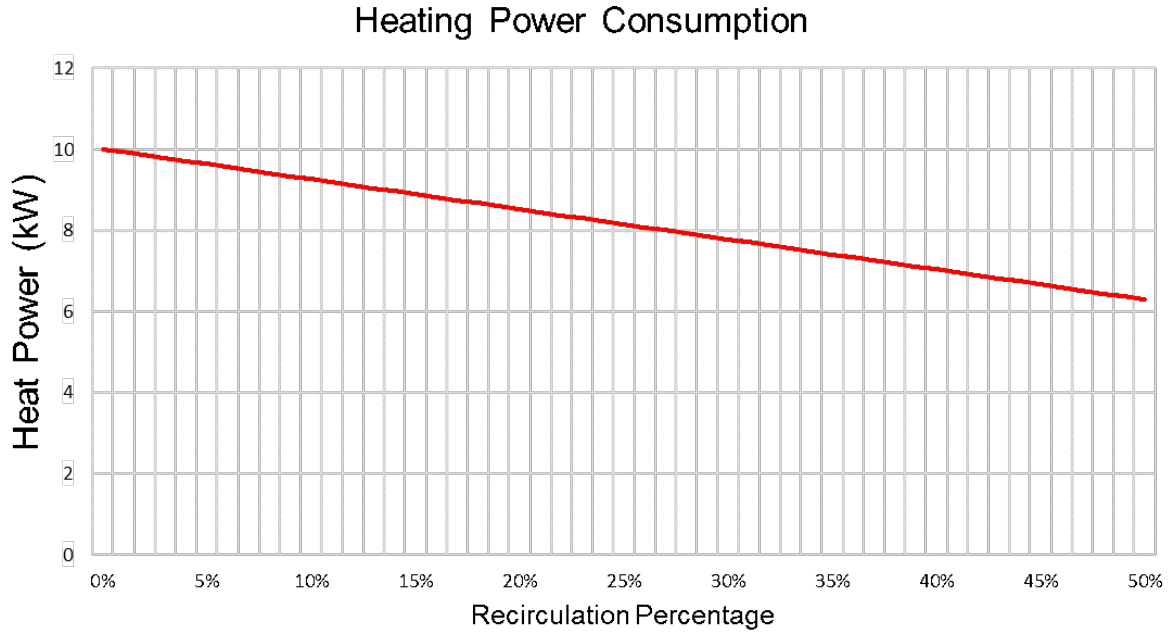


Figure 56: Heat power consumption as a function of the recirculation percentage ξ .

The HVAC unit is capable to withstand the energy consumption with 0% of recirculation. In that case, the heat consumption would be of 10 *kW*. This represents a 62.5% of the maximum heat capacity of BYD K9® heating system. Indeed, it is possible to heat the bus in thermally optimal conditions without any recirculating air flow rate. However, it will be extremely expensive and inefficient. Moreover, the maximum flow rate available is 6000 $\frac{m^3}{h}$, which is much higher than the 900 $\frac{m^3}{h}$ used for the simulations. This makes evident and necessary the usage of recirculation vents, because if the flow rate is increased in order to improve ventilation the HVAC unit will not be able to supply enough heat power to achieve thermal comfort if there is no recirculation.

7 Conclusions and recommendations

Computer-Aided Engineering tools have gained an outstanding importance in mechanical engineering fields. Particularly, in the field of CFD they have no substitute for cheap and faster results. CAD tools, meshing softwares, CFD solvers and post-processing tools have been developed to the point where the workflow connecting these four processes is fluent. Meshing tools must be mentioned; thanks to the new sophisticated algorithms developed, CFD simulations results have much less error due to optimized cell shapes. Software designers are aware of the need of Graphical User Interfaces for non-experienced users who want to start in the meshing field and that is why they create easy-of-use displays in their softwares.

Open source CFD codes are powerful tools. To the point that these are comparable to commercial CFD developed by worldwide known brands. `OpenFOAM` has demonstrated to be a highly reliable free-of-use tool for beginners in CFD coding. From its creation, it has been continuously revised by the fluid research community, making contributions in a non-profit manner. Nevertheless, the lack of GUI is one of the important weaknesses of `OpenFOAM`. For beginners or people who have no background in coding or command lines, it is a hard starting point. But the learning curve of the command lines applied to `OpenFOAM` is certainly steep.

`buoyantSimpleFOAM` is an excellent solving tool for HVAC applications and thermal calculations, but buoyant phenomena must be considered to acknowledge reality in the solutions. Otherwise, the risk is to obtain *GIGO* information which does not represent in any way the fluid behaviour. In addition, steady-state solvers are useful for obtaining quick results, but they do not represent flow motion trough time. These kind of simulations are often interrogated in literature. Mostly because the time needed to reach steady state is an unknown; for instance, if the bus reaches this state after several hours, the result has no practical purpose. Of course it has physical sense, but from an engineering point of view, the results do not give information about the real comfort capabilities.

The results obtained in this research show that thermal comfort is hardly achievable for every person in the bus cabin. It does not exist a midpoint where every occupant is satisfied with the thermal conditions. Indeed, some passengers could feel non-neutral sensations if located in places characterized for the lack of inlet ducts. The analysis must be extended to other passengers: probably there are more seating or standing locations where comfort is not reached. Two simulations were executed and, even so, it was not possible to reach comfort for the seven sampled passengers. Even though, it was possible to determine a theoretical value which optimizes energy consumption, assuming a linear behaviour of the temperature variables. By optimizing the inlet temperature, at the same time the heat power needed to reach thermal comfort is being optimized.

Reaching an optimum and energy efficient temperature for the HVAC system is a matter of concern nowadays. Particularly in the new hybrid and full-electric vehicles, where the energy consumption is, by all means, a critical issue. In fact, the K9 bus from BYD® is an electrical one. Electrical vehicles have assigned a certain threshold of power consumption for the HVAC system. In addition, when the battery of the vehicle is low, the vehicle algorithm powers off the energy of the roof unit, leaving no air conditioning or heating for the bus cabin until the battery is recharged.

The most important recommendations and advices for thermal designers and CFD engineers as a result of this work can be summarized as follows:

- It is extremely important to compare the results with a real experiment. Turbulence models, elaborated numerical schemes and new techniques of Computational Fluid Dynamics cannot replace the real behaviour of the thermal system being analyzed. Computers, servers, supercomputers or workstations are still not capable of emulating with enough accuracy fluid flows or chemical reactions. Turbulence models have proven to be reliable, but only under specific conditions and ranges of operation. The errors obtained by the CFD code are impossible to determine if a point of comparison with reality does not exist.
- Open source tools are a cheap way of making CFD simulations. It is a common belief that commercial software is more reliable and better results are obtained. As a general rule, learning bash command line of Linux, programming in any coding language (Python, C++, C#, pseudo-coding) results in a faster learning of the source code in **OpenFOAM**. For novices and people with no experience, it is highly recommended to learn the basics of coding. This will improve the user's understanding of internal errors in the algorithms and numerical schemes used. Not only in the mentioned software, but also in commercial softwares, such as ANSYS Fluent.
- Throughout the simulations, buoyancy was neglected, as well as time schemes were ignored to let only non-buoyant steady-state simulations be executed. It is clear that buoyancy is a thermal effect that must be accounted for, as well as time derivatives. No conclusion can be stated, since there is no information about floatability effects. However, two important points must be remarked: the source term of gravity in the Navier-Stokes equation may have a major impact in the results, because buoyant currents increase air mixing, generating an homogeneous thermal environment. In addition, these currents maintain the air in continuous movement so time derivatives are likely to be non-zero. That is why a transient simulation should be used instead.
- Even if servers and computing cores are a common resource for industrial CFD, the access to these kind of hardware is expensive. However, cloud computing has

gained importance, making it possible to design CFD code and execute it remotely. Nonetheless, the iterative essence of the design process makes necessary the access to the plot of quantities of interest, residuals and conservation equations errors while simulating. This task is impossible either in servers or cloud computing. Even more, it is needed a visual inspection to ensure that the results have physical sense.

- Thermal systems can be optimized, either by heuristic methods, mathematical modeling or trial and error. The optimization will depend on the objective. In a bus, the objective is to minimize energy consumption, but a prioritization of the occupants' comfort is crucial. Air recirculation is an excellent method for energy saving. This is particularly important in new technological vehicles; either fossil fuel based, hybrid or electric. The latter ones being critical in this aspect, recalling that in this kind of vehicle the HVAC system is the most energy-consuming, according to Göhlich et al. (2018).
- The results obtained in Section 7 should be similar to the ones in the real bus geometry in some aspects. Anyway, the oversimplification in the geometrical features is a matter of concern. The essence of the CFD code is not lost as an overall. Even so, air currents inbetween seats and handrails are lost due to the simplified model, to the point that they could change the air velocities near seating locations.
- As a projection for better results, conjugate heat transfer solvers could be a reliable alternative for developing a complete thermal model. Surface heat transfer is evaluated accurately, so it is possible to determine heat losses through solid elements. By doing so, the 'adiabatic' boundary condition assigned for floor, seats and rear cabin of the bus can be evaluated to assess if they are safe assumptions or not.
- Radiation models must be considered in thermal simulations. They affect noticeably the human perception of thermal comfort according to ASHRAE-55 standards. Nonetheless, analytical methods require to measure on the field the radiation, surface temperature and solid angles for each passenger. The surface-to-surface radiation model is an example for this mechanism of heat transfer that can be implemented in CFD code.
- High quality CFD for thermal simulations need to use real human geometries. Human thermoregulation system is complex to model. Mostly because of its unsteady behaviour, which depends not only on thermal variables, but also on physiological ones. ASHRAE-55 models for thermal perception assume statistically averaged humans in healthy conditions. However, there are more innovative models, such as the Berkeley model for human comfort. It divides the human body into sections that might have different temperatures. The existing models use a unique temperature representing an homogeneous body.

In a general perspective about CFD and thermal comfort, new processor types have been developed by the biggest brands in the world. Thus, making possible to run highly complex simulations in personal computers. However, Moore's law is reaching its theoretical limit and it does not seem that in the near future it will be possible to perform accurate and transient simulations in a personal computer. Quantum processing and new electric materials must be researched more deeply.

Thermal comfort is a multivariable function and human models are being improved. Multidisciplinary teams must design human regulatory models that can be implemented into a CFD code. The final consequence will be better understanding of the human response under environmental conditions and, when materialized, the aftereffect will be the creation of energy efficient and ecofriendly HVAC systems.

8 Bibliography

References

- [1] Merriam-Webster. (n.d.). HVAC. In *Merriam-Webster.com dictionary*. Retrieved from <https://www.merriam-webster.com/dictionary/HVAC>
- [2] Eye Witness to History (2007) *Air Conditioning Goes to the Movies, 1925*. Retrieved from www.eyewitnesstohistory.com
- [3] Country Life Press, 1952, p. 101. *Willis Haviland Carrier died in New York on October 7, 1950, shortly before his seventy-fourth birthday*.
- [4] Pasamos 9 horas y 35 minutos de media semanales metidos en el coche. (27 April 2017). Retrieved from https://www.abc.es/motor/reportajes/abci-pasamos-9-horas-y-35-minutos-media-semanales-metidos-coche-201704271427_noticia.html?ref=https%3A%2F%2Fwww.google.com%2F
- [5] El clima en Finlandia. (23 May 2019). Retrieved from <https://www.infofinland.fi/es/informacion-sobre-finlandia/informacion-sobre-finlandia/el-clima-en-finlandia>
- [6] Markets and Markets (2020). *HVAC System Market by Heating Equipment (Heat Pumps, Furnaces), Ventilation Equipment (Air-Handling Units, Air Filters), Cooling Equipment (Unitary Air Conditioners, VRF Systems), Application, Implementation Type, and Geography - Global Forecast to 2025*. Retrieved from https://www.marketsandmarkets.com/Market-Reports/hvac-system-market-202111288.html?gclid=EAIaIQobChMIgoH568uC6QIVw-R3Ch317gBZEAAYAIAAEgKFWfD_BwE
- [7] McDowall, R. (2007). *Fundamentals of HVAC Systems*. Retrieved from <http://www.sciencedirect.com/science/article/pii/B978012373998850011X>
- [8] Tochihara, Y., & Ohnaka, T. (2005). *Environmental Ergonomics-The Ergonomics of Human Comfort, Health, and Performance in the Thermal Environment*. Elsevier. Retrieved from <https://www.sciencedirect.com/pucdechile.idm.oclc.org/bookseries/elsevier-ergonomics-book-series/vol/3/suppl/C>
- [9] Wiker, S. (2012). Ergonomics. In *Injury Research: Theories, Methods, and Approaches* (pp. 139-185). Springer US.
- [10] Tosi, F. (2020). Design for Ergonomics. In *Design for Ergonomics* (pp. 31-45). Springer, Cham.
- [11] Standard, A. S. H. R. A. E. (2010). Standard 55-2010, *Thermal environmental conditions for human occupancy*. American Society of Heating, Refrigerating and Air Conditioning Engineers.
- [12] Pala, U., & Oz, H. R. (2015). *An investigation of thermal comfort inside a bus during heating period within a climatic chamber*. Applied Ergonomics, 48, 164-176.
- [13] Alahmer, A., Omar, M., Mayyas, A. R., & Qattawi, A. (2012). *Analysis of vehicular cabins' thermal sensation and comfort state, under relative humidity and temperature control, using Berkeley and Fanger models*. Building and environment, 48, 146-163.
- [14] Daanen, H., Van de Vliert, E., & Huang, X. (2003). Driving performance in cold, warm, and thermoneutral environments. *Applied Ergonomics*, 34(6), 597-602.
- [15] Pimenta, A. M., & Assunção, A. Á. (2015). Thermal discomfort and hypertension in bus drivers and chargers in the metropolitan region of Belo Horizonte, Brazil. *Applied ergonomics*, 47, 236-241.
- [16] Scurtu, I. L., & Jurco, A. N. (2019). AIRFLOW AND THERMAL COMFORT OF THE BUS PASSENGERS. *Journal of Industrial Design and Engineering Graphics*, 14(1), 171-174. Retrieved from <http://ezproxy.puc.cl/docview/2231816539?accountid=16788>

- [17] Walgama, C., Fackrell, S., Karimi, M., Fartaj, A., & Rankin, G. (2006). Passenger Thermal Comfort in Vehicles - A Review. *Proceedings of the Institution of Mechanical Engineers, Part D: Journal of Automobile Engineering*, 220(5), 543-562.
- [18] Danca, P., Bode, F., Nastase, I., & Meslem, A. (2017). On the Possibility of CFD Modeling of the Indoor Environment in a Vehicle. *Energy Procedia*, 112, 656-663.
- [19] Kottek, M., Grieser, J., Beck, C., Rudolf, B., & Rubel, F. (2006). World map of the Köppen-Geiger climate classification updated. *Meteorologische Zeitschrift*, 15(3), 259-263.
- [20] Versteeg, H. K. & Malalasekera, W. (2007). *An introduction to computational fluid dynamics: the finite volume method*. Pearson education. [Online]. Available: https://books.google.it/books?hl=es&lr=&id=RvBZ-UMpGzIC&oi=fnd&pg=PA7&dq=related:9PTiyTcuXxEJ:scholar.google.com/&ots=u2DYz6EhDb&sig=6eaE_XJevPpjBn3-yvdugN87BQY&redir_esc=y. [Accessed: April 24, 2020]
- [21] Kundu, P. K., & Cohen, I. M. (2001) *Fluid mechanics*. Elsevier.
- [22] Jasak, H. (1996). *Error analysis and estimation for the finite volume method with applications to fluid flows*.
- [23] Shewchuk, J. R. (1994). *An introduction to the conjugate gradient method without the agonizing pain*.
- [24] Cengel, Y. A., Klein, S., & Beckman, W. (1998). *Heat transfer: a practical approach* (Vol. 141). New York: McGraw-Hill.
- [25] Rodriguez, S. (2017). *Applied Computational Fluid Dynamics and Turbulence Modeling* (No. SAND2017-13577B). Sandia National Lab.(SNL-NM), Albuquerque, NM (United States).
- [26] Jahn, W. (2019). *Fluidodinamica Computacional*. Santiago, Chile: Pontificia Universidad Catolica de Chile.
- [27] Canuto, C. (2019) *Numerical Modelling*. Turin, Italy: Politecnico di Torino.
- [28] Asinari, P. (2019) *Advanced Engineering Thermodynamics*. Turin, Italy: Politecnico di Torino.
- [29] Rivera, J. (2007) *Refrigeracion, Climatizacion y Aire acondicionado*. Santiago, Chile: Pontificia Universidad Catolica de Chile.
- [30] Ferziger, J. H., Perić, M., & Street, R. L. (2002). *Computational methods for fluid dynamics* (Vol. 3, pp. 196-200). Berlin: springer.
- [31] Weatherbase.com, “Turin, Italy”, 2020. [Online]. Available: <https://www.weatherbase.com/weather/weatherall.php3?s=95061&units=>. [Accessed: May 4, 2020]
- [32] Göhlich, D., Fay, T. A., Jefferies, D., Lauth, E., Kunith, A., & Zhang, X. (2018). Design of urban electric bus systems. *Design Science*, 4.
- [33] Schlichting, H., & Gersten, K. (2016). *Boundary-layer theory*. Springer.
- [34] Kestin, J., & Richardson, P. D. (1963). Heat transfer across turbulent, incompressible boundary layers. *International Journal of Heat and Mass Transfer*, 6(2), 147-189.
- [35] Candas, V. (2005). To be or not to be comfortable: basis and prediction. In *Elsevier ergonomics book series* (Vol. 3, pp. 207-215). Elsevier.
- [36] Olesen, B. W. (2005). International standards for the thermal environment. Where are we and what is still needed?. In *Elsevier Ergonomics Book Series* (Vol. 3, pp. 479-485). Elsevier.
- [37] Tanabe, S. I., Ozeki, Y., & Takabayashi, T. (2005). Numerical comfort simulator for evaluating thermal environment. In *Elsevier Ergonomics Book Series* (Vol. 3, pp. 459-466). Elsevier.

- [38] Holmér, I. (2005). Evaluation of vehicle climate. *Environmental ergonomics*, 283-288.
- [39] Smith, W. J. (2010). Can EV (electric vehicles) address Ireland's CO2 emissions from transport?. *Energy*, 35(12), 4514-4521.
- [40] Kühne, R. (2010). Electric buses—An energy efficient urban transportation means. *Energy*, 35(12), 4510-4513.
- [41] Velt, K. B., & Daanen, H. A. M. (2017). Optimal bus temperature for thermal comfort during a cool day. *Applied Ergonomics*, 62, 72-76.
- [42] Suh, I. S., Lee, M., Kim, J., Oh, S. T., & Won, J. P. (2015). Design and experimental analysis of an efficient HVAC (heating, ventilation, air-conditioning) system on an electric bus with dynamic on-road wireless charging. *Energy*, 81, 262-273.

9 Annexes

A1 Technical datasheet of GTT bus.

		CARATTERISTICHE TECNICHE DEL VEICOLO AUTOBUS ELETTRICI 12 m	Allegato 6 pag. 3/13
larghezza utile vani porte (ant. / cent. /post.)	[mm]	1,200/1,200/1,200	
diagnostica integrata con CAN BUS	SI/NO	SI	
tipo intervento in caso di ostacolo frapposto in fase di chiusura		Le porte hanno un dispositivo di rilevazione dell'ostacolo in chiusura e in apertura. Nel movimento di chiusura è presente anche un bordo sensibile.	
tipo intervento in caso di ostacolo frapposto in fase di apertura		Le porte hanno un dispositivo di rilevazione dell'ostacolo in chiusura e in apertura.	
II.3 - CAPACITA' DI TRASPORTO CON SEDIA A ROTELLE A BORDO			
posti a sedere : (incluso disabile in carrozzella)	[nr.]	22	
posti in piedi:	[nr.]	55	
posti totali: (escluso conducente)	[nr.]	77	
area S1 destinata ai passeggeri in piedi	[m ²]	8.7	
II.3 - CAPACITA' DI TRASPORTO SENZA SEDIA A ROTELLE A BORDO			
posti a sedere :	[nr.]	21	
posti in piedi :	[nr.]	62	
posti totali : (escluso conducente)	[nr.]	83	
area S1 destinata ai passeggeri in piedi	[m ²]	10	
ALLESTIMENTI			
II.4.2 SBRINAMENTO			
presa d'aria in posizione alta (CUNA NC 586-06)	SI/NO	NO	
rubinetto sezionamento impianto sbrinamento (front-box)	SI/NO	SI	
finestrino laterale sinistro con resistenza	SI/NO	SI	
prima porta con dispositivo antiappannamento	SI/NO	SI	
II.4.3 - IMPIANTO CLIMATIZZAZIONE POSTO GUIDA			
marca e tipo:		BYD AK411	
Alimentazione		BYD	
potenza termica totale (riscaldamento):	[kW]	4	
potenza termica totale (raffreddamento):	[kW]	4	
portata totale aria:	[m ³ /h]	1,000(aria-out)	
velocità aria min e max dalle bocchette con ventilazione massima:	[m/s]	3-6m/s	
numero regolazioni velocità ventilazione:	[nr.]	3	
II.3.4 - IMPIANTO CLIMATIZZAZIONE VANO PASSEGGGERI			
marca e tipo:		BYD AK421	
Alimentazione		BYD	
potenza termica totale (riscaldamento):	[kW]	20	
potenza termica totale (raffreddamento):	[kW]	14	

6 ACQUISTO AUTOBUS ELETTRICI 12 m Allegato 6 - Caratteristiche
BYD Europe B.V.
 14
 BYD Europe B.V.
 (signature)

portata totale aria:	[m ³ /h]	1,500(aria-in)/6,000(aria-out)
ricambi aria/h :	[nr./h]	/
velocità aria min e max dalle bocchette con ventilazione massima:	[m/s]	3-6m/s
tenuta impianto senza necessità ricarica	[anni]	3
diagnostica integrata con CAN BUS	SI/NO	SI
SEDILI (allegare scheda tecnica)		
II.4.4- Sedile autista - marca e tipo:		Isri 6860/875 NTS2
Seduta : tipo materiale / rivestimento		Cover Inca/Laos TU01-3042/TU01-3044
Schienale : tipo materiale / rivestimento		Cover Inca/Laos TU01-3042/TU01-3044
II.11.2 - Sedili passeggeri (marca, tipo, classe) tipo trattamento antigraffiti		Ruspa Citipro Classe 1
		A causa della loro struttura molecolare non possono essere danneggiati da differenti tipo di inchiostro, quindi nessun trattamento particolare è necessario.
II.12- INDICATORI DI LINEA / INFOMOBILITA'		
Indicatori di linea Marca e tipo:		Aesys Anteriore: 1,930*240mm (160*19 pixel) MA475*500.160*19/1 SL2 M2 ETH M12 Laterale: 1,219*203mm (120*16 pixel) MA 400*500.120*16/1 YW SL2 M2 ETH M12 Posteriore: 420*203mm (33*16 pixel) MA500.33*16/1 SL2 M2 ETH M12 Interni: 720*80mm (144*16 pixel) RG 5M-144*16 ETH
Informazioni ai passeggeri Marca e tipo:		Aesys TFT 18.5" Master RS485 Wi-Fi
II.3.3 - RAMPA E POSTAZIONE DISABILI		
marca, tipo		Ventura S605
Portata	[kg]	19
dimensioni rampa: (lunghezza-larghezza)	[mm]	920*960mm
peso della pedana parte ribaltabile	[kg]	350
II.12.5 - BOTOLE DI AERAZIONE E SICUREZZA		
marca e tipo:		Lam
quantità:	[nr]	2
azionamento:		Elettrico
II.5.1 - PRESTAZIONI A PIENO CARICO		
velocità massima:	[km/h]	70
accelerazione (CUNA 503-06): (15m)	[s]	4.64

6 ACQUISTO AUTOBUS ELETTRICI 12 m Allegato 6 - Caratteristiche

For and on behalf

BYD Europe (I.V.)

authorized sign

A2 Technical description of heating and air conditioning system.



In assenza del disabile a bordo lo stesso spazio potrà essere dedicato allo stazionamento di una carrozzina per bambini e sarà dotato di posti a sedere su sedili chiudubuli.

Lo schienale della postazione disabile in carrozzella e gli strapuntini saranno imbottiti e rivestiti dello stesso materiale.

La porta in corrispondenza dello spazio riservato al trasporto della carrozzella è dotata di una apposita rampa di accesso a ribalta manuale, rispondente ai requisiti normativi applicabili.

4.11. Climatizzazione del comparto passeggeri e vano autista

Il posto guida e il comparto passeggeri sono equipaggiati con un impianto di climatizzazione integrato (condizionatore + riscaldatore), con regolazione della temperatura separata; il comando di attivazione e regolazione del climatizzatore posto guida è a disposizione del conducente, mentre per il comparto passeggeri la regolazione avviene in modo automatico. I parametri di funzionamento sono essere configurati tramite l'elettronica di controllo.

L'impianto garantisce il trattamento dell'aria esterna (stagione invernale -5°C; stagione estiva +38°C), climatizzandola a temperatura ottimale ed immettendola con adeguati flussi all'interno del comparto passeggeri e vano autista. La distribuzione dell'aria lungo il veicolo avviene tramite opportune canalizzazioni dedicate solo al passaggio dell'aria.

Le caratteristiche tecniche dell'impianto prevedono l'uso di tubazioni in rame per il tratto interno vettura e in gomma per le connessioni flessibili; la giunzioni sono realizzate con l'ausilio di connessioni che garantiscano la massima tenuta e consentano agevolmente interventi riparativi o sostituzioni.

L'impianto prevede la funzione di ricircolo dell'aria.

In caso di raggiungimento del 20% di carica delle batterie l'impianto di climatizzazione si disattiva automaticamente.

In sede di offerta deve essere dettagliatamente presentata ed illustrata la soluzione proposta, precisando le caratteristiche tecniche dell'impianto climatizzatore ed il posizionamento dei componenti, con particolare riguardo alle potenze in gioco.

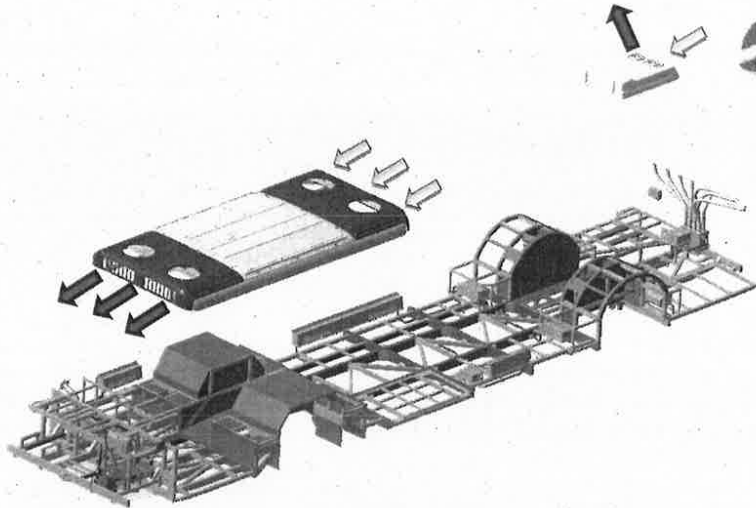
4.11.1. Climatizzazione vano passeggeri

Il veicolo è dotato di un sistema di climatizzazione dell'aria con compressore elettrico, con impianti separati per il vano passeggeri e per il posto guida, realizzato in maniera tale da consentire la regolazione indipendente dei due spazi.

GTT Appalto n.124/2015 – Fornitura autobus elettrici – Descrizione Tecnica. Questo documento è riservato tra BYD e GTT.

97

For and on behalf
of
BYD Europe B.V.
authorized signature(s)



L'impianto di condizionamento del vano passeggeri è stato completamente sviluppato da BYD realizzando un controllo completo della qualità dell'aria con l'impianto installato sul tetto.



Figura 98: Impianto aria condizionata passeggeri

Tipo di Unità	Integrabile con riscaldamento PTC
Tipo installazione	Montaggio a tetto
Fluido refrigerante	R134a
Tensione di lavoro	DC540V (DC210~580V)
Tensione ausiliaria	DC24V
Peso	300kg
Dimensioni	3700mm(L)×1860mm(W)×220mm(H)

Figura 99: Tabella impianto aria condizionata integrato a pompa di calore con riscaldamento PTC

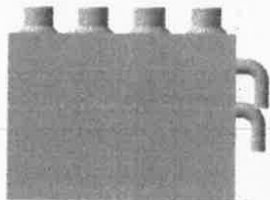
For and on behalf
of
BYD Europe B.V.
authorized signature(s)



Table 4- 1 Caratteristiche impianto AC

Potenza nominale di raffreddamento	25KW
Volume aria trattata	6000m ³ /h
Potenza massima assorbita	16KW
Potenza massima compressore	12KW
Potenza massima accessori (PTC)	16KW
Picco Massimo di corrente	≤120A
Rapporto di efficienza	2.5
Livello del rumore del gruppo	≤68dBA
Rumore all'interno	≤68dBA
Regolazione della temperatura	16~30°C

Figura 100: Tabella caratteristiche impianto AC



Parameter	
Rated voltage	DC24V
Motor power	240W
heat released quantity	9Kw(80°C)
dimension	450X173X341(LXWXH)

Rated voltage/ Tensione nominale; Motor power/Potenza motore;

Heat released quantity/radiazione di calore; Dimension/ Dimensione

Figura 101: Sbrinator



Parameter	
Rated voltage	DC24V
Motor power	55W
Heat released quantity	2Kw
Air output	300m ³ /h
dimension	476X150X191 (LXWXH)

Rated voltage/ Tensione nominale; Motor power/Potenza motore;

Heat released quantity/radiazione di calore; Air output/ Erogazione d'aria; Dimension/ Dimensione

Figura 102: Riscaldatore

GTT Appalto n.124/2015 – Fornitura autobus elettrici – Descrizione Tecnica. Questo documento è riservato tra BYD e GTT.

for and on behalf
of
BYD Europe B.V.
Authorized signature(s)



parameter	
Rated voltage	DC24V
Motor power	40W
heat released quantity	8Kw
Air output	900m ³ /h
dimension	1931X147X207.5 (LXWXH)

Rated voltage/ Tensione nominale; Motor power/Potenza motore;

Heat released quantity/radiazione di calore; Air output/ Erogazione d'aria; Dimension/ Dimensione

Figura 103: Montaggio a pavimento



Parameter	
Rated voltage	DC24V
Motor power	20W
heat released quantity	2Kw
Air output	450m ³ /h
dimension	755X147X207.5 (LXWXH)

Rated voltage/ Tensione nominale; Motor power/Potenza motore;

Heat released quantity/radiazione di calore; Air output/ Erogazione d'aria; Dimension/ Dimensione

Figura 104: Montaggio a parete

4.11.1.1. Filtrazione aria

L'impianto di climatizzazione è previsto di sistemi di filtrazione dell'aria immessa nell'abitacolo per abbattere le impurità, sia in aspirazione dall'interno del veicolo (ricircolo) che dall'esterno.

La presa d'aria esterna deve si trova nella parte superiore del veicolo.

GTT Appalto n.124/2015 – Fornitura autobus elettrici – Descrizione Tecnica. Questo documento è riservato tra BYD e GTT.

for and on behalf
of
BYD Europe B.V.

Authorized signature(s)



4.11.2. Regolazione e impostazioni dell'impianto di condizionamento

4.11.2.1. Modalità automatica

Selezione: modalità automatica oppure comando manuale in caso di necessità.

Uscita: Cambio modalità o spegnimento il sistema.

Algoritmo:

- $Test \geq 26^{\circ}C$, entra in modalità refrigerazione e opera in questa modalità, impostando la temperatura $T_{int} = 26^{\circ}C$;
- $25^{\circ}C \leq Test < 26^{\circ}C$, entra in modalità refrigerazione e opera in questa modalità, impostando la temperatura $T_{int} = Tr - 2^{\circ}C$;
- $23^{\circ}C \leq Test < 25^{\circ}C$, entra in modalità deumidificazione e opera in modalità riscaldamento, impostando la temperatura $T_{int} = Tr - 2^{\circ}C$;
- $Test < 23^{\circ}C$, entra in modalità riscaldamento e opera in questa modalità, impostando la temperatura $T_{int} = 26^{\circ}C$;
- Dopo aver impostato questa modalità, se i compressori sono in funzione da più di 2 ore, la modalità non cambierà più in base alla temperatura;
- Il volume di aria in uscita è regolato automaticamente e fluisce attraverso il condotto d'aerazione con velocità variabile tramite la regolazione delle ventole.

4.11.2.2. Modalità refrigerazione

Selezione: Impostare la modalità refrigerazione, comunque il sistema entra automaticamente in questa modalità anche in determinate condizioni automatiche.

Uscita: Impostare un'altra modalità o spegnere il sistema.

4.11.2.3. Algoritmo di controllo:

- Impostare la temperatura dal pannello, scegliendo una temperatura tra i $16^{\circ}C$ e i $30^{\circ}C$ (la tolleranza della temperatura è di $0,5^{\circ}C$).
- La temperatura può essere regolata premendo i pulsanti "Incremento temperatura" e "Riduzione temperatura".
- Il sistema di controllo verificherà la differenza tra la temperatura impostata e quella effettiva, per poi trasmettere il segnale al compressore;
- Controllo della velocità del flusso d'aria e della rotazione delle ventole: In questa modalità la velocità del flusso d'aria può essere impostata in: automatica, alta, media, bassa, massima e silenziosa.

4.11.2.4. Modalità deumidificazione

Selezione: Impostare la modalità deumidificazione, altrimenti il sistema entra automaticamente in questa modalità in determinate condizioni.

Uscita: Impostare un'altra modalità o spegnere il sistema.

Algoritmo di controllo:

- In modalità deumidificazione, dopo aver impostato la temperatura, opererà come ultimo segnale dal comando;
- $Test > T_{int} + 2^{\circ}C$, funziona in modalità refrigerazione e la velocità del flusso d'aria è regolata dal pannello;
- $Test \leq T_{int} + 2^{\circ}C$, il compressore funziona in modalità refrigerazione e la ventola interna lavora a velocità bassa;
- $Test \leq T_{int}$, il compressore funziona secondo il ciclo: 10 minuti in funzione e 6 minuti spento. In queste condizioni viene considerato un intervallo di 3 minuti per la protezione del compressore in base al suo ciclo.

GTT Appalto n.124/2015 – Fornitura autobus elettrici – Descrizione Tecnica. Questo documento è riservato tra BYD Europe B.V.



di funzionamento. La ventola interna lavora a velocità bassa quando il compressore è in funzione, mentre si ferma quando il compressore è fermo;

- Test $\leq 15^{\circ}\text{C}$, Il sistema e la ventola interna si spengono automaticamente;
- In modalità deumidificazione la frequenza varia di più o meno 1Hz/s ed è sottoposta alle limitazioni della modalità refrigerazione;
- In modalità deumidificazione la velocità del flusso d'aria può essere impostata in: automatica, alta, media, bassa.

4.11.2.5. Modalità riscaldamento

Selezione: Impostare la modalità riscaldamento, il sistema entra comunque in modalità riscaldamento in determinate condizioni del programma automatico.

Uscita: Impostare un'altra modalità o spegnere il sistema.

Algoritmo di controllo:

- Impostare la temperatura dal pannello scegliendo una temperatura tra i 16°C e i 30°C (la tolleranza della temperatura è di $0,5^{\circ}\text{C}$).
- La temperatura può essere regolata premendo i pulsanti "Incremento temperatura" e "Riduzione temperatura".
- Il sistema di controllo verificherà la differenza tra la temperatura impostata e quella effettiva, per poi trasmettere il segnale al compressore;
- Controllo della velocità del flusso d'aria e della rotazione delle ventole: In questa modalità la velocità del flusso d'aria può essere impostata in: automatica, alta, media, bassa, forte e silenziosa.

4.11.2.6. Modalità ventilazione

Selezione:

- Impostare la modalità ventilazione dal telecomando;
- l'impianto si accende se è in stand-by o spento;
- Il comando della modalità ventilazione deve durare 3 secondi.

Uscita: Cambiare modalità entro 3 secondi o spegnere il sistema.

4.11.2.7. Integrazioni del sistema di aria condizionata e del sistema di riscaldamento

E' possibile passare dal sistema di aria condizionata al sistema di riscaldamento e viceversa. Il comando ha tre modalità: spento, modalità aria condizionata e modalità riscaldamento. Passando in modalità aria condizionata, si può attivare il sistema premendo il pulsante Acceso/Spento e si può scegliere una delle tre modalità (automatico, refrigerazione, riscaldamento). In queste condizioni funziona solo l'aria condizionata, il condotto d'aerazione fornirà solo aria fresca per scongelamento anche se il sistema di riscaldamento è impostato su "ACCESO". Passando in modalità riscaldamento entra in funzione la resistenza di riscaldamento. Può essere impostata l'aria calda per i piedi dell'autista e per il vano passeggeri. Ogni modalità del scongelamento è operativa, ma non l'aria condizionata.

Algoritmo controllo aria condizionata: Il sistema di controllo per l'aria condizionata della cabina dell'autista e per l'aria condizionata per il vano passeggeri sono integrati in un unico pannello. Ogni modalità può essere scelta attraverso questo pannello.

4.11.2.8. Pre-riscaldamento

L'autista può impostare il tempo di pre-riscaldamento sul cruscotto in base alle necessità. Raggiunto il tempo prestabilito, le resistenze PTC inizieranno a pre-riscaldare l'autobus. Appena acceso l'autobus il pre-riscaldamento si interrompe.

GTT Appalto n.124/2015 – Fornitura autobus elettrici – Descrizione Tecnica. Questo documento è riservato tra

for and on behalf
of
BYD Europe B.V.

signature

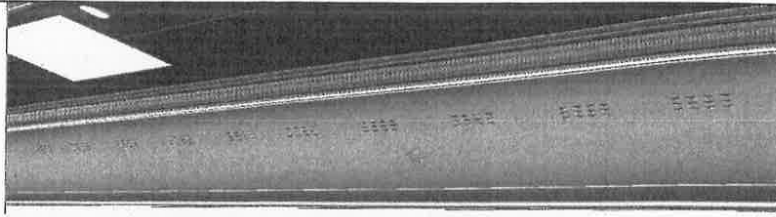


Figura 111: bocchette dell'aria

Durante la ricarica è attivata la funzionalità di mantenimento della temperatura interna del veicolo (10°C in inverno, 28 °C in estate); la funzione è abilitata a chiave servizi estratta e porte chiuse.

4.11.3. Prestazioni del climatizzatore

L'impianto di climatizzazione offerto è opportunamente dimensionato affinché garantisca le seguenti prestazioni:

4.11.3.1. Stagione Estiva

Temperatura interna $\leq 33^{\circ}\text{C}$ con temperatura esterna di $38 \pm 2^{\circ}\text{C}$; in ogni caso è assicurata almeno una differenza di temperatura $\Delta T \geq 5^{\circ}\text{C}$ ($\Delta T = T_{\text{esterna media}} - T_{\text{interna finale}}$) in ogni punto di misura alle condizioni della prova come richiesto.

4.11.3.2. Stagione Invernale

Temperatura interna $\geq 10^{\circ}\text{C}$ con temperatura esterna ed interna iniziale di -5°C ; in ogni caso è assicurata almeno una differenza di temperatura $\Delta T \geq 15^{\circ}\text{C}$ ($\Delta T = T_{\text{interna finale}} - T_{\text{esterna media}}$) in ogni punto di misura alle condizioni della prova come richiesto.

A3 Visual Basic code for PMV calculation

```

Function FNPS(T)
    FNPS = Exp(16.6536 - 4030.183 / (T + 235))
End Function

Function PMV(CLO, MET, WME, TA, TR, VEL, RH, pa)
If VEL <= 0.2 Then
    If pa = 0 Then pa = RH * 10 * FNPS(TA) '
    ICL = 0.155
    M = MET * 58.15
    W = WME * 58.15
    mw = M - W
    If ICL < 0.078 Then fcl = 1 + 1.29 * ICL Else fcl = 1.05 + 0.645 * ICL
    hcf = 12.1 * Sqr(VEL)
    taa = TA + 273
    tra = TR + 273
    'calculate surface temperature for clothing by iterating'
    tcla = taa + (35.5 - TA) / (3.5 * (6.45 * ICL + 0.1))
    'first guess temp'
    p1 = ICL * fcl
    p2 = p1 * 3.96
    p3 = p1 * 100
    p4 = p1 * taa
    p5 = 308.7 - 0.028 * mw + p2 * (tra / 100) ^ 4
    xn = tcla / 100
    xf = xn
    n = 0
    eps = 0.00015
    Do While n < 150
        xf = (xf + xn) / 2
        'heat transf. coeff. by natural convection
        hcn = 2.38 * Abs(100 * xf - taa) ^ 0.25
        If hcf > hcn Then hc = hcf Else hc = hcn
        xn = (p5 + p4 * hc - p2 * xf ^ 4) / (100 + p3 * hc)
        n = n + 1
        If Abs(xn - xf) < eps Then
            Exit Do
        End If
    Loop
    TCL = 100 * xn - 273
    'heat loss components
    h11 = 3.05 * 0.001 * (5733 - 6.99 * mw - pa)
    If mw > 58.15 Then h12 = 0.42 * (mw - 58.15) Else h12 = 0!
    h13 = 1.7 * 0.00001 * M * (5867 - pa)
    h14 = 0.0014 * M * (34 - TA)
    h15 = 3.96 * fcl * (xn ^ 4 - (tra / 100) ^ 4)
    h16 = fcl * hc * (TCL - TA)
    'PMV and PPD
    ts = 0.303 * Exp(-0.036 * M) + 0.028
    'PMV
    PMV = ts * (mw - h11 - h12 - h13 - h14 - h15 - h16)
Else
    PATM = 101.325
    vstill = 0.1
    coolingEffect = coolEffect(TA, TR, VEL, RH, MET, CLO, WME, PATM)
    PMV = PMV(CLO, MET, WME, TA - coolingEffect, TR - coolingEffect, vstill, RH, pa)
End If

End Function
Function PPD(PMV)
    PPD = 100 - 95 * Exp(-0.03353 * PMV ^ 4 - 0.2179 * PMV ^ 2)
End Function

```